Photocontrolling the Diels-Alder Reaction

DISSERTATION

zur Erlangung des akademischen Grades
doctor rerum naturalium
(Dr. rer. nat.)
im Fach Chemie
eingereicht an der

Mathematisch-Naturwissenschaftlichen Fakultät
der Humboldt-Universität zu Berlin
von

Dipl.-Chem. Robert Göstl

Präsident der Humboldt-Universität zu Berlin
Prof. Dr. Jan-Hendrik Olbertz

Dekan der Mathematisch-Naturwissenschaftlichen Fakultät
Prof. Dr. Elmar Kulke

Gutachter:	1. Prof. Stefan Hecht, Ph.D.
	2. Prof. Dr. Hans-Werner Abraham
	3. Prof. Neil R. Branda, Ph.D.
Tag der mündlichen Prüfung:	10. November 2014

Die vorliegende Arbeit wurde in der Zeit von Juni 2011 bis August 2014 am Institut für Chemie der Humboldt-Universität zu Berlin unter der Anleitung von Prof. Stefan Hecht, Ph.D. angefertigt.

Teile dieser Arbeit wurden bereits veröffentlicht in: / Parts of this work have already been published in:

[1] R. Göstl, S. Hecht, *Angew. Chem. Int. Ed.* **2014**, *53*, 8784–8787.

[2] R. Göstl, A. Senf, S. Hecht, *Chem. Soc. Rev.* **2014**, *43*, 1982–1996.

Danksagung

Ich möchte mich bei Prof. Stefan Hecht, Ph.D. für das Ermöglichen dieser Dissertation bedanken. Unter seiner Anleitung habe ich mich nicht nur fachlich ausgezeichnet weiterentwickeln können und stets hervorragende Arbeitsbedingungen vorgefunden, sondern habe von ihm im Besonderen auch die Dinge über das wissenschaftliche Arbeiten gelernt, die in Lehrbüchern nicht abgedruckt werden.

Mein weiterer Dank geht an Martin Herder, Dr. Jan J. Klein, Dr. Maria-Melanie Russew, Dr. Sonia Castellanos Ortega, Dr. Bernd M. Schmidt, Dr. Philipp Viehmann, Derk Jan van Dijken und Dr. Alexis Goulet-Hanssens ohne deren fachliche Kompetenz und Freundschaft meine Dissertation in dieser Form nicht zustande gekommen wäre. Damit einher geht mein Dank an den gesamten AK Hecht, der sich in seinem stetigen Wandel immer wieder von einer neuen Seite präsentiert hat. Herauszuheben ist mein Dank an die Frühstücksrunde bestehend aus Dr. Michael Pätzel, Dr. Lutz Grubert und Dr. Joachim Leistner, die mich stets motiviert in den Tag entlassen haben.

Für zahlreiche Lösungen meiner NMR-Probleme danke ich Prof. Dr. Clemens Mügge, Angela Thiesies und Katharina Pfaff. Prof. Dr. Rainer Mahrwald danke ich für stets abwechslungsreiche Gespräche im Fahrstuhl. Felix Hanßke möchte ich für das Durchführen von DLS-Messungen danken.

Bei der Deutschen Forschungsgemeinschaft möchte ich mich für die finanzielle und fachliche Unterstützung durch den SFB 658 bedanken, ohne die diese Dissertation nicht möglich gewesen wäre.

An meine Lebensgefährtin Linda Hübner geht mein besonderer Dank dafür, dass sie es schafft in meiner Gegenwart nicht wahnsinnig zu werden und für die beste Mischung aus intellektueller und kulinarischer Unterstützung. Schließlich geht großer Dank an meine Mutter Anne Göstl und meine Großmutter Charlotte Göstl, die mich nicht nur moralisch sondern auch finanziell sehr ausführlich gestützt haben.

Abstract

The synthetic chemist's profession is devoted to the formation of chemical bonds to create new molecules, building blocks, or drugs from basic starting materials. However, the growing complexity of these synthetic products necessitates that the development of the tools to fulfill this task must also keep pace. Light as a stimulus with its superior spatial, temporal, as well as energetic resolution in combination with its non-invasive character outperforms the traditional means to control a chemical reaction, such as heat, pressure, or *p*H, clearly. In this work, the unprecedented reversible photocontrol over a dynamic covalent reaction was established by the combination of a molecular photoswitch and the well-known Diels-Alder reaction. The outcome of the reaction of a furyl-substituted diarylethene and maleimide could be determined exclusively by illumination with differently colored light. This prototypical system was then advanced for the application under physiological conditions while retaining its superior photochemical properties. The release of therapeutically effective concentrations of different antitumor agents could be photoreversibly triggered in buffered, aqueous solution at body temperature employing bioorthogonal visible light. It is shown how the release properties of these photoswitchable prodrugs can be fine-tuned and a thorough investigation of the release dynamics is presented promoting this system to a level where *in vivo* application can be considered. Furthermore, the foundations for the implementation of the photocontrollable Diels-Alder reaction in the reversible covalent functionalization of carbon nanotubes have been laid. Despite the fact that a successful functionalization has not yet been achieved, the basic principles were investigated and have paved the way for the application of more advanced techniques to effectively modulate the physicochemical properties of sp^2-carbon allotropes.

Zusammenfassung

Die Aufgabe des synthetischen Chemikers besteht darin neue Moleküle, Bauelemente oder Medikamente aus einfachen Edukten herzustellen. Die wachsende Komplexität dieser synthetischen Produkte bedingt jedoch, dass die Entwicklung der dazu benötigten Werkzeuge ebenso schritthalten muss. Licht ist mit seiner herausragenden räumlichen, zeitlichen und energetischen Auflösung sowie seinem nicht-invasiven Charakter den traditionell verwendeten Stimuli überlegen. In dieser Arbeit wurde durch die Kombination eines molekularen Photoschalters mit der Diels-Alder-Reaktion die Photokontrolle über eine dynamisch-kovalente Reaktion erlangt. Das Ergebnis der Reaktion eines furyl-substituierten Diarylethens mit Maleinimid konnte ausschließlich durch die Bestrahlung mit Licht unterschiedlicher Farbe bestimmt werden. Dieses prototypische System wurde dann unter Erhalt seiner photochemischen Eigenschaften für die Anwendung unter physiologischen Bedingungen weiterentwickelt. Es konnte die photoreversible Freisetzung therapeutisch wirksamer Konzentrationen verschiedener Anti-Tumor-Medikamente in gepufferter, wässriger Lösung bei Körpertemperatur durch bioorthogonales sichtbares Licht ausgelöst werden. Weiterhin wurden die Feinabstimmung der Freisetzung dieser photoschaltbaren Diels-Alder-Addukte und eine ausführliche Untersuchung der Freisetzungs-Dynamiken gezeigt. Hierdurch wurde das System auf eine Stufe gehoben, an der *in vivo* Anwendungen erwägt werden können. Des Weiteren wurden die Grundlagen zur Implementierung der photokontrollierbaren Diels-Alder-Reaktion in der reversiblen kovalenten Funktionalisierung von Kohlenstoffnanoröhren gelegt. Trotzdem noch keine erfolgreiche Funktionalisierung nachgewiesen werden konnte, wurde durch die Untersuchung der zugrundeliegenden Prinzipien der Weg für die Anwendung fortgeschrittener Techniken zur Modulation physikochemischer Eigenschaften von sp^2-Kohlenstoff Allotropen geebnet.

Table of Contents

1. Introduction

1.1 Preliminary Remarks

Besides its analytical and theoretical element, chemistry has always been a creative and constructive science. The synthetic chemist utilizes compounds that are readily available and converts them to a desired product through a chemical reaction constructing new materials, drugs, and technologically basic modules. As the demand for complexity and finesse of these products increases with the proceeding industrial advancement of our society, it becomes imperative that the methods to control a chemical reaction must also keep pace. Whereas so far it was enough to exert control over a chemical transformation by varying reaction temperature and time, the tailor-made molecules of the future clearly demand for stimuli featuring higher precision and orthogonality. Many physical and chemical stimuli, such as pressure and *p*H, exist that could possibly be employed to incorporate a higher dimension of control into a reaction system. Light, however, with its superior spatial, temporal, and energetic resolution in combination with its non-invasive character offers the possibility to remote control different processes simultaneously with molecular scale resolution. It is thus only consequential to design molecules that respond to light as a stimulus and that can transfer the acquired information to manipulate the outcome of a chemical reaction.

In this work the reader is guided through a process starting with the design of a photoresponsive molecule that is then applied to influence the outcome of the well-known and heavily used Diels-Alder reaction. This system is then advanced towards an application where the additional stimulus enables the unprecedented control over the release of antitumor agents in physiological systems – an application that would not be possible without the extra dimension in control. Additionally, the foundations for the implementation of the photocontrollable Diels-Alder reaction in the reversible covalent functionalization of carbon nanotubes are laid. The results and accompanying experimental details follow a short introduction to the basic principles used which are necessary to fully recognize the extent of this work.

1.2 Photochromism

Simply put, photochromism is defined as a *light-induced reversible change of color*. A more precise formulation would be helpful and translated into the realm of the sciences photochromism indicates *a reversible transformation of a chemical species induced in one or both directions by absorption of electromagnetic radiation between two forms, A and B, having different absorption spectra* (Scheme 1-1).[1,2]

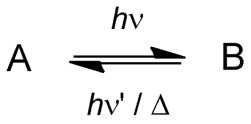

Scheme 1-1: General expression of a photochromic transformation.

However, over the last decade research on photochromes has reached a new quality as we consistently progress from seeing photochromism as simple switching between two colored states towards employing it as a tool to control chemical, physical, and biological processes through the application of external light stimuli.[3–7] The outcome of this is an ever-growing academic interest in photochromic molecules[8–10] that directly reflects the chemist's desire to control diverse chemical transformations on the molecular level resolved in time as well as in space.

There exists a considerable amount of classes of photochromic molecules, the most popular derivatives of which are depicted in Scheme 1-2. The azobenzene class has been known for decades but still enjoys an unimpaired popularity amongst its users (Scheme 1-2a). The huge geometrical change upon UV-light induced isomerization from the thermodynamically more stable *E*-form to the *Z*-azobenzene is accompanied by a large variation in the dipole moment rendering it especially useful for the alteration of molecular geometries,[11] directed modification of shapes in preorganized ensembles on materials and surfaces,[12,13] or conformational changes in biomacromolecules.[14] The *Z*- to *E*-isomerization is possible *via* the photochemical as well as the thermal pathway since azobenzene is a T-type photochrome, meaning that it reconverts to its thermodynamically more stable *E*-isomer thermally over time. The spiropyran class complements the azobenzene class as the UV-light induced formation of the merocyanine form is reversible by both visible light as well as thermally (Scheme 1-2b). Besides the advantageously large spectral separation of the two isomers, the switching to the merocyanine form entails a charge separation, which renders the

alteration of the dipole moment much more pronounced as compared to the azobenzene class.[15] Unfortunately, spiropyran is prone to a number of irreversible side-reactions (fatigue) in solution. As a direct result, the most impressive research results incorporating spiropyrans as switches rely on the molecule being attached to a bulk surface or nanoparticles limiting its translational freedom and thus inhibiting unwanted intermolecular fatigue-reactions.[16] This immobilization can also be realized through the incorporation of the switch into polymer blends and accordingly to this day the only industrial application of organic photochromes is that of spiropyran or spirooxazine derivatives in photochromic lenses.[17]

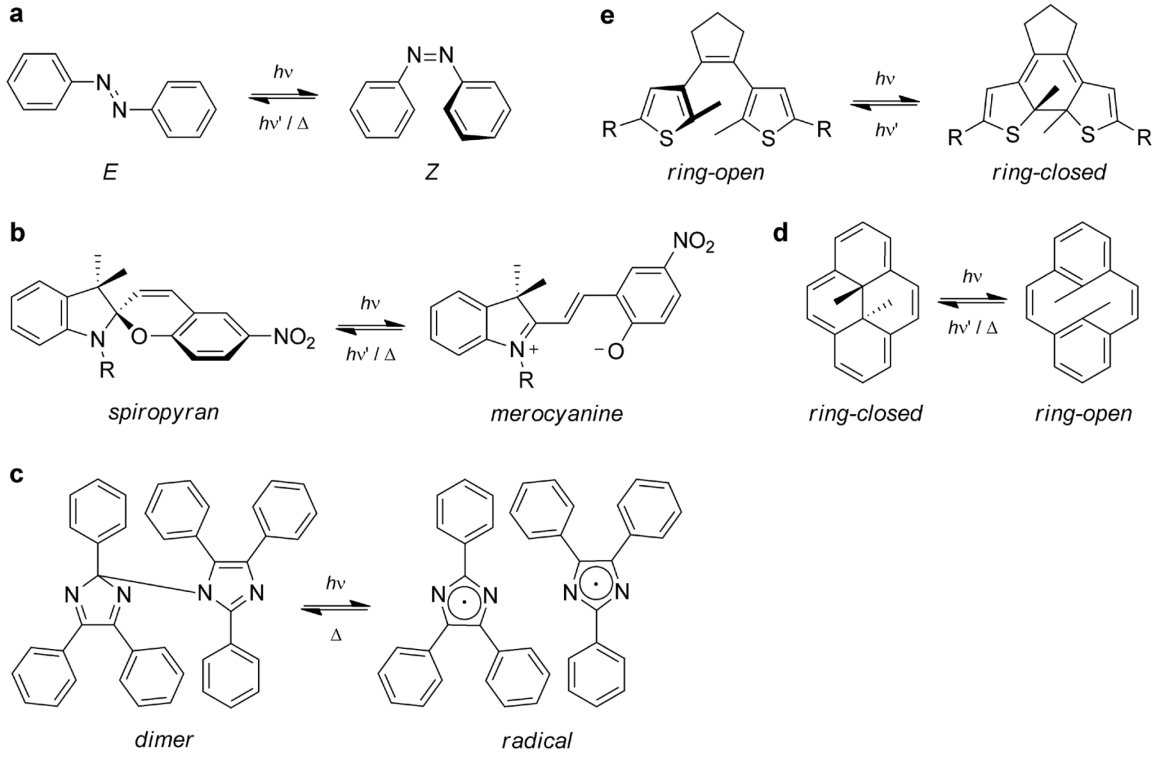

Scheme 1-2: Classes of popular photochromic molecules depicted in their respective switching states. a) Azobenzene, b) spiropyran, c) triphenylimidazole dimer, d) dihydropyrene, and e) diarylethene.

A relatively new kind of T-type photochromic compounds is the triphenylimidazole dimer class (Scheme 1-2c). By irradiation with UV-light a triphenylimidazole dimer breaks into two aromatically stabilized, colored triphenylimidazolyl radicals.[18,19] The significance of this system lies in its tremendously fast thermal back reaction (tens of milliseconds) rendering it potentially interesting for time-dependent applications that are only executed under irradiation and cease to function as soon as the light source is removed.[20]

The aforementioned T-type photochromes all have in common that the uncolored isomer is the thermodynamically more stable form and thus the default position of the

switching system. Contrarily, dihydropyrenes are colored in their thermodynamically more stable ring-closed form classifying these compounds as negative photochromes (Scheme 1-2d).[21,22] This characteristic switching behavior appears to be especially advantageous for possible *in vivo* applications as the default state can be addressed with vis-light lying in the therapeutic optical window of biological tissue.[23]

By far one of the most popular photochromes is the diarylethene (DAE) class of molecules (Scheme 1-2e).[24,25] These differ considerably from the switches mentioned earlier in a number of characteristics. DAEs can be rendered P-type photochromes and thus both the ring-open as well as the ring-closed isomers can be thermally stable constituting a system that is addressable with light exclusively. Besides featuring high photocyclization quantum yields with low fatigue – offering reversible switching over hundreds to thousands of cycles – the isomerization process is accompanied by a rather small change in the molecular geometry and can thus be induced in very confined spaces, such as densely packed single crystals.[26] Conversely, the electronic modulation during the isomerization process is quite remarkable: When the reactive sp^2-carbon centers are connected, a conjugation pathway is opened throughout the molecule in a way that the two aryl moieties can 'communicate' electronically with each other. This permits reactivity modulation for functional sites located on the switch by connecting electronically modifying groups into the conjugated π-system.[3,27–29] Hence, the synthetically convenient modifiability, high switching efficiency, and superior fatigue resistance accompanied by pronounced changes between the ring-open and ring-closed forms render DAEs the molecule of choice for applications where reliable photoswitching is demanded.

1.3 The Diarylethene Class Photochromes

1.3.1 Molecular Construction

Historically, all DAEs are related to their parent compound stilbene. Besides the *E*-*Z*-isomerization, stilbene can undergo a 6π-electrocyclization yielding dihydrophenanthrene upon irradiation with UV-light (Scheme 1-3). This photoreaction is, however, only poorly reversible as the ring-closed dihydrophenanthrene oxidizes easily to phenanthrene under aerated conditions. As useful as the photocyclization with following oxidative dehydrogenation is for the synthesis of condensed ring systems, it is just as counterproductive for providing reversible photochromism. Hence, replacing the oxidatively labile protons in the dihydrophenanthrene with more inert, yet sterically low-demanding, substituents, such as methyl residues, has proven to successfully inhibit the oxidation to the aromatically stabilized phenanthrene.

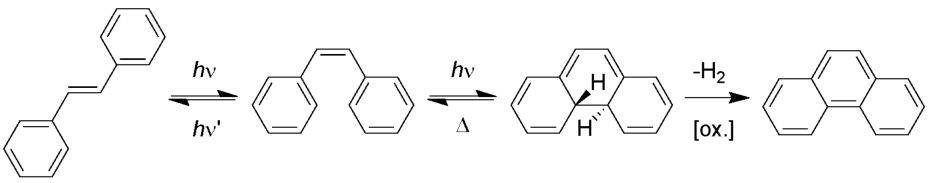

Scheme 1-3: *E*-*Z*-isomerization, electrocyclization, and oxidation of stilbene.

Despite the considerable improvement, methylated stilbene still makes for a poor bistable photoswitch, the main reason being the phenyl residues. When the aromatic stabilization energy of the ring-open form is large as compared to the ring-closed dihydrophenanthrene derivative, the latter is destabilized considerably and the system becomes thermally reversible. It was, however, found that the incorporation of aromatically less stabilized moieties, such as thienyl-residues, reduces the effective energy difference between the ring-open and the ring-closed forms enough to prolong the thermal half-life of the ring-closed forms almost indefinitely (Scheme 1-4).[30] Furthermore, elongation of the conjugated π-system induces a bathochromic shift of the S_1-transition in the ring-closed form. This spectral separation considerably accounts for the independent addressability of ring-open and ring-closed forms. As research on DAEs has intensified over the past few decades, a vast amount of different aryl substituents has been successfully incorporated. Amongst them are benzothiophene,[31–34] furan,[30,35–39] benzofuran,[40–44] indole,[45,46] isoxazole,[47] thiazole,[48–54], pyrrole,[55] pyrimidine,[56] pyridine,[43,57–60] tetrathiafulvalene,[61] and various polycyclic

aromatic hydrocarbons.[52,62–64] Furthermore, the attachment of the heterocycle can be varied leading to inverse type DAEs that exhibit distinctively different spectral characteristics and increased cycloreversion quantum yields. For details on this type of switch the reader is referred to Chapter 1.3.3.

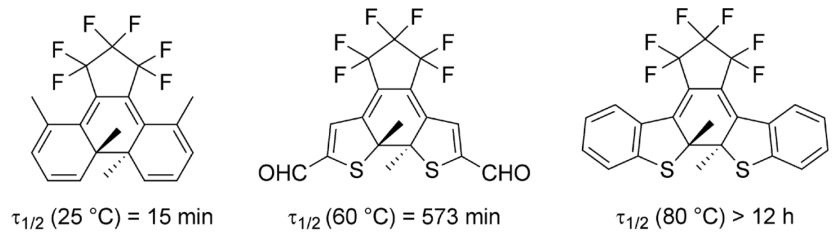

Scheme 1-4: Thermal half-life values ($\tau_{1/2}$) of the ring-closed forms of different diarylethenes.

Having suppressed the oxidation to the phenanthrene derivative and improved the thermal half-life considerably, another design flaw becomes obvious: The *E*-*Z*-isomerization can compete with the 6π-electrocyclization, severely diminishing the quantum yields of the desired ring-closing and ring-opening reactions. This issue is addressed by the mechanical fixation of the central C–C double bond in its *Z*-geometry *via* the introduction of a bridging moiety linking its 1- and 2-positions. Although four- and six-membered rings have already been incorporated into DAEs, five-membered rings, especially cyclopentene and hexafluorocyclopentene, are generally employed for this purpose.[65,66] The latter two motifs, are seen as the ideal compromise between the distinct planarity of the four-membered ring bridges and the overemphasized aryl-bridge torsion angle of the six-membered bridges.[67,68] Moreover, the bridge moiety partially governs the optical and electronic properties of the DAE. While cyclopentene can be seen as electron-rich and thus donating residue, hexafluorocyclopentene withdraws electron density from the photoswitch (Scheme 1-5a).

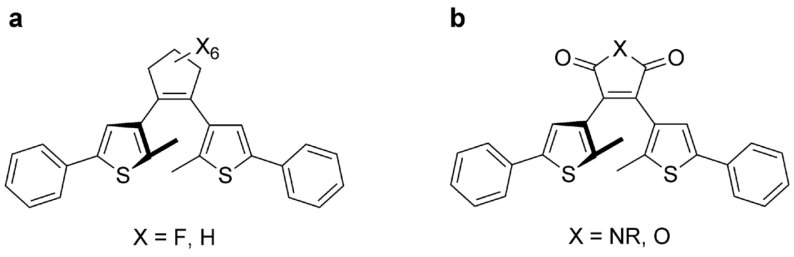

Scheme 1-5: Popular bridge motifs for the design of DAEs. a) Hexafluorocyclopentene and cyclopentene, b) maleimide and maleic anhydride.

Concomitantly, maleimide or maleic anhydride bridged DAEs exhibit a considerable bathochromic shift in their ring-open form allowing for vis-light induced photocyclization (Scheme 1-5b).[51,53]

Naturally, countless other bridge substituents have been successfully incorporated into DAEs so far, amongst them furan,[69–71] imidazole and imidazoline,[49,72] dihydrophosphole and dihydrosilole,[73] thiazole,[34,74–76] thiophene and dihydrothiophene,[34,77–79] substituted and unsubstituted polycyclic aromatic hydrocarbons,[80–86] and various substituted cyclopentenes.[87–91] Particularly the latter can be employed to enhance photocyclization quantum yields, as described later in Chapter 1.3.3.

Many successful routes for the synthesis of differently substituted DAEs have been published in the literature, the most important and general of which are depicted in Scheme 1-6.[92] Amongst the first popular DAE derivatives stand the hexafluorocyclopentenes that were – and still are – mostly synthesized by an organolithium reagent induced halogen-metal exchange on an aryl moiety followed by a nucleophilic addition/elimination sequence employing octafluorocyclopentene (Scheme 1-6a).[65] This route has proven reliable and typically provides good yields. However, the volatility of octafluorocyclopentene under ambient conditions as well as its high cost have inspired researchers to find an alternate route to the desired hexafluorocyclopentene switches. Hence, the palladium-catalyzed cross coupling of aryl boronic acids to dichlorohexafluorocyclopentene, being less volatile and costly, was reported (Scheme 1-6b).[93] As the Suzuki-Miyaura type coupling usually results in poor yields or does not work at all when oxidative insertion has to take place into a C–Cl bond, specific organophosphorous ligands, such as XPhos (2-dicyclohexylphosphino-2‘,4‘,6‘-triisopropylbiphenyl), have to be employed to ensure sufficient reactivity.

Conversely, cyclopentene bridged DAEs are generally synthesized by Friedel-Crafts acylation of the aryl moiety to a glutaric acid derivative and subsequent reductive McMurry coupling of the resulting diketone (Scheme 1-6c).[66] This route is also a reasonable alternative towards hexafluorocyclopentene bridged DAEs even though the perfluorinated glutaric acid esters are quite costly. As supposed, the synthesis of non-symmetric cyclopentene DAEs is synthetically more challenging and was approached by a consecutive Friedel-Crafts ring-opening reaction of an aryl moiety to glutaric acid anhydride followed by generation of the acid chloride and a Friedel-Crafts acylation with the second aryl moiety (Scheme 1-6d).[94] Simultaneously, we developed a route towards substituted cyclopentene bridged DAEs by

relying on a base catalyzed Michael addition of an acetylated aryl moiety to an α-β-unsaturated heteroaryl compound of a different origin.[88] We further improved and modified this reaction during the course of this work[95] (Scheme 1-6e) and the reader is referred to Chapter 2.1.2 for a detailed description of this novel approach. Only recently discovered was a novel route towards a series of terarylenes that have been synthesized by Pd-catalyzed C–H activation.[96]

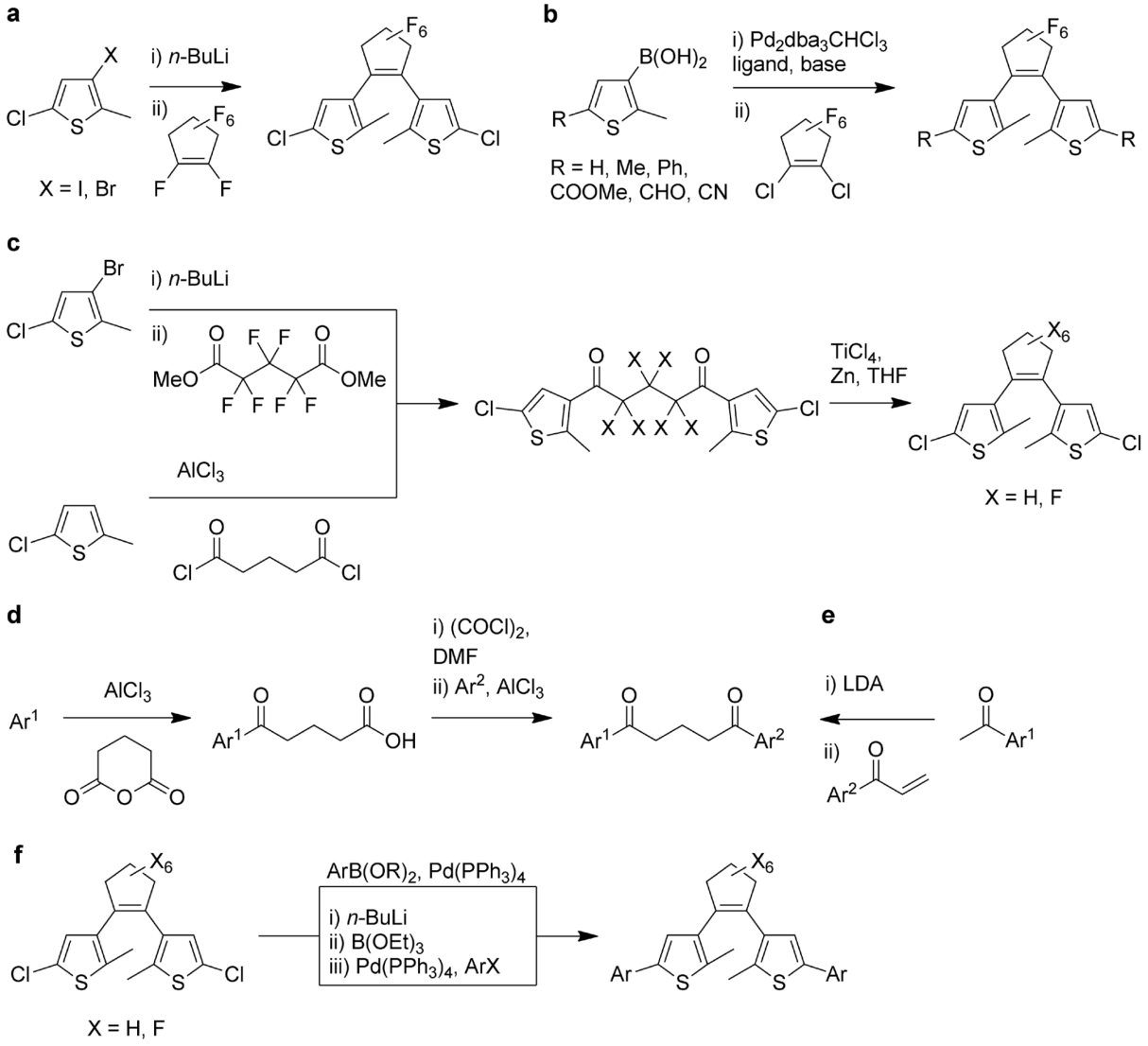

Scheme 1-6: Different synthetic approaches towards DAEs.

Once the aryl moieties are connected to the central double bond, subsequent post-functionalization offers the possibility to introduce a vast amount of different substituents (Scheme 1-6f).[92] This is generally carried out by halogen-metal exchange of the remaining aryl halide with an organolithium reagent. Subsequently, the resulting metalated aryl moieties are either quenched with an electrophile producing the final switch or are boronated for

further conversion *via* a palladium-catalyzed cross-coupling reaction. Equally, the functionalization employing Suzuki-Miyaura type conditions can be performed directly on the aryl halide using a boronate as the coupling partner.

1.3.2 Fatigue Behavior

Most research articles on DAEs (as does this work in Chapter 1.2) boldly claim that DAEs can undergo hundreds if not thousands of switching cycles without any notable fatigue. Yet, thorough investigation of a DAE over several switching cycles usually reveals that this statement is rather euphemistic. Besides the unspecific, triplet self-sensitized degradation involving singlet-oxygen and other reactive oxygen species,[97,98] DAEs' fatigue mechanism generally lies in the formation of an irreversible by-product upon prolonged irradiation of the ring-closed isomer with UV-light (Scheme 1-7). This acenaphthene type by-product was first observed and isolated by Irie and coworkers, who then also managed to grow single-crystals of the compound and perform a respective X-ray crystallographic analysis for its structure determination.[99]

While a particular derivative (Scheme 1-7, X = Me) was reported not to undergo by-product formation upon thousands of switching cycles, this is a fortunate design resulting in an exceptional shape of the excited state potential energy surface and of no universal validity. Calculations suggest that this distinct derivative's slightly higher activation energy (5 kcal/mol) from the intermediate to the by-product arising from steric hindrance is the reason for the effective suppression of its formation.[100] However, as the by-product's mechanism of formation is still only scarcely investigated,[101] no universal guidelines for the molecular design of fatigue resistant DAEs are currently available.

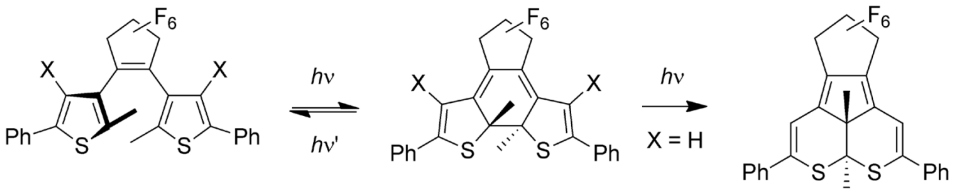

Scheme 1-7: Photochemical by-product formation of DAEs upon prolonged irradiation of the ring-closed form with UV-light.

As long as researchers avoid facing the optimization towards truly fatigue resistant modifiable DAEs, these switches will not find uses in long term application as they will

always be limited in recyclability and lifetime, thus making them inferior to their more fatigue resistant non-organic counterparts.

1.3.3 Photochemical Efficiency

The photochemical efficiency of an organic photochromic system is generally expressed by two parameters: i) the reaction quantum yield for the desired photoprocess and ii) the composition of the two isomers at the photostationary state. For a uniform photoreaction of a distinct chemical entity A to entity B (compare Scheme 1-1), an integral photochemical reaction quantum yield γ_{AB} can be intuitively defined and is expressed through

$$\gamma_{AB} = \frac{N_{reac}}{N_{absA}} \tag{1.1}$$

where N_{absA} are the number of photons absorbed by species A and N_{reac} the number of photons that have induced the photoreaction of A to B.[102] For ease of use, however, the differential quantum yield ϕ_{AB} defined by

$$\phi_{AB} = -\frac{\mathrm{d}c_A}{\mathrm{d}t} \cdot \frac{1}{I_{absA}} = -\dot{c}_A \cdot \frac{1}{I_{absA}} \tag{1.2}$$

is usually favored as it assumes an infinitesimally small change in concentration over a given time interval.[8] Here, $\dot{c}_A$ is the differential change of the concentration of species A over time and I_{absA} the amount of light absorbed by species A as a function of c_A. According to Lambert-Beer's law I_{absA} can be defined as

$$I_{absA} = 1000 \cdot I_0 \cdot \varepsilon_A \cdot c_A \cdot \frac{1-10^{-A'}}{A'} \tag{1.3}$$

with a correction factor of 1000 cm^3L^{-1}, the incident photon irradiance I_0 $\left[\mathrm{E} \cdot \mathrm{cm}^{-2} \cdot \mathrm{s}^{-1}\right]$,[103] the molar absorptivity of species A ε_A, and the overall absorbance at the irradiation wavelength A'.[8,104–106] Equations (1.2) and (1.3) combine to give the differential expression of a uniform photochemical reaction where the product B is photoinactive

$$\frac{\mathrm{d}c_A}{\mathrm{d}t} = -1000 \cdot I_0 \cdot \varepsilon_A \cdot \phi_{AB} \cdot c_A \cdot \frac{1-10^{-A'}}{A'}. \tag{1.4}$$

However, if both species A as well as B absorb at the irradiation wavelength, *i.e.* their molar absorptivities ε are different from 0, and the reaction is photoreversible, forward and backward reactions have to be taken into account with

$$\frac{\mathrm{d}c_\mathrm{A}}{\mathrm{d}t} = -1000 \cdot I_0 \cdot \left(\varepsilon_\mathrm{A} \cdot \phi_\mathrm{AB} \cdot c_\mathrm{A} - \varepsilon_\mathrm{B} \cdot \phi_\mathrm{BA} \cdot c_\mathrm{B}\right) \cdot \frac{1-10^{-A'}}{A'}. \tag{1.5}$$

This equation cannot be solved to give a closed-form expression and consequently it is practical to make an approximation. The initial slope method (or 'method of initial rates') is an approach to measure ϕ_AB in a regime where the contribution of species B to the overall absorbance is assumed to be negligible $\left(c_\mathrm{B} < 0.05 \cdot c_\mathrm{A}^0 \approx 0\right)$ and thus the rate of the back reaction can be neglected. Additionally, within the 5% conversion limit the photokinetic factor $\frac{1-10^{-A'}}{A'}$ is assumed to remain constant. Applying these restraints to Equation (1.5) while considering that $\dot{c}_\mathrm{A} = -\dot{c}_\mathrm{B}$ gives the term

$$\frac{\mathrm{d}c_\mathrm{B}}{\mathrm{d}t} = 1000 \cdot I_0 \cdot \varepsilon_\mathrm{A} \cdot \phi_\mathrm{AB} \cdot c_\mathrm{A} \cdot \frac{1-10^{-A'}}{A'}. \tag{1.6}$$

A' can be expressed as the sum of the overall absorbances of the species existing in solution

$$A' = \varepsilon_\mathrm{A} \cdot c_\mathrm{A} + \varepsilon_\mathrm{B} \cdot c_\mathrm{B} \tag{1.7}$$

and as $c_\mathrm{B} \approx 0$, Equation (1.6) can be altered accordingly to

$$\frac{\mathrm{d}c_\mathrm{B}}{\mathrm{d}t} = 1000 \cdot I_0 \cdot \phi_\mathrm{AB} \cdot \left(1-10^{-A'}\right). \tag{1.8}$$

If the reaction is monitored by absorption spectroscopy at a wavelength where $\varepsilon_\mathrm{A} = 0$, the concentration of species B can be directly expressed through its absorbance A_B at that wavelength and subsequently results in the equation

$$\frac{\mathrm{d}A_\mathrm{B}}{\mathrm{d}t} = \phi_\mathrm{AB} \cdot 1000 \cdot I_0 \cdot \varepsilon_\mathrm{B} \left(1-10^{-A'}\right) \tag{1.9}$$

where the quantum yield ϕ_AB can be extracted as the slope of a pseudo-linear relation.

A direct consequence of the overlapping absorption bands of species A and B in the UV-range is that the conversion to the photoproduct usually converges non-quantitatively during the photocyclization reaction and a photostationary state (PSS) is reached. This can be explained by consulting Equation (1.5) and the fact that $\dot{c}_A = 0$ at $t = \infty$ and results in the expression

$$\frac{c_A^\infty}{c_B^\infty} = \frac{\phi_{BA} \cdot \varepsilon_B}{\phi_{AB} \cdot \varepsilon_A} \tag{1.10}$$

that directly determines the composition at the PSS through the ratio of $\phi_{BA} \cdot \varepsilon_B$ and $\phi_{AB} \cdot \varepsilon_A$.

As can be expected, ample research has been devoted to unveil the structure-property relationships governing the photochemical efficiency in DAEs and some general design guidelines have been established. A universal approach to increase the ring-opening quantum yield is, for instance, the inverse attachment of the aryl moiety to the bridging unit (Scheme 1-8).[107–109]

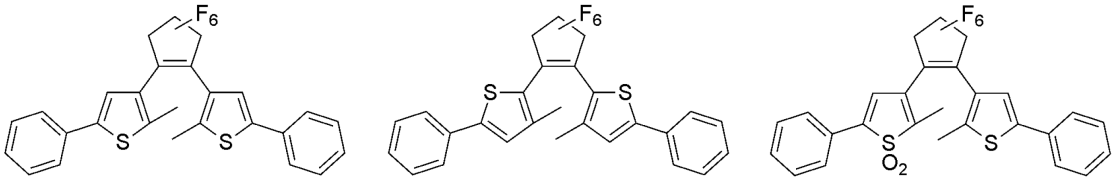

Scheme 1-8: Comparison of the photocyclization and cycloreversion quantum yields of normal, inverse, and oxidized type DAEs.

The enhancement of the cycloreversion quantum yield ϕ_{co} is quite remarkable as it comprises typically more than a whole order of magnitude. However, for this advantage these inverse type DAEs sacrifice the beneficial spectral separation of ring-open and -closed isomers and a high photocyclization quantum yield ϕ_{oc}, and are thus considered not the best choice for photoreversible DAEs.[110] Contrarily to the inverse type architecture, ϕ_{co} can be diminished by two orders of magnitude *via* oxidation of one thienyl residue while retaining the spectral separation of ring-open and -closed form (Scheme 1-8).[111] This can be attributed to the oxidized type DAEs' strong fluorescent decay pathway from the excited state in the ring-closed form inhibiting effective cycloreversion. In addition, it was only recently shown that

the cycloreversion quantum yield can be significantly enhanced by photoinduced oxidation of the ring-closed isomer in an electrocatalytic process.[34,112]

Despite the fact that the cycloreversion quantum yield can be tuned by adhering to some general molecular design principles, the role of the photocyclization quantum yield is usually regarded as more important since the default state of DAEs is the ring-open form. The most common approach to improve ϕ_{oc} is to bias the ground state dynamic conformational equilibrium of the ring-open DAE between the parallel (p) and anti-parallel (a-p) form. According to the Woodward-Hoffman rules the electrocyclization of a 6π-electron system can only take place in a conrotatory manner from the excited state (Scheme 1-9).[113] As the photoactive a-p form and the photoinactive p form are constantly equilibrating at ambient conditions because the rotational barrier is small, the a-p conformer is generally populated to about 50%. Consequently, the highest possible photocyclization quantum yield that can be achieved with an unbiased system is 0.50.

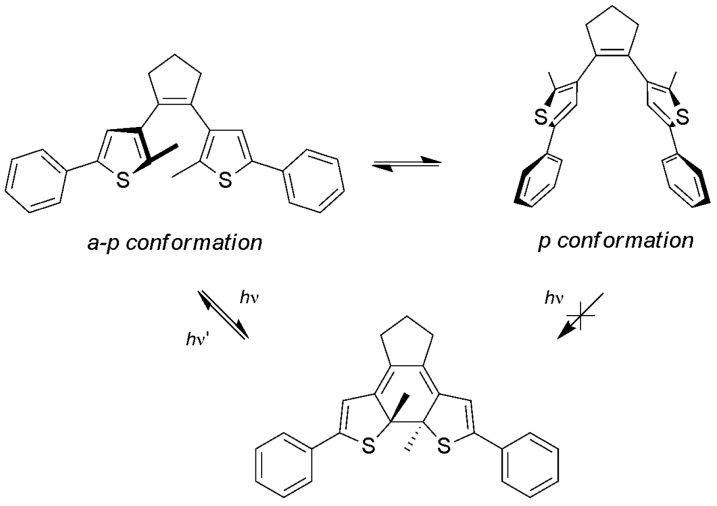

Scheme 1-9: Dynamic equilibrium between the p and a-p form with subsequent photocyclization from the a-p conformer only.

Efforts have been undertaken to bias this conformational equilibrium towards the side of the a-p conformer ranging from the incorporation of a DAE in a polymer backbone,[114] sterically crowding the aryl substituents,[115–119] locking the a-p form by attaching covalent bridges,[120–122] physical separation of the a-p conformer,[123] over incorporation into films or single crystals,[10,124,125] to intramolecular non-covalent interactions.[59,83] Amongst these efforts, two examples are especially remarkable: Firstly, Kawai and coworkers synthesized a dithiazolylarylene that locks the ring-open DAE in the a-p form through intramolecular

hydrogen bond as well as attractive S–N interactions (Scheme 1-10a).[84] By thorough photokinetic measurements it was confirmed that the photocyclization amounts to a quantum yield of 0.98 for this derivative, essentially enabling a photon-quantitative reaction. However, the intramolecular interactions are weakened in polar and in protic solvents rendering the system not universally applicable. In 2012 we reported on a system that addresses this disadvantage by employing steric repulsion of substituents incorporated in the bridge moiety as a design principle to improve the quantum yield of dithienylethenes from the unbiased 0.50 up to 0.83 (Scheme 1-10b).[88] As the modification of the bridge moiety is the only prerequisite for the improvement and the synthetic route remains straightforward and modifiable, this approach remains as one of the few general molecular design guidelines towards enhanced photo-performance of DAEs.

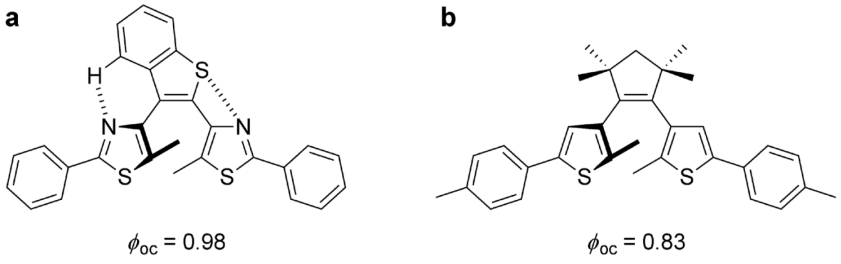

Scheme 1-10: Attempts to bias the conformational equilibrium of DAEs in the ring-open form. a) Dithiazolylarylene investigated by Kawai and coworkers, b) Tetramethylcyclopentene derivative designed by Hecht and coworkers.

Regardless of the success that has been accomplished improving DAE switching efficiency, there is still huge demand for more generally applicable design principles. It has become clear over iterations of DAE improvements that the increased population of the a-p conformer is not the sole solution towards a higher photocyclization quantum yield and that other factors, such as C–C bond distance of the reacting carbon atoms or electronic effects contribute significantly. These latter two factors, however, cannot be rationalized as easily as the equilibration of the conformers.

1.4 Photoswitchable Stoichiometric Reactions

1.4.1 General Aspects

In order to design photoswitchable systems that are capable of controlling ground-state, *i.e.* thermal chemical reactions, photochromic 'gates' (introduced in Chapter 1.2) have to be incorporated into the system in a manner that the structural differences between their two switching states are translated into different chemical reactivity. Therefore, one has to optimize the intrinsic switching properties of the photochrome itself as well as the way it is intersecting with the chemical reaction to be gated. To translate molecular changes during the course of photoswitching into differences in reactivity, the photochrome should undergo significant geometrical or electronic changes. Large geometrical changes are typically achieved via *E*-*Z*-photoisomerization reactions of azobenzene (or stilbenes), leading to largely reduced distances between the phenyl termini in the bent, non-planar *Z*-configuration when compared to the extended, planar *E*-configuration. Complementary to the systems with large geometrical changes, the electrocyclic ring-closing/ring-opening reactions of 1,3,5-hexatriene systems, for example in DAEs, result in substantially different electronic properties of the ring-closed isomer as compared to the ring-open form. Most notably the double bonds relocate during the switching process – a characteristic that has been exploited in the literature[71,126–129] and will be used as well in Chapter 2.1. It is important to maintain the switching behavior throughout the reaction and therefore the excitation of the photochromic moiety should be selective and local, without interfering quenching processes by energy or electron transfer.

The photochromic gate can be incorporated either directly by covalent connection to one of the components participating in the reaction, or indirectly by non-covalent interaction with the same. This chapter will focus on the former as covalent constructs offer the advantage that they operate more independently of concentration as opposed to supramolecular approaches. For an overview regarding the non-covalent interactions of switches on reactivity-controlling entities the reader is referred to the existing literature.[130] In general, the coupling of a photochromic system to gate another thermal reaction can be realized using various concepts depending on the particular geometrical or electronic alteration of the switch and the point of interference. Such interference can occur either at the level of the substrate, product, or template, leading to stoichiometric processes with maximum overall quantum yields of unity ($\phi \leq 1$). When these changes occur at the level of the catalyst

or effector, a rise in amplification of the light stimulus and overall reaction quantum yields exceeding unity ($\phi > 1$) can be seen. This chapter focusses on the former, as light controlled catalysts have been reviewed in the literature extensively.[3,5,130]

The introduction of light as a gating stimulus means enabling manipulation of one reaction component in a way that it can be switched from an unreactive state to a reactive state or vice versa. This can be achieved through three different approaches. (i) Switching one of the starting materials from an inactive to an active form allows the respective compound to participate in the reaction and to form the desired product on demand (starting material control). (ii) Switching the reaction product from an active form to an inactive form removes the compound from the initial equilibrium between the reactants and thus locks the product in an unreactive state (product control). (iii) Switching neither substrate(s) nor product but a 'reaction mediator', namely a template, from an inactive to an active form and thereby controlling conversion by supramolecular complexation (template control).

1.4.2 Starting Material Control

The photoreversible activation of a starting material allowing it to participate in a chemical reaction is conceptually depicted in Figure 1-1. As opposed to photocaging, true reversibility can only be achieved if the photodynamic reaction is coupled to a dynamic thermal equilibrium, *i.e*. the starting material can be reformed thermally and subsequently deactivated by light.

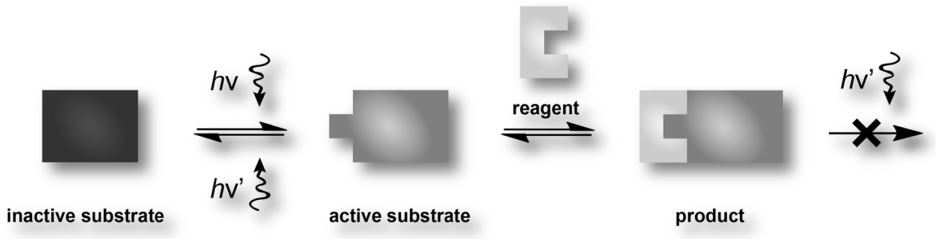

Figure 1-1: Concept of starting material control: Photoswitching a substrate between inactive and active forms allows for controlled feeding or removal of a starting material to or from a dynamic covalent equilibrium.

Kawashima and coworkers reported silicon fluoride derivatives bearing a covalently attached azobenzene ligand as early as 2001 where the photochemical *Z*- to *E*-isomerization of the azobenzene could reversibly change the complex from the pentacoordinate to the hexacoordinate geometry.[131] The group then transferred this reversible geometry change to an azobenzene-substituted allyldifluorosilane.[132] Photoisomerization of the *Z*- to the *E*-

isomer followed by subsequent treatment with 18-crown-6 and potassium fluoride induces an allyl-shift to the azobenzene reducing it to the diphenylhydrazine (Scheme 1-11). However, the original *Z*-isomer is unreactive under those reaction conditions. Further work on this system enabled photocontrol not only over the allyl-shift but also over disiloxane formation[133] and intermolecular hydrosilylation and desilylation reactions.[134] The latter is an exceptional example, as it not only allows the 'on'/'off'-switching of a reaction but offers the choice between two different reaction types.

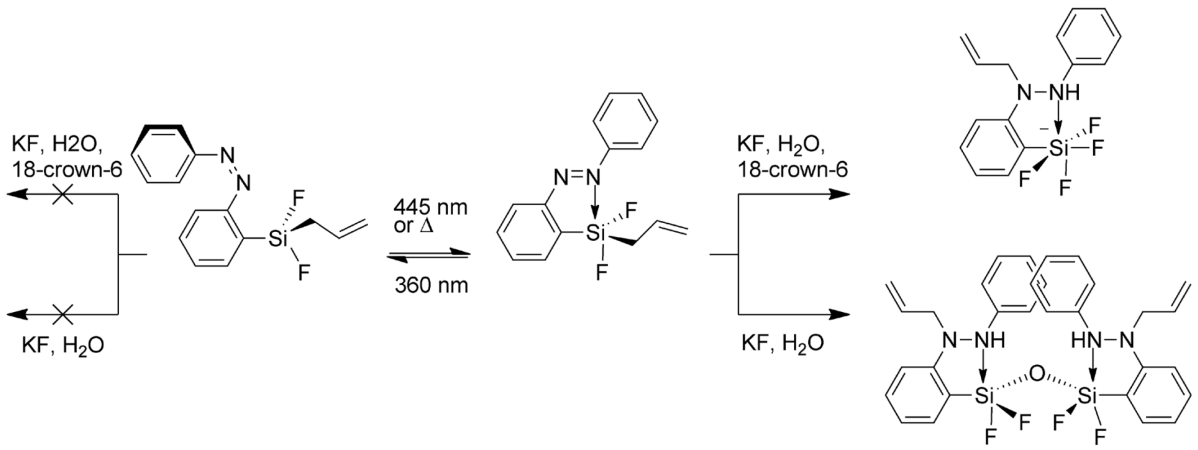

Scheme 1-11: Photocontrolled allyl transfer reaction of silyl azobenzenes with fluoride yielding hydrazine rearrangement products.

Another elaborate example of starting material control is the incorporation of an aromatic imidazolium moiety into the bridge position of a diarylethene reported by Kawai and coworkers (Scheme 1-12).[49] Due to its aromatic stabilization, the imidazolium ion is not prone to the nucleophilic addition of methoxide. However, upon photocyclization to the ring-closed form the bridge moiety is transformed into an imidazolinium ion removing the crucial double bond as well as the aromatic stabilization. The closed form switch can then react reversibly to yield the methanol adduct.

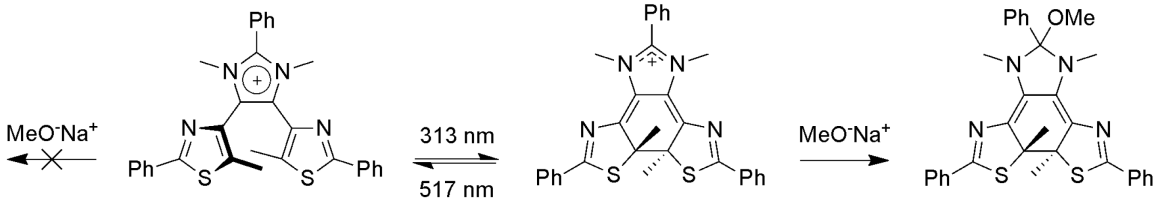

Scheme 1-12: Photocontrolled addition of methanol to imidazol(in)ium ions embedded in a diarylethene framework.

Kawai and coworkers further exploited the combination of photoswitching and aromatic stabilization in benzothienyl-substituted terarylenes.[33] The crucial methyl substituent in the 2-position of the aryl moieties was omitted on one benzothiophene and replaced by a methoxy group on the other. UV-induced photocyclization of this switch to the dihydrophenanthrene derivative enables the elimination of methanol under acidic conditions while generating the aromatically stabilized phenanthrene derivative. This system could be tuned to the point where the authors were also able to achieve photocontrol over the elimination of ethanol and reversible nucleophilic addition-elimination cascades.[76]

Photomodulation of nucleophilicity could be achieved by Branda and coworkers, who reported a diarylethene incorporating a pyridyl substituent into one aryl moiety and an electron-withdrawing pyridinium group into the other (Scheme 1-13).[28,29] In the ring-open form the two aryl moieties are not in conjugation and thus the nucleophilicity of the pyridyl-lone pair is unbiased in a reaction with *p*-bromobenzyl bromide. However, upon UV-induced photocyclization a conjugation pathway between the two aryl moieties is opened up and electron density is removed from the pyridyl-lone pair lowering its nucleophilic character and hampering the reaction with *p*-bromobenzyl bromide severely.

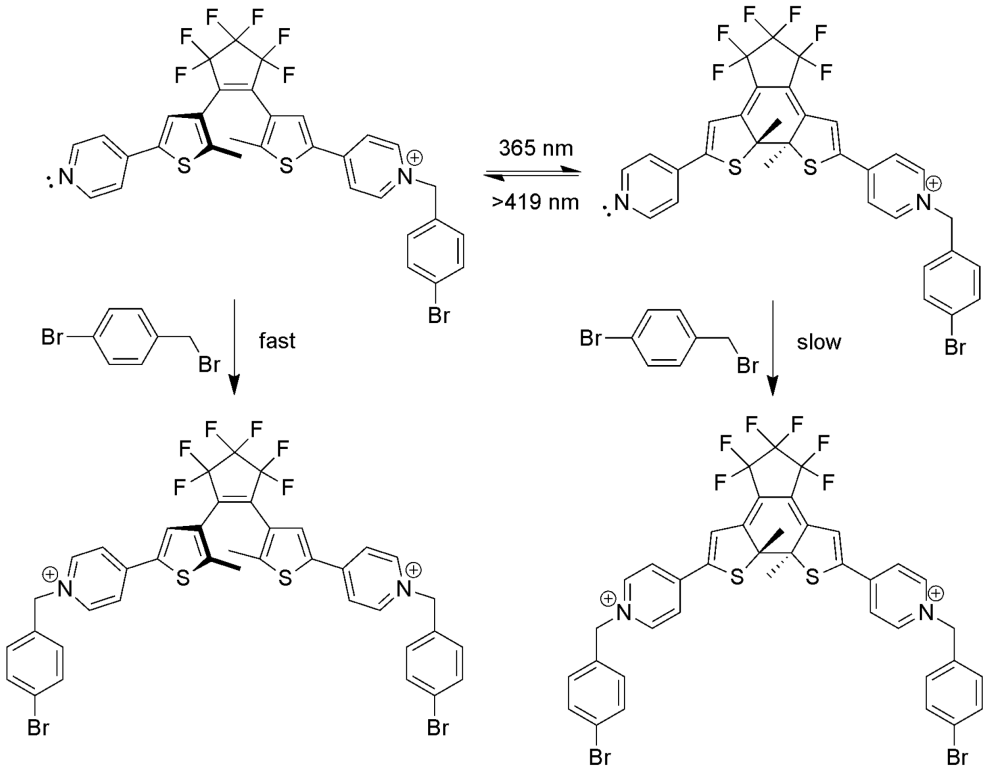

Scheme 1-13: Photomodulation of nucleophilicity by switchable coupling to an acceptor moiety through a diarylethene bridge.

In the same manner, a further example of switching on the starting materials of a chemical reaction was reported by Morimoto, Murata, and Michinobu in 2011. They synthesized a phenylacetylene-substituted dithienylethene that upon photocyclization to the ring-closed form coupled an electron-donating dimethylaminophenyl residue into the conjugated π-system of the molecule rendering the alkyne moiety reactive towards the addition of tetracyanoethylene.[135]

1.4.3 Product Control

Analogously to switching on the starting materials in a covalent chemical reaction, switching of a reaction product crucially demands for the thermal reaction to be in a dynamic equilibrium. Only in this way can the reaction products be removed from the initial reaction mixture and locked in an unreactive state (Figure 1-2).

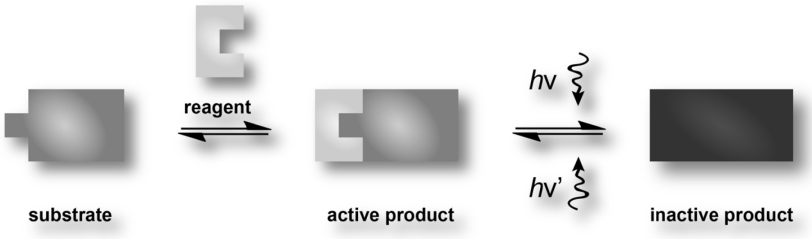

Figure 1-2: Concept of product control: Photoswitching a product to an inactive 'locked' form removes it from a dynamic covalent equilibrium, while switching it back into its active 'unleashed' form re-introduces it to the system.

Branda and coworkers synthesized a number of pro-diarylethenes incorporating a cisoid diene moiety that can undergo a Diels-Alder reaction with the corresponding dienophile. Upon adduct formation, a diarylethene 6π-electron system is generated and photocyclization can be induced by UV-light removing the diarylethene adduct from the chemical equilibrium and locking it in an unreactive state.

The first work employing this concept relied on a hexadiene motif in the bridge position of a pro-diarylethene that could undergo the Diels-Alder reaction with maleic anhydride to yield the target photochrome.[126] Since the equilibrium was shifted to the product side, this system proved to be especially useful for gating photochromism through chemical reactivity. However, the potential of the overall concept was quickly recognized and a publication followed that advanced the bridge motif of a pro-diarylethene to the

photochromically more advantageous fulvenyl moiety.[127] Reaction of this pro-photochrome with dicyanofumarate yielded the respective diarylethene that could undergo photocyclization locking it in its unreactive state (Scheme 1-14).

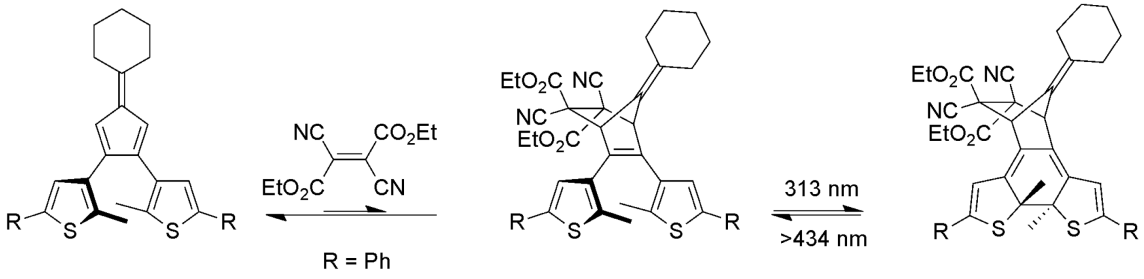

Scheme 1-14: Photoswitching locks the Diels-Alder adduct and removes it from the dynamic equilibrium.

However, the equilibrium between diene and dienophile was lying strongly on the starting materials side at room temperature. This allows exploitation of the design for photo-release of the dicyanofumarate from the pure locked Diels-Alder adduct, which was isolated beforehand. Only recently the scope was expanded by incorporating a furyl moiety in the bridge position as the diene in another pro-dithienylethene enabling the use of maleimide derivatives as dienophiles (Scheme 1-15).[71] Since the furan-maleimide couple exists in a highly reversible regime under ambient conditions, the system could be exploited far beyond the simple photorelease adding new potential applications for the light controlled adduct-locking in materials sciences and biological environments. Consequentially, the motif was exploited to design an elaborate photoswitchable adhesive relying on the switching 'on' of the retro Diels-Alder reaction.[129]

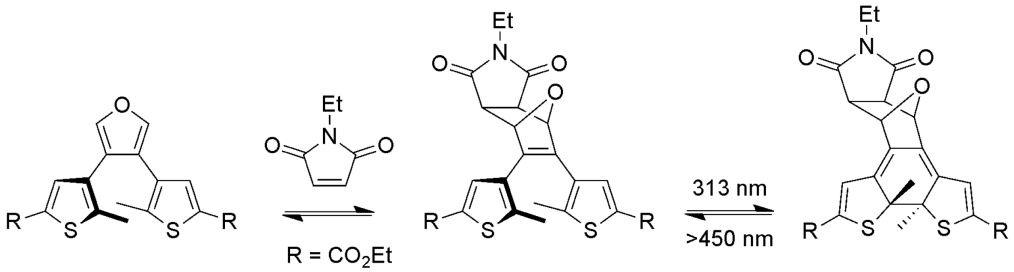

Scheme 1-15: Photoswitching locks the Diels-Alder adduct and removes it from the dynamic equilibrium.

Note that the concept to control the Diels-Alder reaction *via* the adduct exclusively significantly differs from our efforts to introduce photocontrol over starting materials *as well as* products of the Diels-Alder reaction outlined in Chapter 2.1.

1.4.4 Template Control

Substrate switching offers convenient possibilities of enabling or disabling a chemical reaction. However, since the photoswitchable unit has to be incorporated into one of the reaction partners, its inherent disadvantage lies in the lack of flexibility in choosing the substrates. Template switching addresses this issue by outsourcing the photocontrollable unit from the substrate to an external molecule that pre-arranges the reactive centers of the starting materials so that a previously inhibited reaction can take place (Figure 1-3).

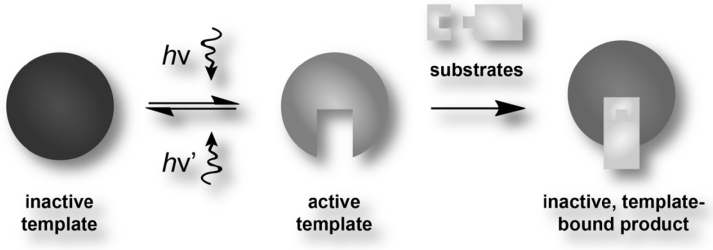

Figure 1-3: Concept of template control: Photoswitching a template between inactive and active forms allows for conversion control of starting materials to products.

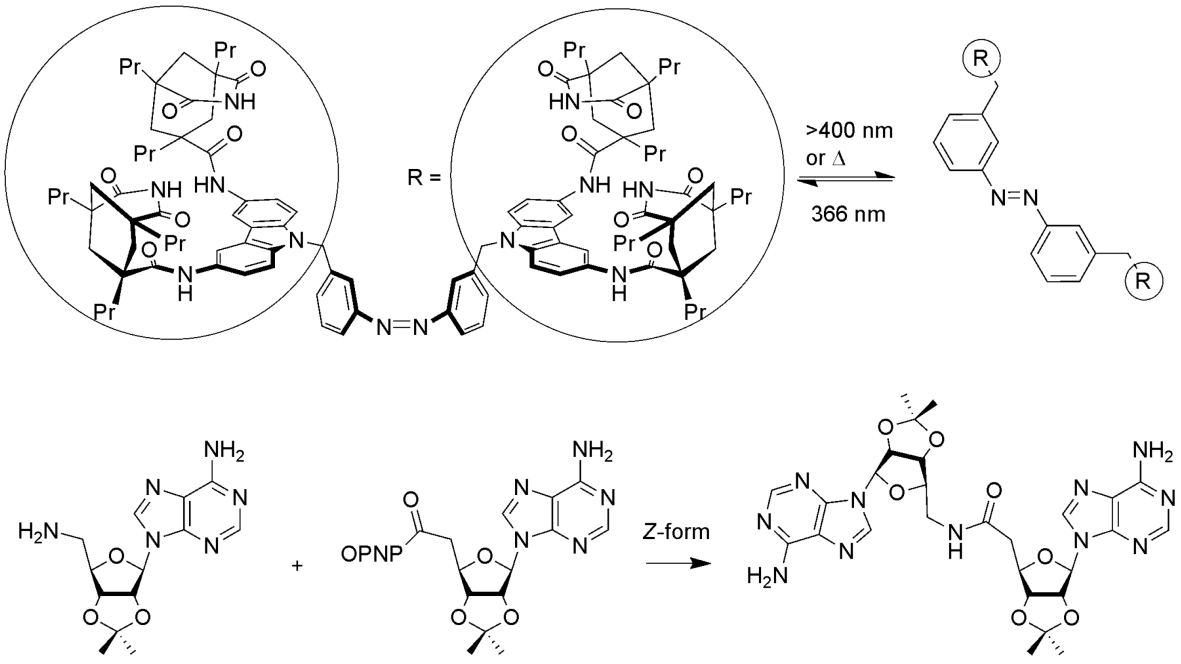

Scheme 1-16: Photoswitchable template, which in its *Z*-form enables the coupling of an amine and an activated acid to the corresponding amide.

The first photoswitchable template was synthesized as early as 1995 by Würthner and Rebek.[136] They designed a complex biscarbazolylimide terminated azobenzene (Scheme

1-16). In the *E*-form this template is inactive and shows no conversion in the coupling reaction between aminoadenosine and a *p*-nitrophenyl ester to the corresponding amide, whereas upon UV-induced isomerization to the *Z*-form the formed cavity acts as an ideal host to promote the coupling reaction. However, the coupling product remains bound to the host upon bond formation, thereby not completely fulfilling the ambitious task of designing a photoswitchable catalyst. The authors later showed that product inhibition as well as inhibition by competitive binders are observed during the reaction and neither photochemical nor thermal *Z*- to *E*-isomerization could be induced into the host while being bound to the coupled product.[137]

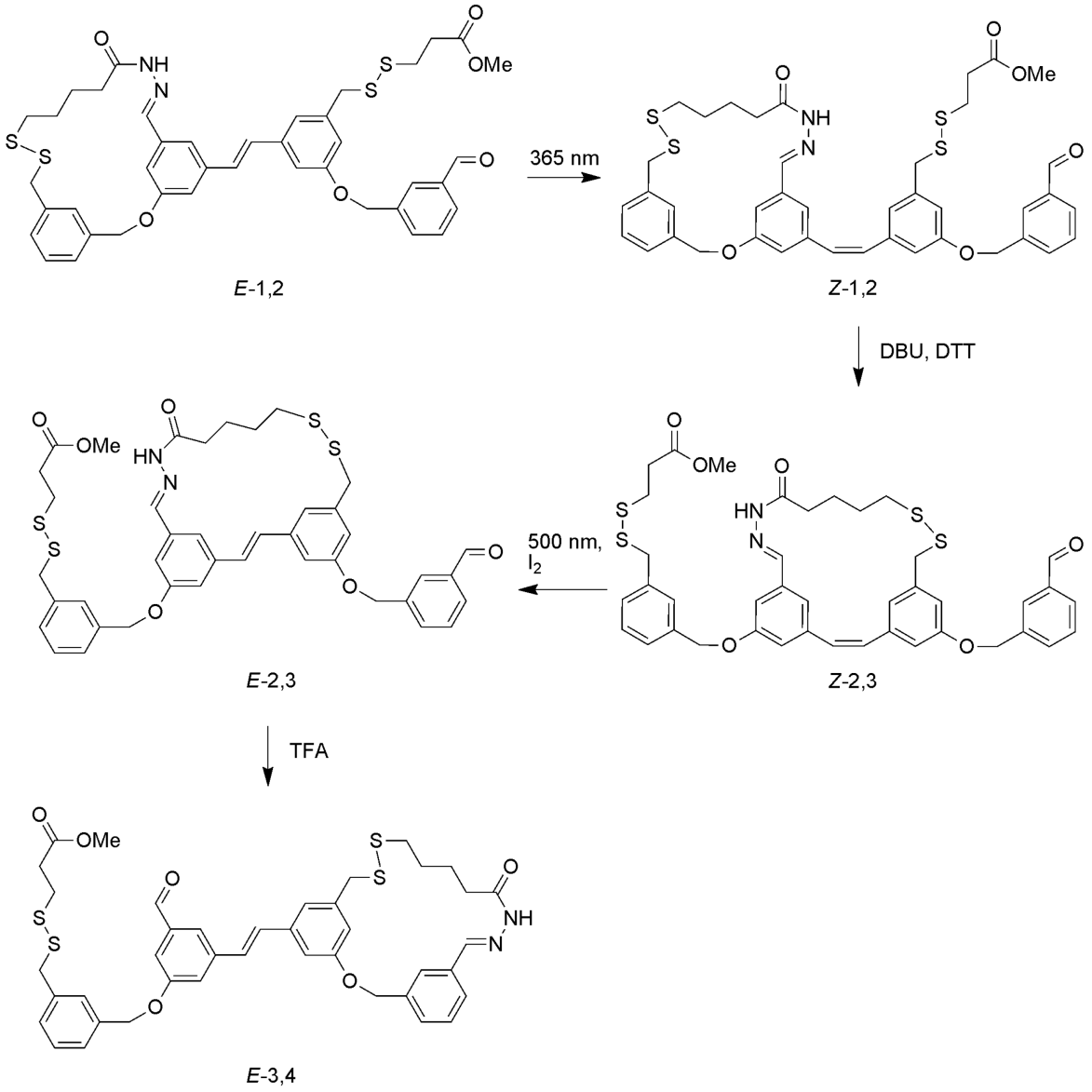

Scheme 1-17: In a molecular walker-track conjugate, a photoswitchable stilbene moiety in the track guides the walker along the track by biasing the individual dynamic covalent equilibria for disulfide and hydrazone formation.

Switching of the template can, in a broader sense, also be achieved by manipulating the track of a molecular walker by light.[138] Leigh and coworkers synthesized a walker-track conjugate offering different possibilities for hydrazone and disulfide binding (Scheme 1-17). The key step in the movement of the walker is the isomerization of the stilbene moiety incorporated into the center of the track. Upon UV-induced isomerization from *E*-1,2 to *Z*-1,2 the equilibrium between disulfide formation on the first position and the third position is highly biased toward the latter position and the walker moves along the track to form *Z*-2,3. Subsequent vis-light induced back isomerization from *Z*-2,3 to *E*-2,3 shifts the equilibrium between the hydrazone formation on the second and fourth position towards the fourth position to form *E*-3,4. Overall, the walker was moved successfully along the track by dynamically breaking and forming covalent bonds and biasing the associated equilibria by photoisomerization.

Besides directly switching the template 'on' or 'off', the assembly of the template itself can be dynamic and controlled by light (Figure 1-4). As opposed to the switching of a stable and inert template molecule, the formation of the template itself can be rendered photoswitchable by coupling the template-assembly to dynamic covalent chemistry. Typically, a dynamic combinatorial library consists of a large number of equilibrated host structures, derived from a quantity of building blocks connected via reversible covalent bonds, and the equilibria present in the library can be biased towards one or a few particular structures by stabilizing non-covalent interactions with a certain guest molecule, thereby leading to a selection and amplification of the best binder. If one of the building blocks of the library consists of a photochrome, one should be able to modulate the initial composition of the unbiased library and therefore also the selection and amplification process by light.

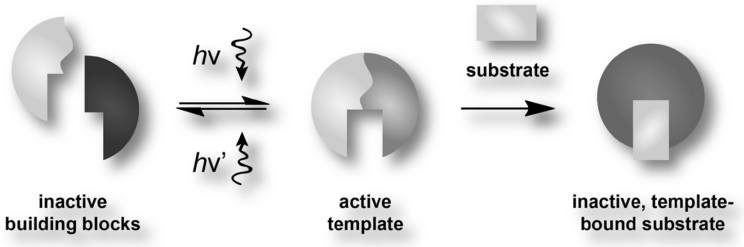

Figure 1-4: Concept of dynamic template control: Photoswitching a building block of a dynamic constitutional library between reactive and non-reactive forms allows for the assembly of an active template, which facilitates the conversion of starting materials to products.

Such a system has been described by Waters and Ingerman, who employed a dynamic constitutional library consisting of one azobenzene and two proline building blocks (Scheme 1-18).[139] The library was equilibrated in the presence of an oligoproline guest and yielded a distinct distribution of host molecules. However, upon UV-induced isomerization of the building blocks from the *E*-form to the *Z*-form the distribution amongst the possible macrocycles changed significantly, therefore amplifying one macrocycle by more than 60%. This shows that in addition to switching the template 'on' or 'off', it is also possible to switch between different receptor states.

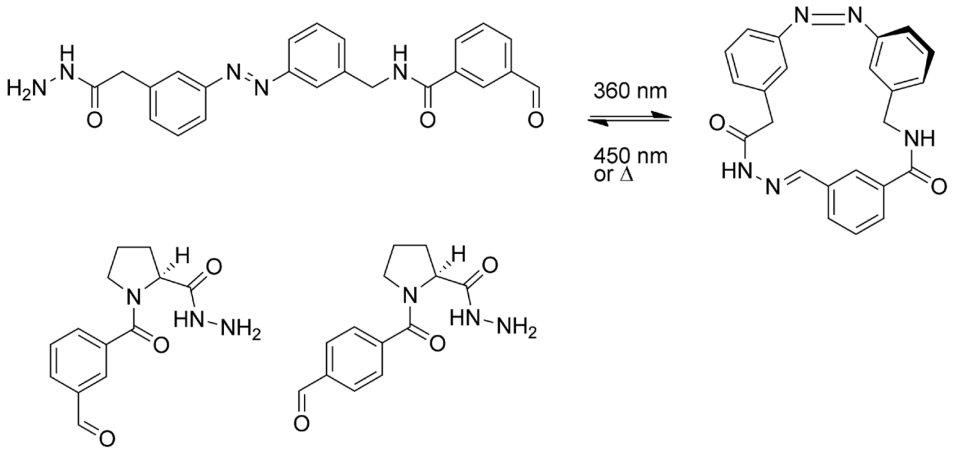

Scheme 1-18: Photoswitching the composition of a dynamic constitutional library by incorporating a photochromic building block leads to a change of the host distribution in the presence of an oligoproline guest.

The photoswitching of stoichiometric reactions remains a comparably young and unexplored field. As it becomes necessary to control increasingly complex reactions on a continuously shrinking scale, advancements in this field are of high importance and relevance for the proceeding of nanosciences and -technology.[3,140] However, a few intrinsic difficulties still have to be overcome by future reaction systems to raise it beyond the level of pure academic interest.

Most studies, for example, are performed with isolated (*i.e. ex situ* switched) molecules and thus produce effects of magnitudes, perhaps unachievable while switching the molecules *in situ*. This problem originates mainly from the large discrepancy of concentrations at which chemical reactions take place, namely in the molar to millimolar range, and the concentrations at which the overall optical density of the system is low enough to perform clean and fast photochemistry, *i.e.* the micromolar range. Marrying these two worlds has been a challenge since the beginning of photochemistry and requires careful

engineering of the employed reactants' absorption characteristics to avoid low conversions at the PSS or total absorption preventing light to reach and therefore 'switch' all molecules inside the solution. Furthermore, organic photochromes are prone to degradation and might perhaps always fall behind their inorganic counterparts with regards to photostability. Here, the inherent advantage of organic chemistry, the modularity in synthesis regarding structure-property relationship, will have to be exploited to design and engineer organic molecules that circumvent or compensate their intrinsic weaknesses in novel and unexpected ways.

It thus becomes clear that there lies a tremendous amount of work ahead until the control over chemical reactivity will leave the safe confines of academic research. Although only a glimpse of the possibilities of what these techniques could yield has been seen, the potential of amalgamating reversible photochemistry and traditional chemical reactivity promise very interesting research for decades to come.

1.5 The Diels-Alder Reaction with Furan

1.5.1 General Aspects

The mechanism and enormous potential of the reversible [4+2] cycloaddition of an electron-rich diene and an electron-poor dienophile was first realized at the beginning of the 20th century by Otto Diels and Kurt Alder and is since then widely known as the Diels-Alder (DA) reaction (Scheme 1-19).[141]

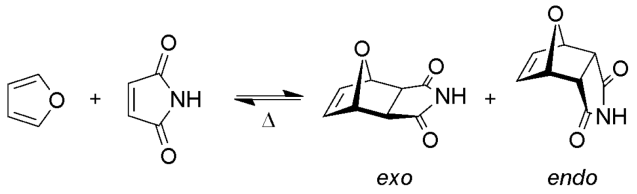

Scheme 1-19: Diels-Alder reaction between furan and maleimide.

Since its discovery, the DA reaction has evolved into one of the most powerful synthetic protocols in the organic chemist's toolbox for the assembly of complex six-membered ring-systems.[142,143] The reaction of an annulated diene usually yields a mixture of the *endo* and *exo* addition products with the *exo* product being the sterically less strained and thus thermodynamically more stable isomer. However, in many cases the *endo* isomer is preferably formed due to kinetic control – a phenomenon widely known as the '*endo*-rule'. Furthermore, Lewis acid- and salt-catalyzed and homo-DA reactions (in which the diene is not conjugated) are literature-known today and applied widely.[144,145] The back reaction is called the retro DA reaction and can be induced by applying high temperatures, though this pathway is usually unwanted in the course of a reaction leading to C–C bond formation.

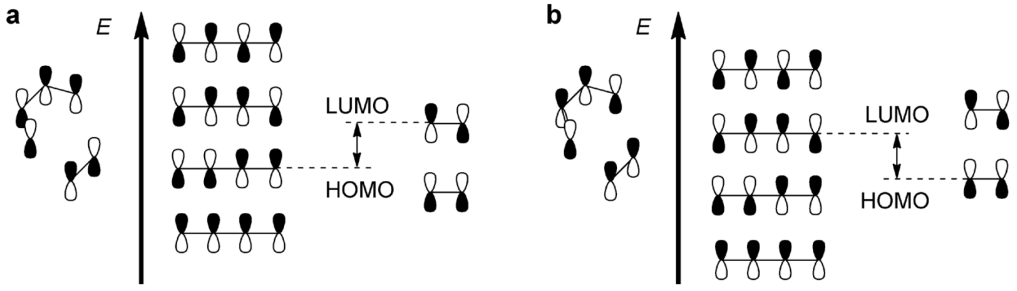

Figure 1-5: Qualitative frontier orbital energy diagram of the DA reaction. a) Normal case, b) inverse case.

A prerequisite for the DA reaction is a sufficient overlap of orbitals between the reacting diene and the dienophile that can be explained by consulting the frontier molecular orbital theory

(Figure 1-5). To permit a high orbital overlap and thus a high DA reactivity, diene and dienophile must exhibit orthogonal electronic character, *i.e.* the diene's HOMO has to be electron-rich and the dienophile's LUMO electron-poor (normal case) or *vice versa* (inverse case).

Furan is one of the most popular diene building blocks employed in synthetic DA reactions[146] as its aromatic character is pronounced enough to be stable at ambient conditions allowing for the introduction of substituents but low enough that its double bonds exhibit a high degree of localization necessary for the orbital overlap with the dienophile (Scheme 1-20). Moreover, the resulting oxanorbonene adducts can be aromatized easily by acid induced ring-opening enabling for the easy construction of aromatic systems subsequent to the DA reaction (Scheme 1-21).[146]

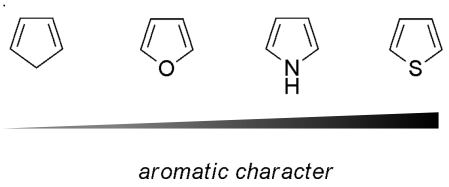

Scheme 1-20: Aromatic character of five-membered (hetero-)cycles.

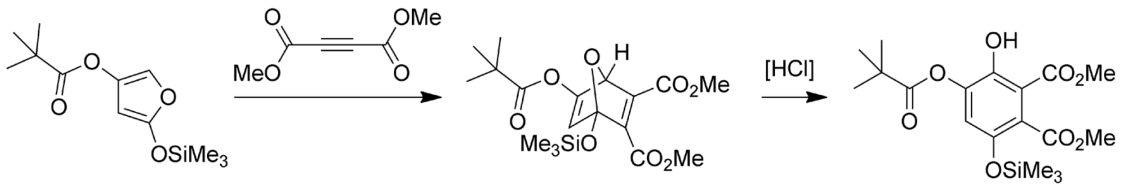

Scheme 1-21: Synthetic application of furan to build six-membered, aromatic carbocycles.

Beyond its mere use as a synthetic auxiliary, furan proves to be a versatile and powerful diene for diverse applications of the DA reaction, particularly in the field of reversibly crosslinkable polymers with maleimide[147–150] and the reversible covalent functionalization of sp^2-carbon,[151] both of which are elucidated in later sections.

1.5.2 The Furan-Maleimide Couple

As the DA reaction is a bimolecular reaction, a dienophile with a compatible reactivity towards furan is desirable. Maleimide has been established as a very popular partner to furan already decades ago[152] as their characteristic reaction temperatures lie between 25 °C and 50 °C for the forward reaction and above 70 °C to 100 °C for the retro DA reaction to occur.

This renders the furan-maleimide couple one of the few self-containing (*i.e.* by-product free) systems that exhibit fully dynamic covalent properties at relatively mild conditions. In addition to the complete reversibility, maleimide and furan can be easily functionalized and thus their incorporation as practical linker units into larger chemical entities is effortlessly achieved. While maleimides are generally substituted at the *N*-terminus by condensation of maleic anhydride with functionalized amines, furan can be modified simply by employing one of its low cost commercial precursors, such as furfural, furfuryl alcohol, or 2,5-dimethylfuran. As a direct consequence the furan-maleimide couple is employed in a vast amount of reversible crosslinkable polymeric materials to impart self-healing properties.[147–150] It is used in reversible interpenetrating hybrid networks[153] and thermally responsive dendrons and dendrimers,[154,155] as well as for reversible, modular printing and lithography.[156,157]

Despite this ostensibly simple reactant system, a closer look at the DA reaction between furan and maleimide reveals important details. To begin with and as already touched on in Scheme 1-19, this reaction yields two different stereoisomers, *endo* and *exo*. Scheme 1-22 briefly summarizes the underlying equilibria with the corresponding reaction rate constants for forward k^f and backward reaction k^b to the respective stereoisomers.

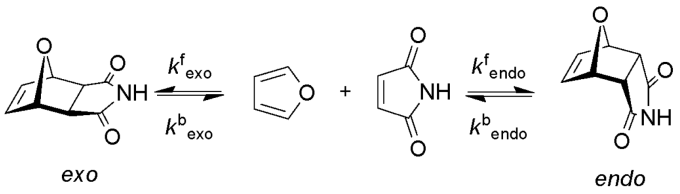

Scheme 1-22: Itemized equilibria leading to the *endo* or *exo* adduct in the course of a DA reaction between furan and maleimide.

Kinetic ^{1}H-NMR experiments have been carried out on this system to gain an insight into the driving force governing the outcome of this particular DA equilibrium. This offers the possibility to derive a potential energy diagram out of the data reported in the literature.[158] At room temperature it was shown that with

$$2k^f_{exo} = k^f_{endo} \tag{1.11}$$

the rate constant for the formation of the *endo* stereoisomer is about twice the magnitude of the rate constant for the formation of the *exo* stereoisomer. Taking into account the dimension of the back reactions of both isomers it became clear that with

$$\frac{k^{\mathrm{f}}_{\mathrm{exo}}}{k^{\mathrm{b}}_{\mathrm{exo}}} > \frac{k^{\mathrm{f}}_{\mathrm{endo}}}{k^{\mathrm{b}}_{\mathrm{endo}}} \tag{1.12}$$

at room temperature the formation of the *exo* isomer is slightly thermodynamically favored but that the formation of the *endo* isomer is considerably faster. When this experiment is repeated at 65 °C it becomes clear that with

$$k^{\mathrm{f}}_{\mathrm{exo}} = k^{\mathrm{f}}_{\mathrm{endo}} \tag{1.13}$$

the rate constants for the formation of both isomers are of comparable magnitude. However, as $k^{\mathrm{b}}_{\mathrm{endo}}$ grows extraordinarily as compared to $k^{\mathrm{b}}_{\mathrm{exo}}$, the formation of the *exo* isomer becomes thermodynamically extremely predominant since

$$\frac{k^{\mathrm{f}}_{\mathrm{exo}}}{k^{\mathrm{b}}_{\mathrm{exo}}} >> \frac{k^{\mathrm{f}}_{\mathrm{endo}}}{k^{\mathrm{b}}_{\mathrm{endo}}} \tag{1.14}$$

Out of these data a qualitative potential energy diagram for the DA reaction between furan and maleimide can be derived (Figure 1-6).

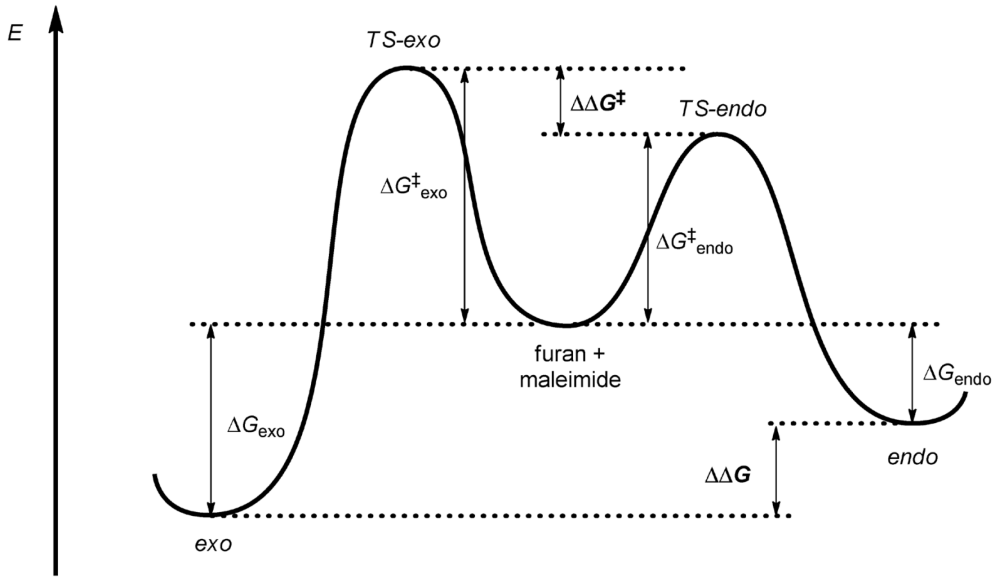

Figure 1-6: Qualitative potential energy diagram of the DA reaction of furan with maleimide.

It is obvious that when the reaction temperature is low, the difference in both transition states' Gibbs free energies $\Delta\Delta G^{\ddagger}$ is the governing quantity, the reaction is under kinetic control, and the *endo* stereoisomer is the preferred product. Contrarily, if the reaction temperature is high, both transition states are accessible and hence the difference in ground state Gibbs free

energies $\Delta\Delta G$ is the prevalent factor, the reaction is under thermodynamic control, and the *exo* stereoisomer is the main product.

Moreover, the ratio between *exo* and *endo* adducts can be biased by attaching Substituents with different electronic properties (Scheme 1-23).[159] While the *N*-terminal functionalization of maleimide seems to have little to no effect on the stereoselectivity, the introduction of electron-withdrawing substituents in the 2- or 3-positions of the furan lowers the Gibbs free energy of the *exo* transition state $\Delta G^{\ddagger}_{exo}$ more significantly than $\Delta G^{\ddagger}_{endo}$. Whereas electron-donating substituents appear to favor the *endo* adduct as the main product with a low $\Delta G^{\ddagger}_{endo}$ (at low temperatures), residues exhibiting large electron-withdrawing properties tend to prefer the *exo* stereoisomer even under kinetically controlled conditions.

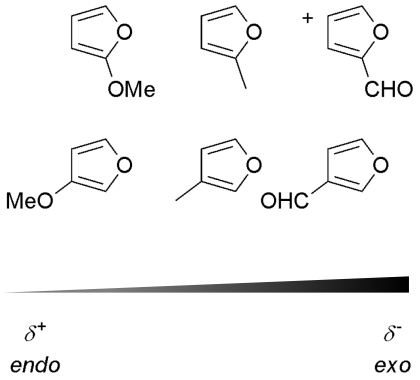

Scheme 1-23: Influence of the substituent's electron-withdrawing effect on the stereodiscrimination in the DA reaction between furan and maleimide.

It should be noted, however, that these data are specifically valid only for furan and maleimide and that from these, no general trend for other DA reactant systems can be deduced. Nevertheless, the thorough kinetic analysis of the particular furan-maleimide couple shows that the frequently stressed *endo*-rule[160–162] assuming transition state discrimination as cause for the effective stereoselectivity should be taken with a pinch of salt when predicting *endo*-*exo*-selectivity on paper.

1.6 Maleimide Derivatives and Their Potential use in Photopharmacology

1.6.1 Principles of Photopharmacology

Photopharmacology describes the incorporation of photoswitches into drugs used in pharmacotherapy to gain control over their therapeutic properties through the application of light.[23] With this goal, photopharmacology emerged from the efforts to achieve photocontrol over structure and function of biological systems.[163,164] Today's drug administration oftentimes faces challenges associated with poor selectivity resulting in high toxicity and drug resistance, both of which have their origin in the limited spatiotemporal control offered by conventional drugs. That means that there is generally no possibility to control where and when, in- or outside the organism the drug is active. For example, most antitumor agents unselectively impair mitosis, which particularly affects the fast-dividing cells in tumors, but also causes many unwanted side effects. Also, poor drug selectivity severely narrows the therapeutic window as oftentimes the toxic side effects predominate over the drug's therapeutic value. Moreover, gratuitous drug administration based on poor selectivity contributes to the development of drug resistant strains of pathogenic agents.

As highlighted before in Chapters 1.2 and 1.4, light as a non-invasive stimulus with superior spatial, temporal, and energetic resolution in combination with its high orthogonality to biological processes would make for an excellent gate to control drug activity with higher precision. Photocontrol over drug activity can be achieved in two ways: i) irreversibly releasing or activating the drug from a prodrug by the photochemical reaction of a one-cycle photoswitch or a photoprotecting group or ii) employing a multi-cycle photoswitch that allows not only for activating the drug inside of the organism but also for its deactivation after leaving the organism and the desired therapeutic effect has been achieved. Photodynamic therapy (PTD) takes a special place in the context of photopharmacology as it relies on the triplet sensitized generation of singlet oxygen $^1O_2$ by photoexcitation.[165–170] Since the physiologically active component $^1O_2$ invokes unspecific cell death, PTD has rather low selectivity and is mainly useful where the locally resolved destruction of tissue is necessary, *e.g.* for the treatment of tumors. Also, the employed sensitizers remain active within the body for weeks complicating the patients' post-treatment phases.

The photoswitch governing the drug's activity or selectivity must certainly fulfill multiple criteria for the successful application in the organism. One key criterion is that the

drug needs to retain its biological activity and also should not be active towards secondary targets upon incorporation of the photoswitch. As modern drugs are usually highly optimized molecules, this is a major challenge for the design of novel photoswitch-drug conjugates. Since bioavailability is of importance, sufficient solubility in physiological media of the photoswitch-drug conjugate has to be guaranteed. A direct follow-up requirement is that the photochrome still maintains its switchability in the aqueous environment as well while being attached to the drug. Ideally, the compositions at the respective photostationary states in the active and inactive form should be high to achieve the best possible modulation in the drug's bioavailable concentration. Furthermore, there exists a so-called 'phototherapeutic window' in which electromagnetic radiation can penetrate tissue most efficiently, lying in the visible range of the spectrum. Due to its cytotoxic side effects as well as its low penetration depth, UV-light is generally not regarded as the best option in view of highly selective drug design incorporating photoswitches. Hence, special design considerations have to be made when choosing an appropriate photoswitch for the task.

The pioneering examples in the field of photopharmacology have been reported by the groups of Erlanger and Nachmansohn that reported on a variety of differently substituted azobenzene photoswitches that could modulate the activity of acetylcholine receptors by light-induced isomerization from the inactive *E*-form to the active *Z*-form.[171–173] However, most of the outstanding advances regarding the photoreversible switching of drugs' activities have been made only recently.

Besides Trauner and coworkers' exceptional overall work on photochromic ion channel blockers,[174–177] the reversible control over the induction of pain in organisms is a particularly outstanding example.[178] For that purpose, they designed an azobenzene bearing a moiety that resembles the scaffold of capsaicin, the active compound in chili peppers, that was able to bind to the heat and pain receptor TRPV1. While binding to TRPV1 in its *Z*-form, the photoswitch is able to antagonize the effect of simultaneously administered capsaicin. However, it can be switched to its inactive *E*-form by visible light allowing capsaicin to bind to TRPV1 again inducing a painful sensation upon irradiation (Scheme 1-24).

Trauner and coworkers furthermore synthesized a photoswitchable azopropofol that could be shown to reversibly switch GABA-induced Cl^- currents to control neural systems (Scheme 1-25).[179] While the *E*-form of the azopropofol is active just as its parent compound propofol, the *Z*-form produced by irradiation with violet light is inactive and exhibits lower

anesthetic behavior. This development is particularly important with regard to improved temporal control over anesthetically active drugs.

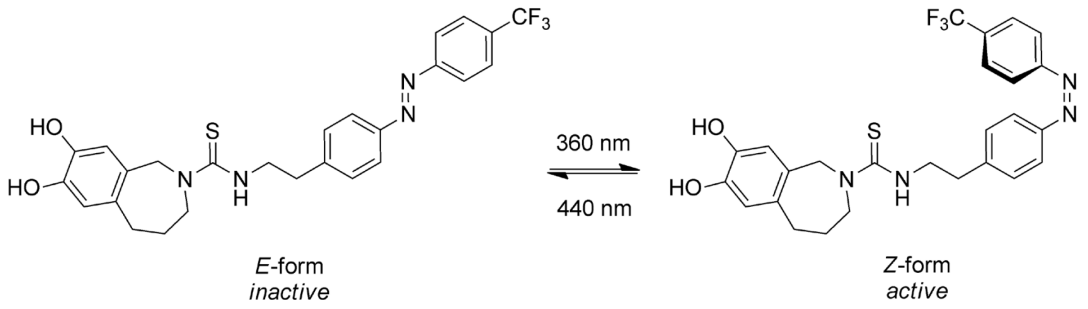

Scheme 1-24: Photoswitchable TRPV1 channel inhibitor that can be switched from its active *Z*-form to the inactive *E*-form by irradiation with blue light.

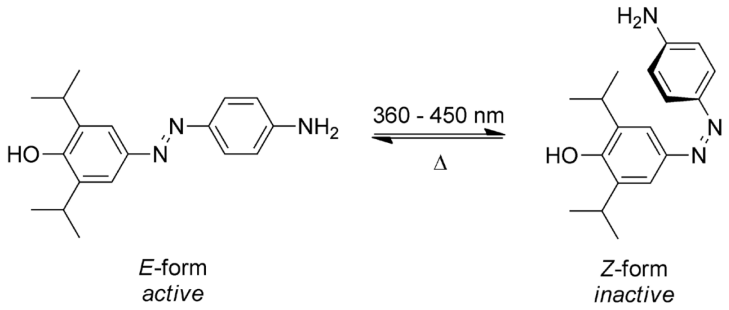

Scheme 1-25: Photoswitchable azopropofol that can be switched from its active *E*-form to the inactive *Z*-form by irradiation with violet light.

Another exceptional work incorporating an azobenzene attached to a drug motif was published only lately by Feringa and coworkers and involves the possibility to photoswitch the activity of a quinolone antibiotic.[180] By attaching an azobenzene moiety it was possible to modulate the quinolone antibiotic's antibacterial activity from high in the *E*-form to low in the *Z*-form and thus to gain spatial control over the growth of bacteria (Scheme 1-26).

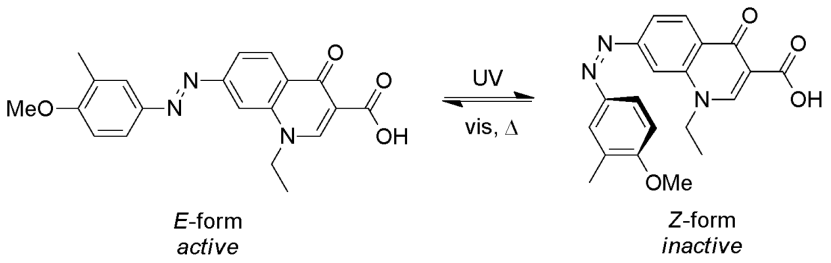

Scheme 1-26: Photoswitchable quinolone that can be switched from its active *E*-form to the inactive *Z*-form by irradiation with UV-light.

Abell and coworkers synthesized a potent photoswitchable m-calpain inhibitor, the molecular design of which is based on common peptide m-calpain and μ-calpain inhibitors.[181] The protease calpain is made responsible for multiple diseases, specifically cataract, and its activity could be successfully inhibited by the azobenzene-drug conjugate in its active *E*-form (Scheme 1-27). Isomerizing the molecule to the *Z*-form by irradiation with UV-light deactivates the m-calpain inhibiting effect thus offering some potential as a means to control cataract.

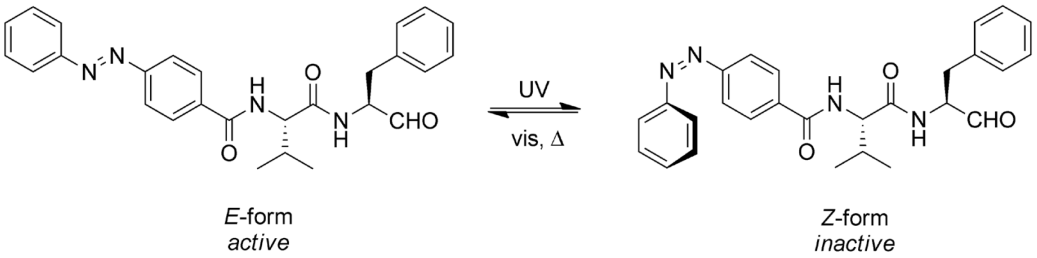

Scheme 1-27: Photoswitchable m-calpain inhibitor that can be switched from its active *E*-form to the inactive *Z*-form by irradiation with UV-light.

Though diarylethenes are less frequently used in the context of photopharmacology, as researchers prefer azobenzene's pronounced geometrical change upon photoisomerization, some notable examples have been reported that incorporate DAEs as the photoswitch. A notable case is the design of a photoswitchable human carbonic anhydrase I (hCAI) inhibitor by the groups of Branda and König.[182] This enzyme is of particular interest as it is central to cellular transport as well as metabolic processes in the organism. A histidine binding Cu iminodiacetate group was incorporated in one aryl moiety of the DAE and a hCAI inhibiting sulfonamide motif on the remaining aryl substituent (Scheme 1-28). In the ring-closed form the DAE backbone is rigid and thus retains the sulfonamide group from binding to hCAI. Upon visible light induced cycloreversion, however, the backbone becomes flexible thus enabling the inhibiting group to bind to its target.

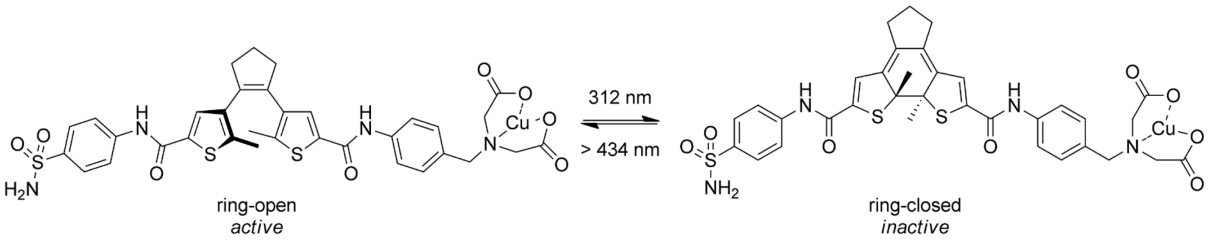

Scheme 1-28: Photoswitchable hCAI inhibitor that can be reversibly switched from its inactive ring-closed form to the active ring-open form by irradiation with blue light.

Only recently the groups of Komarov and Ulrich designed a peptidomimetic macrocycle incorporating a DAE in its backbone.[183] The Gramicidin S analogue exhibits antimicrobial activity in the ring-closed form while irradiation to the ring-open form with visible light disabled this effect. Analogously to the hCAI inhibitor reported by the groups of Branda and König, the decisive difference between the two isomers is the DAE backbone's alteration in flexibility. While the flexible backbone in the ring-open form grants more degrees of freedom allowing for spatial arrangement of the functional groups, the rigid backbone in the ring-closed form forces the molecule into a predetermined conformation.

While the molecules investigated so far generally rely on the change of geometry or modulation of conformational flexibility to achieve the desired pharmacotherapeutic effects, other variable properties, such as the change in the dipole moment or the HOMO-LUMO gap, appear harder to implement. However, this leaves lots of room for creative design that can be realized in future generations of photoresponsive drugs. Eventually, it can be seen that during the last decade the research area of photopharmacology took big steps towards *in vivo* application in humans. Though the main efforts undertaken in this field are currently accomplished by only a handful of research groups, the impact on the academic landscape is considerable. Its interdisciplinary character will provide unprecedented options for collaborations and hopefully establish photopharmacology as a force to be reckoned with in the daily clinical routine.

1.6.2 Maleimide Derivatives as Catalytic DNA Topoisomerase II Inhibitors

DNA topoisomerase II (TOP2) is an enzyme that catalyzes the interconversion of different DNA toposiomers (*e.g.* supercoiled or catenated DNA) by religation of the DNA strands thus promoting chromosome disentanglement (Figure 1-7).[184] The catalytic cycle of TOP2 action is depicted in Figure 1-8.[185] First, a gate segment of DNA ('G segment') is bound to TOP2. A second strand, the transport segment or 'T segment', is then captured by TOP2. Binding and hydrolysis of ATP then lead to the cleavage of the G segment and subsequently the T segment is transported through the G segment as the two strands separate. Finally, the G segment is sealed and release of ADP leads to the reset of the system.

Xenobiotics can act *via* different pathways upon this function leading to lethal DNA strand breaks when TOP2 action is affected.[186–188] Supposedly, many antitumor drugs and antibiotics act upon the scission and ligation reactions of TOP2 by stabilizing the so-called 'cleaved complex' of TOP2 and DNA (Figure 1-8).

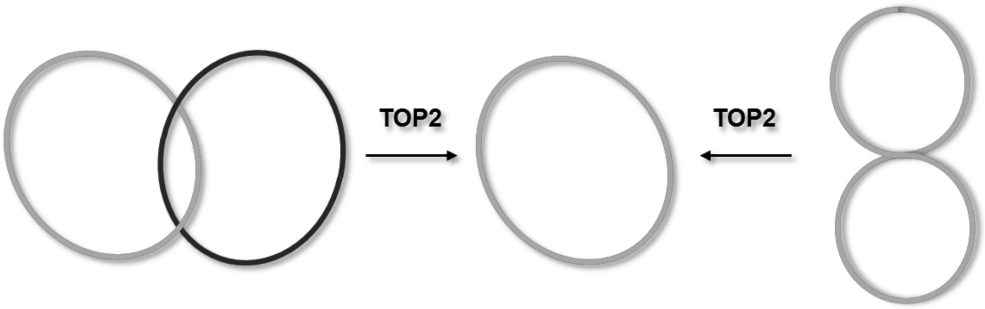

Figure 1-7: Decatenation and relaxation of DNA strands performed by TOP2.

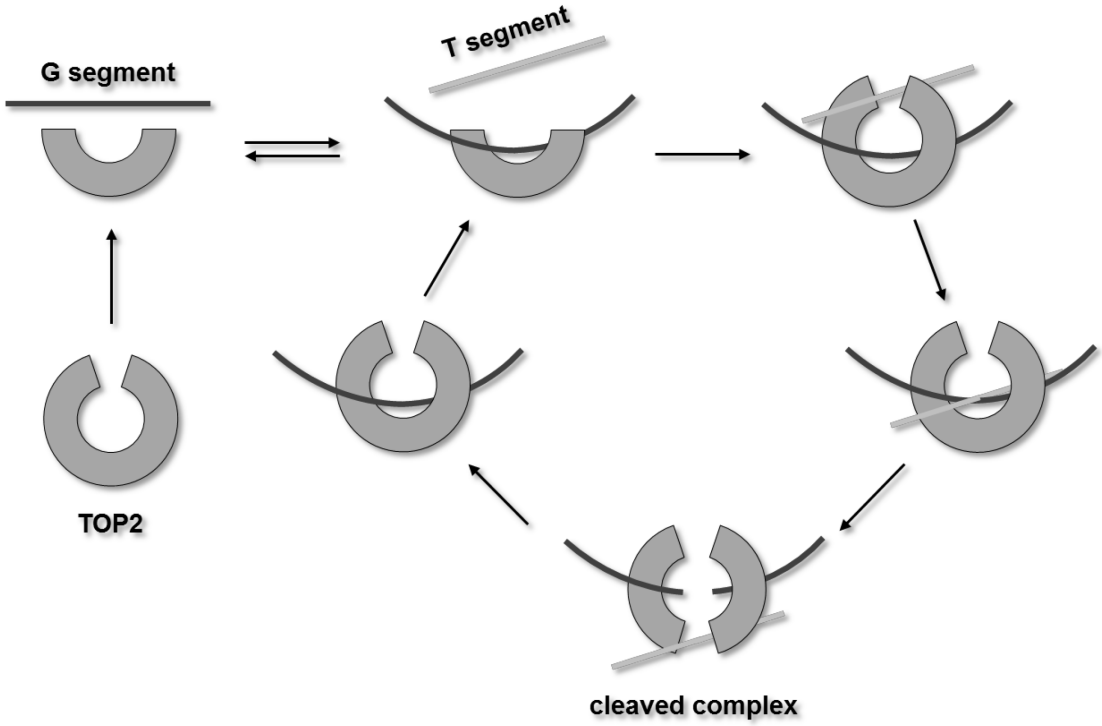

Figure 1-8: Mechanism of TOP2 action upon religation of a DNA strand (G segment) through binding and transport of a T segment.

At that stage the T segment has already passed and cleaved the G segment. However, the T segment cannot leave the complex and TOP2 is halted inhibiting enzyme turnover. This produces enzyme mediated DNA damage that interferes with many DNA metabolic events such as transcription and replication. Drugs that act upon TOP2 in this way, such as doxorubicin, daunorubicin, etoposide, mitoxantrone, and m-AMSA, are classified as TOP2 poisons (compare Scheme 1-29). As TOP2 poisons can provoke unwanted secondary malignancies or topical cell necrosis, it can be necessary to inhibit the formation of stable cleaved complexes between TOP2 and DNA alongside pharmacotherapy.[189] Compared to TOP2 poisons, catalytic TOP2 inhibitors prevent ATP hydrolysis and maintain the TOP2

structure as a closed clamp.[190–192] In this way they do not prevent religation of the G segment thus avoiding the production of loose DNA strands. Hence, this mode of inhibition supposedly leads to less toxic or lethal side effects.

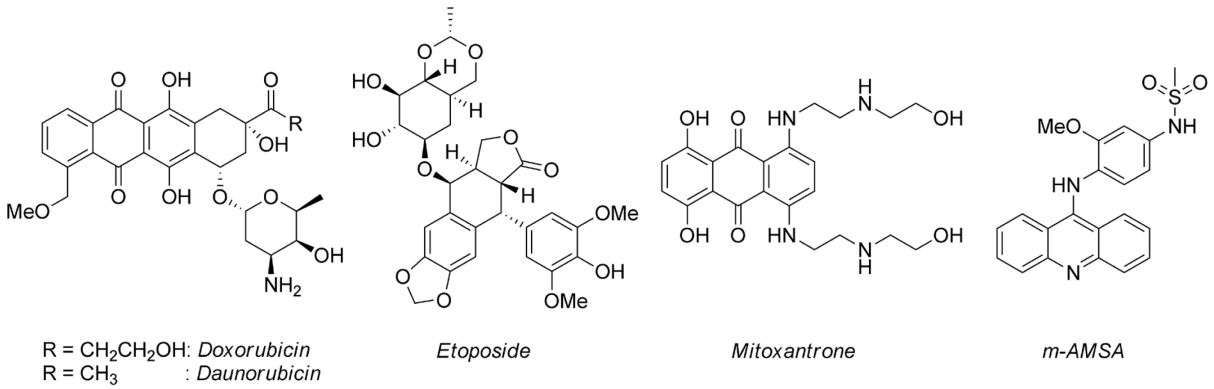

Scheme 1-29: Molecular structures of the common TOP2 poisons doxorubicin, daunorubicin, etoposide, mitoxantrone, and m-AMSA.

Recently it was proposed that maleimide, *N*-methylmaleimide, and *N*-ethylmaleimide belong to the class of catalytic TOP2 inhibitors.[193,194] When assessed as drug for TOP2 depletion, these maleimide derivatives exhibited strong TOP2 inhibiting properties with effective concentrations already showing activity in the micromolar range.[194,195] More importantly, in the same study maleimide derivatives have been shown to antagonize the toxicity caused by TOP2 poisons, such as etoposide. While individual administration of etoposide led to TOP2 depletion as expected, the simultaneous application of different maleimide derivatives antagonized the TOP2 poison's effect. Interestingly, during this simultaneous administration low concentrations of the maleimide drug did not lead to TOP2 inhibition. These results point towards an alternative inhibition mechanism different from the ones known for existing catalytic TOP2 inhibitors. As succinimide did not have an effect on the TOP2 catalytic cycle, it was reasoned that the inhibition is caused by thiol-ene-ligation (a variant of the Michael addition) of exposed thiols belonging to cysteine residues exposed by TOP2.[193,194] Chemical modification would take place before the G segment is initially captured and decrease the overall available concentration of catalytically active TOP2. In that way maleimide derivatives could antagonize the TOP2 related side effects of drugs used for the treatment of cancer *in vitro* as well as *in vivo* preventing uncontrolled DNA cleavage. This is a significant finding as the toxicity of most TOP2 poisons employed in antitumor applications is the factor that restricts their extensive clinical application.

As Michael acceptor systems are generally thought to belong to the class of reactive inhibitors because of their high alkylation potential,[196] it would be advantageous to introduce a new level of control over the activity of maleimide's ability to undergo thiol alkylation reactions. The Diels-Alder reaction with furan seems predestined for this task as it is, to the best of our knowledge, the only effective way of protecting maleimide functionalities. The DA reaction with furan masks the reactive C–C double bond and can be tuned easily to be reversible at physiological temperatures. Gaining additional control over this protecting group *via* an external stimulus, such as light, allowing for the reversible control over the drugs activity would hence be very desirable and will be discussed in detail in Chapter 2.2.

1.7 Furan for the Reversible Covalent Functionalization of Carbon Nanotubes

For a long time graphite, amorphous carbon, and diamond have been the only known major carbon allotropes and their chemistry was regarded as rather dull since elementary carbon exists in a thermodynamic valley rendering it quite unreactive. This changed extraordinarily with the discovery of fullerene, carbon nanotubes (CNTs), and graphene, all of which are modifications of sp^2-hybridized carbon atoms connected to each other, as they possess outstanding physicochemical properties and unique reactivity. Graphene can be seen as a two-dimensional sheet of sp^2-carbon atoms attached to each other in a honeycomb lattice while CNTs are best imagined as a rolled-up graphene sheet to yield a cylindrical nanostructure and fullerenes as a ball resulting from a wrapped-up graphene sheet (Scheme 1-30).[197–199]

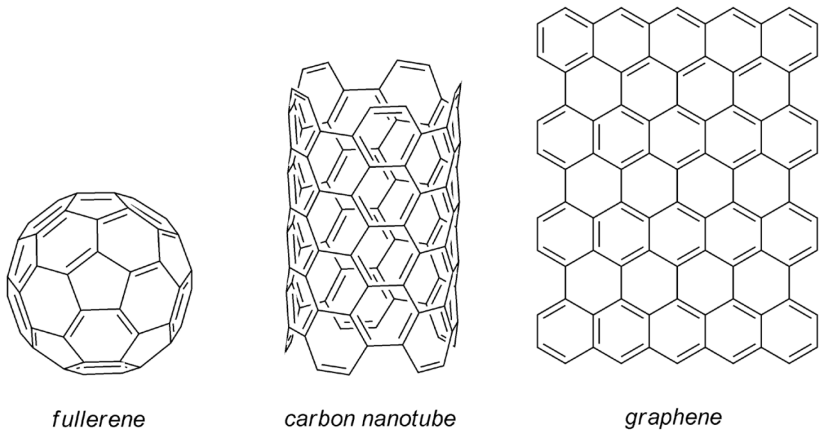

Scheme 1-30: Exemplified depictions of a fullerene (C_{60}), as well as pieces of a carbon nanotube and a graphene sheet.

CNTs demonstrate remarkable properties, such as very high tensile strength while retaining elasticity that outshines conventional materials, metallic or semiconducting electrical properties, excellent thermal conductivity, and particular photoluminescence that renders CNTs promising candidates as nanotechnology materials.[200,201] Besides the difficulties associated with the bulk synthesis of defined species, the lack of easy processability is a major factor hampering the breakthrough of CNTs for most applications on a large industrial scale. Intrinsically, CNTs are hardly soluble in common solvents and thus have to be functionalized with solubilizing groups in order to achieve a minimum degree of processability. This functionalization can also be carried out to adapt and fine-tune CNTs' optoelectronic properties or to add new functional moieties.

Functionalization of CNTs can be achieved either by the non-covalent approach, the covalent approach, or by mechanical interlocking (MINT).[202–205] Non-covalent

functionalization relies on the exploitation of weak interactions between CNT and a functional unit, such as van der Waals and π-π interactions, wrapping around, or filling of the tube. This method has the advantage that the tube's conjugated π-system remains more or less unaffected and the CNTs are easily defunctionalized as the non-covalent interactions can be generally regarded as weak. However, as non-covalent interactions tend to exhibit dynamic character at ambient conditions rendering a fixed, durable, and localized functionalization difficult, this is also the major disadvantage of this approach. Conversely, covalent functionalization relies on the formation of stable covalent bonds through esterification or amidation reactions with oxidized CNTs, radical additions, or various cycloadditions usually irreversibly disrupting the tube's skeleton. Only very recently the MINT approach was established by the group of Martín and coworkers based on the formation of rotaxane-resembling structures that interlock the tube mechanically but do not react with the sp^2-lattice.[205]

It becomes clear that a protocol is desirable that merges the advantages of covalent as well as non-covalent functionalization, *i.e.* which forms stable covalent bonds which can be cleaved on demand to regenerate the tubes' π-systems. The DA reaction fulfills these demands and besides its use for the bottom-up synthesis of defined sp^2-carbon structures, it has been successfully employed for the reversible covalent functionalization of multiwall carbon nanotubes (MWCNTs) as well as single wall carbon nanotubes (SWCNTs).[151] Sp^2-carbon allotropes can react either as diene or dienophile in a DA reaction visualized through the different mesomeric structures that can be drawn for their electronic configuration (Scheme 1-31).[206,207] For CNTs reacting as diene, solely modifications using maleimide or maleic anhydride as dienophile are known.[208–210] Conversely, when the CNTs react as dienophile they can be functionalized by employing anthracene,[211,212] dimethoxybutadiene,[213] arynes,[214] *o*-quinodimethane,[215–218] as well as cyclopentadiene.[219–222] Subsequent to all the advantages mentioned in Chapter 1.5.1, one of the most extensively used dienes in this application remains furan.[209,210] París and coworkers could modulate CNTs fluorescence properties *via* the attachment of a copolymer consisting of polystyrene, BODIPY fluorophores, and furan as a linker diene.[223] Furthermore, Chang and Liu could significantly enhance the bulk electrical conductivity of MWCNTs by reacting a difuryl crosslinker with pristine MWCNTs creating densely connected MWCNT networks that retained their superior mechanical properties.[224] Quijada-Garrido and coworkers synthesized bionanocomposites by reacting furyl-substituted poly(3-hydroxybutyrate-co-3-hydroxyhexanoate) with MWCNTs as potential scaffold for neural growth application.[225]

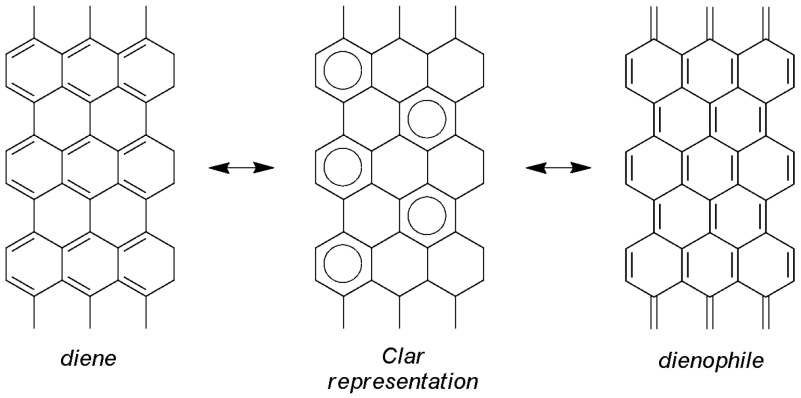

Scheme 1-31: Exemplified depictions of different mesomeric structures that can be drawn for sp^2-carbon allotropes to illustrate their reactivity in DA reactions.

While the DA reaction is usually performed at temperatures slightly above ambient conditions over the course of multiple days with high concentrations of the diene in solution or even in the bulk, the retro DA reaction is generally carried out in several hours at temperatures above 150 °C. The successful functionalization and/or defunctionalization is then verified via thermogravimetric analysis (TGA), Fourier transform infrared (FTIR), or Raman spectroscopy. The CNTs' pronounced reactivity towards cycloadditions is caused by the curvature directivity of the π-bonds[226] and diminishes with increasing radius of the tube.[227,228]

Though the reversible covalent functionalization of sp^2-carbon allotropes clearly has advantages when compared to the simple covalent or non-covalent approaches, a control over where and when these processes happen would be highly desirable. Carbonaceous sp^2-materials in particular unfold most of their strengths not in the bulk solid or in solution but in surface or interface applications where a local addressability is outstandingly useful. Thus, Chapter 2.3 will be devoted to the development of a photocontrolled reversible covalent functionalization approach prospectively leading to resolution of these processes in time and space.

2. Results and Discussion

2.1 Controlling Covalent Connection and Disconnection by Light

2.1.1 Conceptual Outline

Feature miniaturization and the growing complexity of structures used in nanomaterials and nanotechnology demand the precise and controlled formation of covalent bonds on the molecular scale.[140,229,230] In a conventional dynamic reaction,[231–233] the distribution of products can be controlled by applying different chemical and physical triggers, such as temperature, pressure, or light.[139,234,235] As light delivers superior spatial, temporal, as well as energetic resolution, photoaddressable molecular switches are ideal candidates to exploit the typical dynamic covalent reactions available to the organic chemist. These include the reversible formation of imines, hydrazones, oximes, thiols, aldols, boronates, or olefins by metathesis,[233,236–239] and are already employed to control stoichiometric chemical reactions as shown in Chapter 1.4. In addition to the listed reactions, the DA reaction – particularly with furan as diene and maleimide as dienophile – unifies a number of advantageous features that were already explained in detail in Chapter 1.5. The high reversibility of the furan-maleimide couple causes the temperature-dependent conversion to the adduct to be generally not quantitative. Conversely, this dynamic character is the prerequisite for the integration of light as an additional stimulus that offers the possibility to reach a new level of control over this type of reaction. DAEs are the photochromes of choice for this purpose due to their thermal stability and high fatigue resistance in combination with large optical changes between their ring-open and -closed forms (Chapter 1.3).

Branda and coworkers have already reported a series of photoswitchable DAEs with a diene motif incorporated in their bridge moieties that can undergo DA reactions with various dienophiles and inhibit the retro DA reaction through photochemical cyclization of the adduct (Chapter 1.4.3) The intrinsic design margins, however, do not allow for locking the DA reaction to either the side of the starting materials *or* the products by application of light. This is only possible through choice of different diene-dienophile combinations, as the unreacted diene is photochemically inactive. Thus, these truly innovative molecules unfold their capabilities rather as devices for the photocontrolled release of small molecules.[127]

Conversely, having the possibility of using light as a stimulus to switch both starting materials (diene) *and* reaction product (DA adduct) would offer true photocontrol over the dynamic covalent reaction system and enable the precise access to the underlying equilibrium (Figure 2-1a). The desired ability to photoswitch the unreacted DAE as well as the DA adduct sets certain demands on the molecular design of the respective target compound. The need to have a photoswitchable system that removes the reactive double bonds in the diene as well as in the adduct upon irradiation with light, thereby preventing either the DA reaction or the retro DA reaction, is addressed conveniently by replacing one of the thienyl moieties of a dithienylethene by incorporation of a furyl residue as the reactive diene (Figure 2-1b).

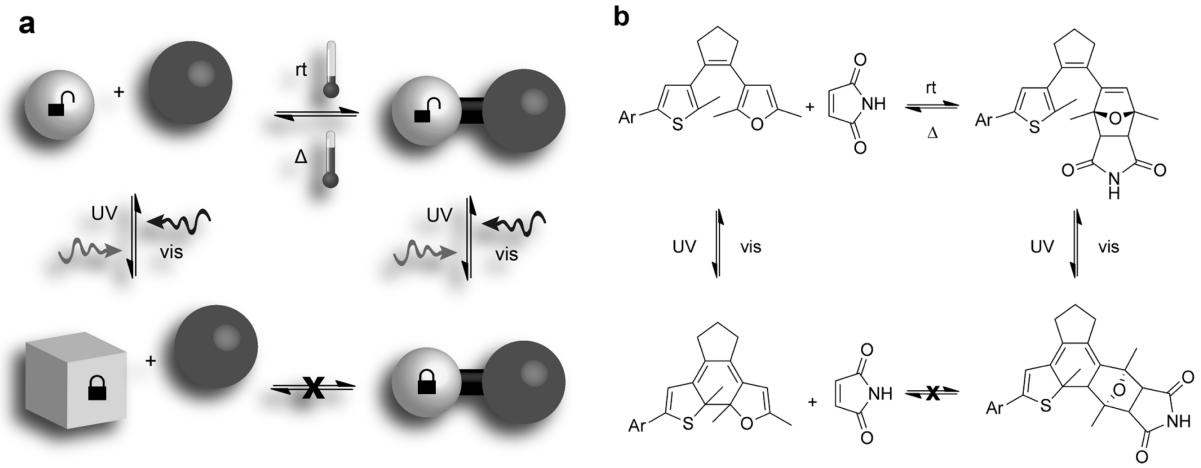

Figure 2-1: Photocontrol over the formation and scission of a dynamic bond using photoswitches as locks. a) Concept. b) A furyl-substituted diarylethene to achieve a photocontrolled DA reaction with maleimide.

2.1.2 Synthesis and Characterization of the Target Molecules

DAE **1o** was the first furylthienylethene synthesized to fulfil the specific demands outlined in Chapter 2.1.1 with the critical intermediate towards it being diketone **11** (Scheme 2-1). The synthesis *en route* to **11** can be approached by two major pathways: i) a subsequent cascade of Friedel-Crafts type reactions or ii) a Michael type enolate addition.

The first path starts with the smooth reaction of thiophene **5** and glutaric acid monoethyl ester chloride to give the acylated ethyl ester **6** with 64% yield. Saponification with excess NaOH in EtOH easily yielded the corresponding carboxylic acid **7** in basically quantitative yields. Note that the supposedly more facile[94] synthesis of acid **7** starting directly with thiophene **5** and glutaric anhydride was also attempted but purification of the received crude carboxylic acid proved to be laborious and inefficient. Subsequently,

chlorination of acid **7** with oxalyl chloride in CH_2Cl_2 efficiently produced the acid chloride **8** which was employed for the subsequent reaction without any further workup.

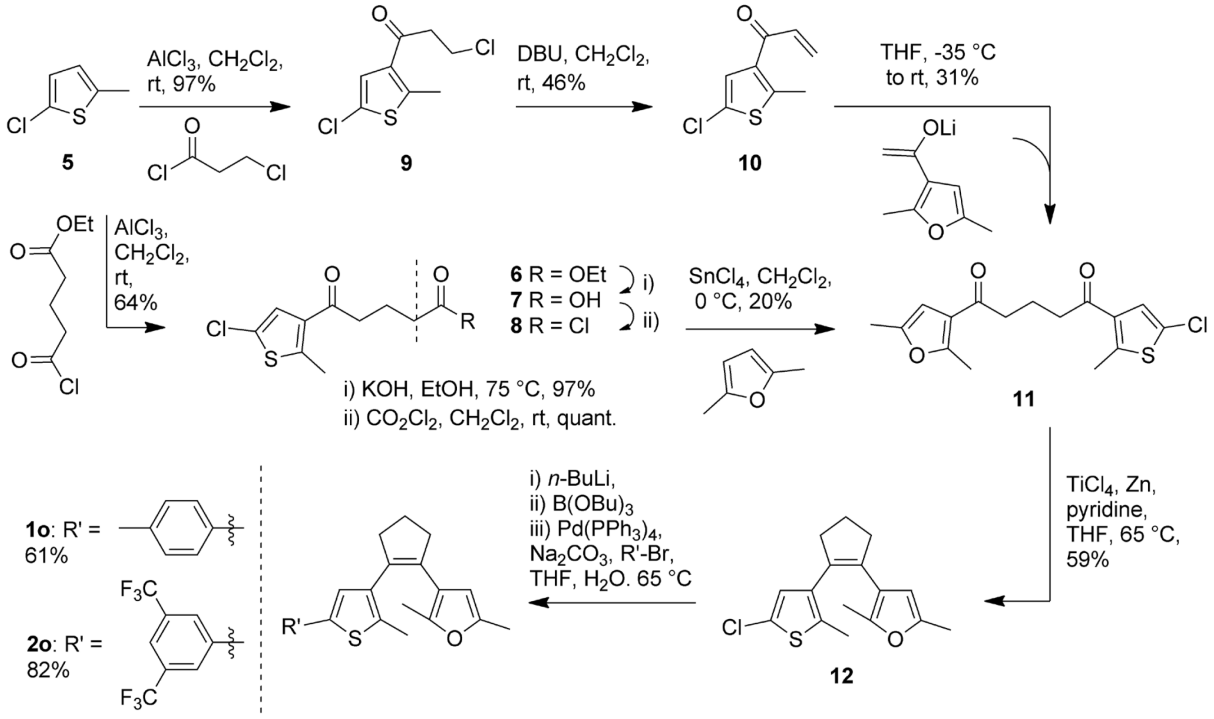

Scheme 2-1: Synthesis of furyl-substituted DAEs **1o** and **2o**.

However, the following Friedel-Crafts acylation of commercially available 2,5-dimethylfuran to the obtained acid chloride **8** was found to be an inefficient process as the yields did not surpass 20% in any attempt. The degradation behavior of furans when exposed to Lewis acids is sufficiently documented[240] and thus only few Lewis acids could be considered in the first place. $SnCl_4$ is known to exhibit the right balance regarding activity and degradative behavior towards furan[146] but even this Lewis acid led to ample destruction of the starting material **8**. Hence, the second route relying on a Michael type addition was selected. Starting with thiophene **5**, the first step gives the acylated compound **9** by Friedel-Crafts acylation with chloropropanoyl chloride in 97% yield as mixture of the 3- and 4-regioisomers. Basic elimination of HCl employing DBU results in the corresponding α,β-unsaturated ketone **10** that can undergo a Michael type addition with the lithium enolate of commercially available 3-acetyl-2,5-dimethylfuran to give diketone **11** with a yield of 31%. Though this reaction pathway apparently produces yields that are only slightly higher compared to pathway 1, the overall effort is lower as there are fewer steps involved and the elimination-addition-cascade can be carried out *in situ*. Then, standard McMurry type conditions produce the reductively coupled precursor **12** in 59% yield which, in turn, can be

functionalized conveniently by an *in situ* boronation with subsequent Suzuki-Miyaura palladium catalyzed cross-coupling yielding the respective diarylethene **1o** with a yield of 61%. DAE **1o** can successfully undergo the DA reaction with *N*-phenylmaleimide to its corresponding DA adduct **3o** – consisting of the stereoisomers ***exo*-3o** and ***endo*-3o** – and exhibits full reversibility to the starting materials at elevated temperatures (Scheme 2-2). Though both stereoisomers were isolated and appear to exhibit the same spectral characteristics, only the thermodynamically more stable ***exo*-3o**, synthesized with a yield of 37%, was employed for thorough analytical characterization and photochemistry.

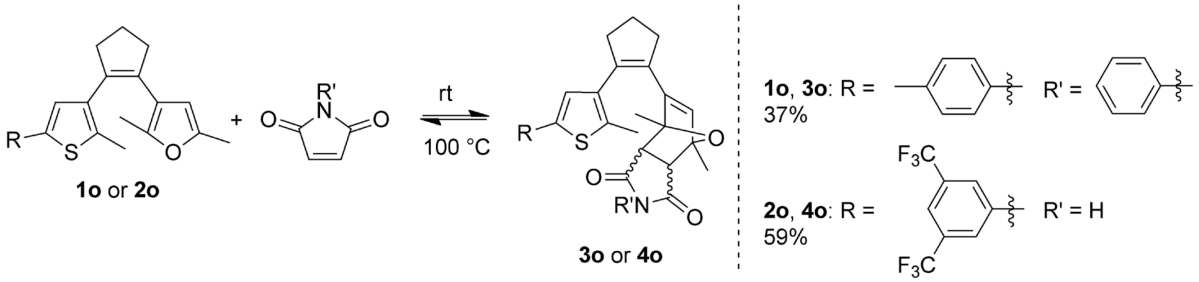

Scheme 2-2: Diels-Alder reaction between DAEs **1o** and **2o** with maleimides towards respective adducts **3o** and **4o**.

Unreacted switch **1o** as well as adduct ***exo*-3o** show fully reversible photochromism and exhibit the appearance of the typical band in the visible part of the spectrum upon photocyclization (Figure 2-2). The photocyclization and cycloreversion quantum yields along with molar absorptivities and compositions and the PSS of switches **1** and ***exo*-3** are combined in Table 2-1 and Table 2-2.

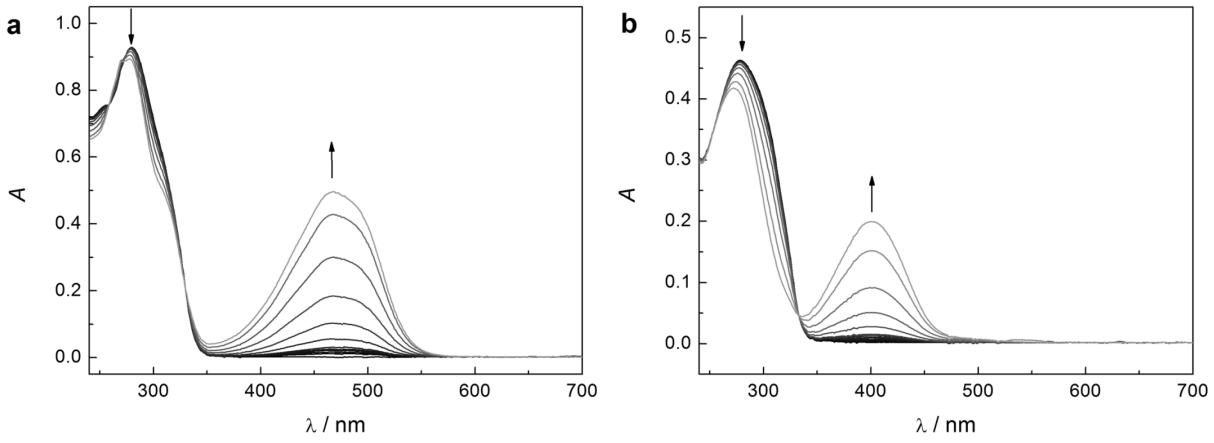

Figure 2-2: UV/vis absorption spectra during the course of ring-closure of a) DAE **1o** and b) respective Diels-Alder adduct ***exo*-3o** in MeCN ($c \sim 10^{-5}$ M), induced by irradiation with UV-light (λ_{irr} = 313 nm) at 25 °C.

Table 2-1: Molar absorptivities, absorption maxima, composition at the PSS, as well as cyclization and cycloreversion quantum yields of DAE **1** in MeCN.

	ε / L mol^{-1}cm^{-1}		λ_{max} / nm			λ_{irr} / nm	
	1o	**1c**	**1o**	**1c**		313 **o→c**	436 **c→o**
MeCN	20000	14600	280	468	ϕ	0.63	0.06
					PSS / %	73	100

Table 2-2: Molar absorptivities, absorption maxima, composition at the PSS, as well as cyclization and cycloreversion quantum yields of DAE ***exo*-3** in MeCN.

	ε / L mol^{-1}cm^{-1}		λ_{max} / nm			λ_{irr} / nm	
	***exo*-3o**	***exo*-3c**	***exo*-3o**	***exo*-3c**		313 **o→c**	436 **c→o**
MeCN	22000	13500	278	400	ϕ	0.25	0.08
					PSS / %	70	100

Despite the fact that the system constituting of diarylethene **1o** and *N*-phenylmaleimide showed full function in reactivity as well as photochemistry, it was not employed for further studies as **1o** is prone to fast oxidation under aerated conditions, the photocyclization and cycloreversion quantum yields of **1** and ***exo*-3** are low, and the amounts of **1c** and ***exo*-3c** at their respective PSSs are dissatisfying. Thus the practicality of this system is widely restricted and instead, the 3,5-bis(trifluoromethyl)phenyl terminated DAE **2o** was synthesized with a yield of 82% analogously to **1o** by varying only the aryl bromide as the coupling partner in the last step of the synthesis (Scheme 2-1). The 3,5-bis(trifluoromethyl)phenyl substituent was chosen as it is known from work in our research group to substantially enhance fatigue resistance and its electron-withdrawing character increases the bathochromic shift of the ring-closed form's absorption band. Similar to **1o**, DAE **2o** can successfully undergo the DA reaction with maleimide to yield the corresponding adduct **4o** as a mixture of *exo* and *endo* stereoisomers, the formation of which are reversible at 100 °C (Scheme 2-2). Again both stereoisomers were isolated, however, for thorough analytical characterization and photochemistry only the thermodynamically more stable ***exo*-4o**, received with a yield of 59%, was employed. Both switches **2o** and ***exo*-4o** show fully reversible photochromism and their photocyclization reactions are each characterized by the typical appearance of a band in the visible part of the spectrum (Figure 2-3). Notably, the

adduct **4c**'s absorption maximum exhibits a strong hypsochromic shift when compared to the unreacted species **2c** of $\Delta\lambda_{max} = 86$ nm, which can be attributed to the additional double bond of the furyl moiety and thus larger π-electron system in **2c**.

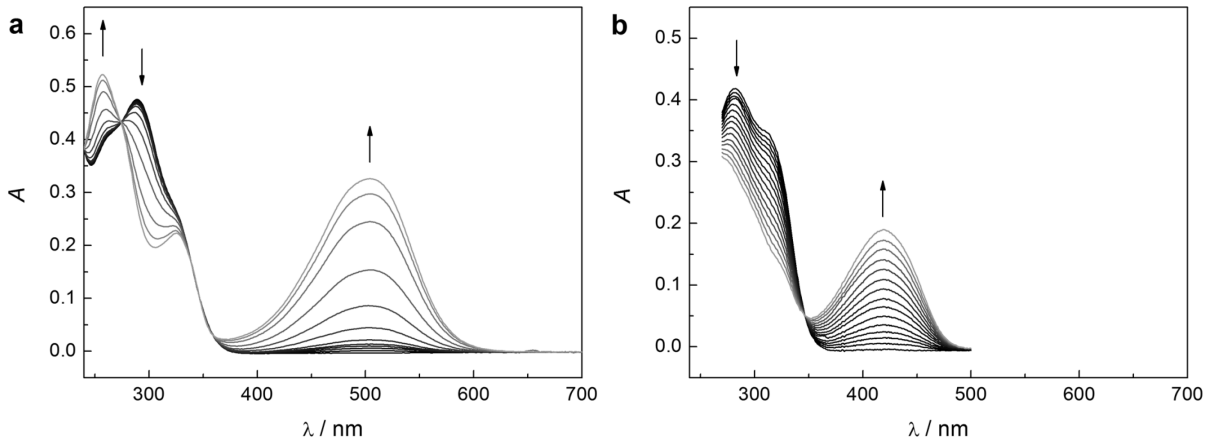

Figure 2-3: UV/vis absorption spectra during the course of ring-closure of a) DAE **2o** and b) respective Diels-Alder adduct ***exo*-4o** in MeCN ($c \sim 10^{-5}$ M), induced by irradiation with UV-light (λ_{irr} = 313 nm) at 25 °C.

The photocyclization quantum yield of **2o** was determined to be as high as 0.80 in acetonitrile at the irradiation wavelength $\lambda_{irr} = 313$ nm (Table 2-3). However, the reason for this extraordinarily high photochemical efficiency is until now still unclear, particularly as ϕ_{oc} drops to 0.40 when the solvent is changed to the less polar toluene. Conversion to **2c** at the PSS is also acceptable in acetonitrile as well as in toluene and suffers only from a small drop to around 84–86% at the irradiation wavelength $\lambda_{irr} = 375$ nm. This can be attributed to the smaller molar absorptivity ε_{2o} and gain in ε_{2c} in this spectral region leading to increased competition of the cycloreversion reaction (Figure 2-3a).

Table 2-3: Molar absorptivities, absorption maxima, composition at the PSS, as well as cyclization and cycloreversion quantum yields in different solvents at different wavelengths of DAE **2**.

	ε / L mol^{-1}cm^{-1}		λ_{max} / nm			λ_{irr} / nm				
	2o	**2c**	**2o**	**2c**		313 **o→c**	334 **o→c**	375 **o→c**	395 **o→c**	546 **c→o**
MeCN	17000	11900	290	505	ϕ	0.80	0.77	-	-	0.04
					PSS / %	97	98	86	9	-
toluene	17000	11900	292	512	ϕ	0.40	0.49	-	-	0.04
					PSS / %	91	94	84	-	-

Though solvent independent, the photocyclization quantum yield of adduct **4** with a value of 0.30 is much lower than the unreacted DAE **2** (Table 2-4). However, the cycloreversion quantum yields are drastically increased to about 0.10 rendering **4** an ideal candidate for dynamic switching that requires acceptable photochemical efficiencies in both directions. The conversion to **4c** at the photostationary state is with values >90% also more than satisfactory.

Table 2-4: Molar absorptivities, absorption maxima, composition at the PSS, as well as cyclization and cycloreversion quantum yields in different solvents at different wavelengths of adduct DAE ***exo*-4**.

	ε / L mol^{-1}cm^{-1}		λ_{max} / nm			λ_{irr} / nm		
	***exo*-4o**	***exo*-4c**	***exo*-4o**	***exo*-4c**		313 **o→c**	334 **o→c**	436 **c→o**
MeCN	15000	10800	283	419	ϕ	0.31	-	0.10
					PSS / %	90	-	-
Toluene	15000	10800	289	425	ϕ	0.30	0.33	0.11
					PSS / %	90	99	-

2.1.3 Amplification or Inhibition of the Diels-Alder Reaction

Two main aspects can be extracted from the findings that have been elucidated in Chapter 2.1.2 so far and are summarized in Scheme 2-3: i) Photocyclization of **2o** to **2c** removes the reactive *cisoid* diene functionality of the furyl moiety and thus detains the molecule from participation in the DA reaction; and ii) ring-closure of **4o** to **4c** removes the reactive double bond from the oxanorbornene skeleton, thereby thermally locking the adduct and preventing the retro DA reaction. As can be seen in Figure 2-4a, reaction of **2o** with maleimide results in conversion to the adducts ***exo*-4o** and ***endo*-4o** even at very low concentrations. To prove that the forward DA reaction can be inhibited by photocyclization, **2o** was irradiated to the PSS consisting almost only of **2c** and then submitted to the same reaction conditions with no apparent conversion to the DA adduct (Figure 2-4b). In an analogous manner Figure 2-4c shows the smooth retro DA reaction from ***exo*-4o** to **2o** upon heating. However, heating a mixture of ***exo*-4c** and residual ***exo*-4o** at the PSS clearly reveals that the ring-closed adduct ***exo*-4c** is unreactive and stable under these conditions and only the residual amount of the ring-open isomer ***exo*-4o** can undergo the retro DA reaction (Figure 2-4d).

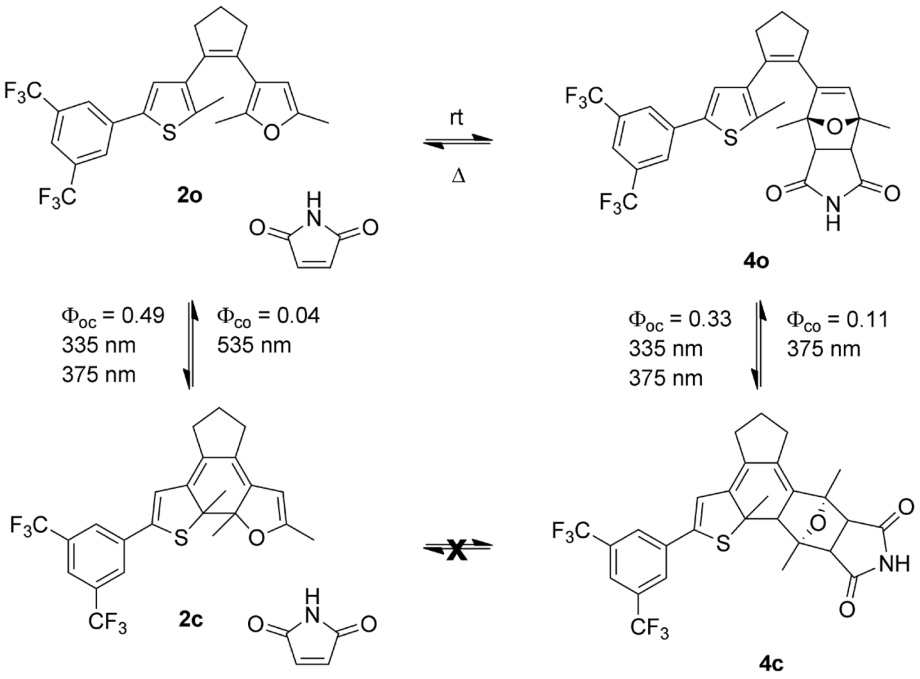

Scheme 2-3: Reaction scheme depicting the different components **2o**, **2c**, **4o**, **4c**, and maleimide in the course of a photocontrolled Diels-Alder reaction with respective photocyclization and cycloreversion quantum yields measured in toluene and irradiation wavelengths employed for the *in situ* reaction.

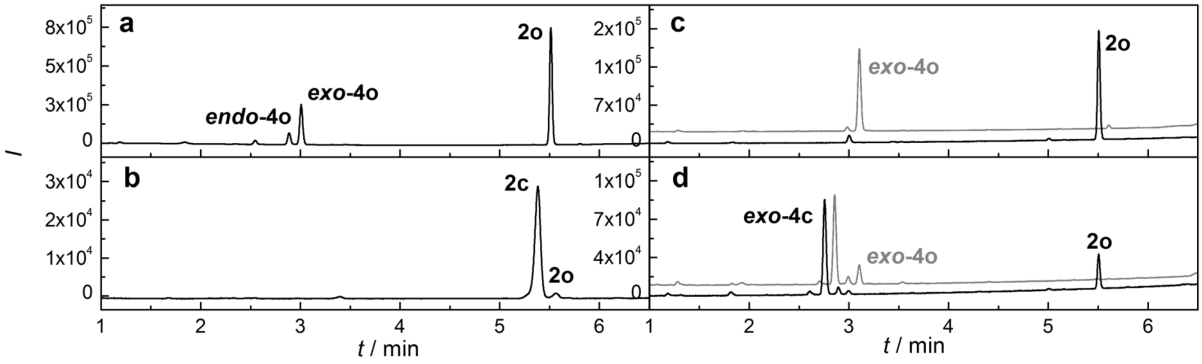

Figure 2-4: Locking the DA as well as the retro DA reaction by light: UPLC diode array detector (DAD) traces at λ = 270 nm of a) formation of ***exo*-4o** and ***endo*-4o** after heating **2o** and maleimide (MI) at 50 °C for 1 d, b) no formation of adduct is visible after heating **2c** and maleimide at 50 °C for 1 d, c) **2o** after heating ***exo*-4o** at 100 °C for 15 min (***exo*-4o** before heating shown in grey with offset for comparison), d) No retro DA for ***exo*-4c** is visible after heating a mixture of ***exo*-4o** and ***exo*-4c** at the PSS for 1 h at 100 °C (PSS of ***exo*-4o** and ***exo*-4c** before heating shown in grey with offset for comparison). Concentrations of switches **2o**, **4o**, **2c**, and **4c** employed were 10^{-5} M, that of maleimide was 10^{-2} M.

The ability to lock **2o** as well as **4o** by converting them to **2c** and **4c**, respectively, with UV-irradiation is remarkable and offers various possibilities to employ these switch prototypes as photocontrollable locks. However, the true value of the system arises from the feature that the reverse photoprocesses to unleash the reactive diene or DA adduct can be

induced each selectively by choosing the proper irradiation wavelength. Comparing the absorption spectra of both ring-closed forms reveals a considerable spectral separation ($\Delta\lambda_{max} = 86$ nm) between the absorption maxima of **2c** absorbing in the green and ***exo*-4c** absorbing in the blue region (Figure 2-5a). Thus, and despite the fact that **2c** absorbs slightly in the region where ***exo*-4c** is addressed, this allows for almost independent initiation of cycloreversion reactions while irradiating a mixture of both ring-closed derivatives – the key to achieve control over a dynamic system with light.

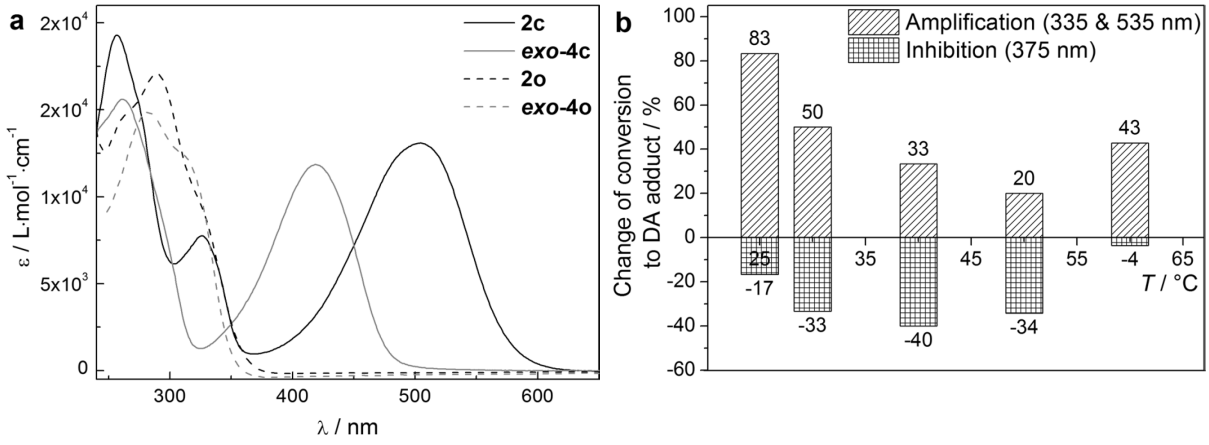

Figure 2-5: a) Comparison of the absorption spectra of **2o**, **2c**, ***exo*-4o**, and ***exo*-4c** in acetonitrile at 25 °C. Residual absorbance of ***exo*-4c** above 500 nm is attributed to minor retro DA reaction taking place during the irradiation process. b) Relative amplification or inhibition of DA adduct formation depending on illumination wavelength. Changes in conversion to **4** (**4o**, **4c** both *exo* and *endo* combined) reacting DAE **2o** (~10^{-5} M) with maleimide (~10^{-2} M) employing irradiation either at 335 nm and 535 nm for 6 h (amplification) or at 375 nm for 24 h (inhibition) as compared to the corresponding dark reaction as a function of temperature. See Table 2-5 for absolute values.

Indeed, simultaneous irradiation of a mixture of **2o** and maleimide with light enables *in situ* control over the outcome of the DA reaction. While thermal reactions of **2o** with maleimide exhibit conversions of 18–35% to **2o** after 24 h depending on the applied temperature (Figure 2-6a and Table 2-5), the formation of the DA adduct can be amplified or inhibited by irradiation with light of the appropriate wavelength and subsequent formation of the respective ring-closed isomers (Figure 2-5b). Irradiating a mixture of **2o** and maleimide with 335 nm and 535 nm light induces cyclization of both ring-open isomers **2o** and **4o** but cycloreversion only in **2c** (Figure 2-5a), therefore effectively leading to an enrichment of **4c** in the reaction mixture. This method leads to an amplification of DA adduct formation already after 6 h as compared to the dark DA reaction (striped bars in Figure 2-5b). The respective liquid chromatography traces for the amplification reaction at 25–60 °C can be found in

Figure 2-6b with the corresponding relative peak areas in Table 2-5. At the temperature of 40 °C the amplification was monitored exemplarily by UV/vis absorption spectroscopy confirming the initial formation of **2c** followed by its depletion over time to form **4c** (Figure 2-7a). Note that the heating time was reduced as prolonged irradiation and heating result in degradation. The same method but using different wavelengths can also be applied to bias the DA reaction in favor of adduct inhibition. Using light of 375 nm cyclizes **2o** to **2c** as well as **4o** to **4c** but simultaneously addresses the vis-band of the ring-closed adduct **4c**, thereby also inducing cycloreversion towards **4o** (Figure 2-5a). According to Le Châtelier's principle, diene **2o** is removed from the dynamic DA equilibrium by conversion to **2c** and thus the reaction is inhibited effectively as compared to the dark, *i.e.* solely thermal, DA reaction (checkered bars in Figure 2-5b). The respective liquid chromatography traces for the inhibition reaction at 25–60 °C can be found in Figure 2-6c with the corresponding relative peak areas in Table 2-5. Again, at the temperature of 40 °C the inhibition was monitored exemplarily by UV/vis absorption spectroscopy revealing the formation of **2c** as the major component absorbing in the visible region in the reaction mixture (Figure 2-7b).

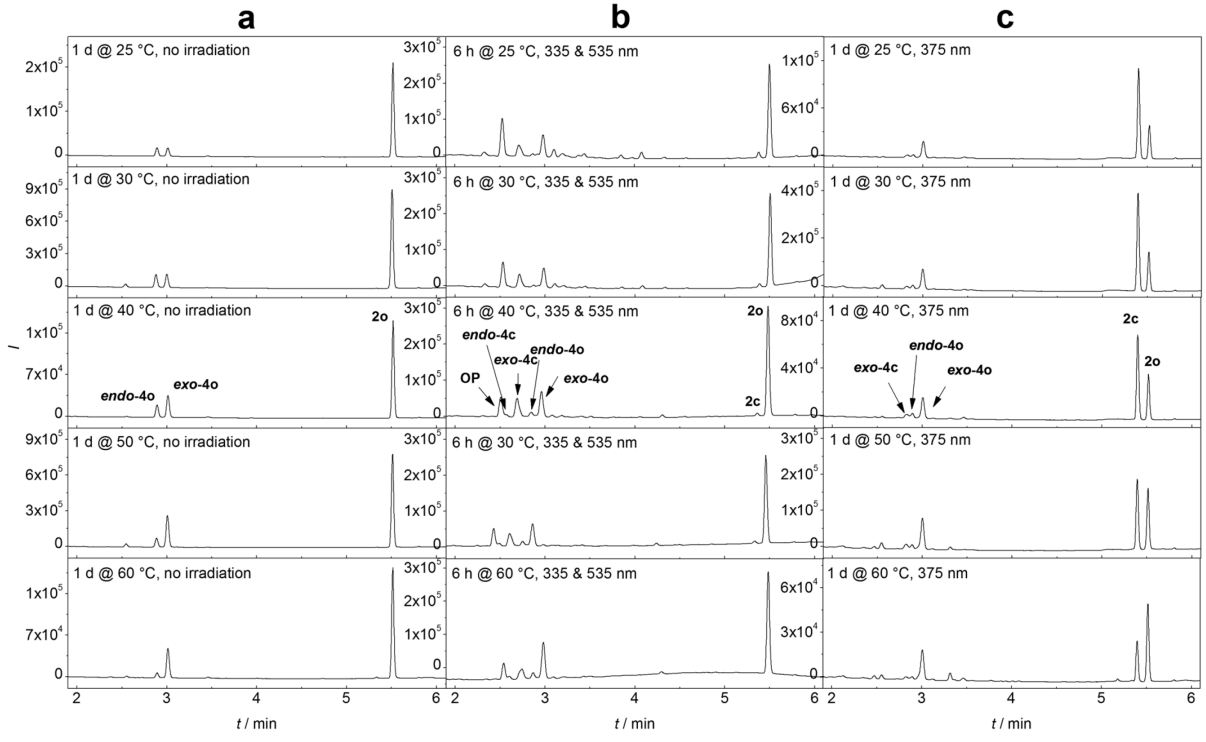

Figure 2-6: UPLC-MS DAD traces at 270 nm after the *in situ* DA reaction of DAE **2o** with maleimide at different temperatures after a) 1 d without irradiation (dark reaction), b) 6 h and irradiation with 335 & 535 nm light (amplification), and c) irradiation with 375 nm light (inhibition). The observed oxidation product **OP** at $t \sim 2.5$ min is not a result of the reaction and was formed over several weeks in the stock solution of **2o**.

Table 2-5: Summarized integrated peak areas during the *in situ* DA reaction of **2o** and maleimide of ***exo*-4** and ***endo*-4** (both ring-open and -closed) at different temperatures employing different irradiation conditions.

T / °C	Peak area / %		
	dark	375 nm	335 & 535 nm
25	18	15	33
30	24	16	36
40	30	18	40
50	35	23	42
60	28	27	40

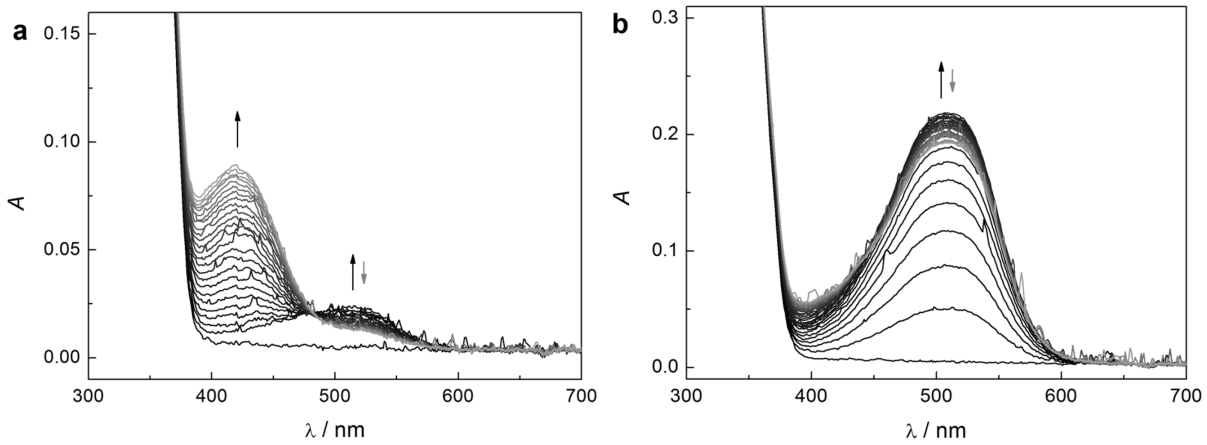

Figure 2-7: Exemplary UV/vis absorption spectra during the course of either *in situ* a) amplification carried out for 6 h at 40 °C irradiating with light of the wavelengths 335 & 535 nm or b) inhibition of the DA reaction between **2o** and maleimide for 1 d at 40 °C irradiating with light of the wavelength 335 nm. Concentration of switch **2o** was 10^{-5} M, that of maleimide was 10^{-2} M.

In addition to the applied irradiation wavelength, the quantity of amplification or inhibition is strongly dependent on the applied temperature (Figure 2-5b). However, rationalization of the process is difficult since the overall outcome is a result of a superposition of thermal and photochemical equilibria in the ground as well as in the excited states. Elevated temperatures, for example, not only promote the retro DA reaction but also increase the ring-opening quantum yields, hence affecting the composition at the PSS noticeably.[241,242] Furthermore, amplification works best at temperatures typically unfavorable for the DA reaction (*i.e.* in the highly reversible regime) while inhibition works best at temperatures yielding already high conversion in the dark. This indicates that amplification and inhibition unfold their potential primarily when the reaction rate constant for the thermal DA reaction at a given temperature favors the opposite direction.

In summary, we have been able to selectively either amplify or inhibit a DA reaction by illumination with light of different wavelengths, thus broadening the repertoire of DCC. Not only could the DA reaction be shifted to either the side of the starting materials or the side of the products *in situ* and on demand, in addition our prototypic DAE has tremendous potential for a variety of possible applications, such as the release of maleimide derivatives in physiological systems or the reversible covalent functionalization of carbon nanotubes, both of which will be discussed in detail in Chapters 2.2 and 2.3.

2.2 Photoinduced Release of Maleimide Derivatives in Physiological Systems

2.2.1 Conceptual Outline

In Chapter 1.6.2, it was highlighted that maleimide derivatives show great potential as DNA Topoisomerase II (TOP2) inhibitors as well as TOP2 poison antagonists. It was emphasized that maleimide derivatives do not stabilize the cleaving complexes of DNA G segment, T segment, and TOP2, but in contrast decrease the bioavailable TOP2 concentration through its respective alkylation. This circumvents side-effects of common antitumor or antibiotic drugs.[193–195]

As pointed out in Chapter 1.6.1 that exerting control over 'where' and 'when' a drug is administered in the organism is regarded as highly beneficial to bypass poor selectivity and toxicity, a release of maleimide derivatives activated by an external stimulus would be highly sought after.[23] It was clarified in the earlier sections that light as a stimulus has many advantages, including its high bioorthogonality, and thus a photoactivatable release system can be seen as promising with view on actual *in vivo* application. Additionally, conventional drug administration usually suffers from an initially high but comparatively short bioavailability of the drug as reactive sites are generally metabolized quickly. Hence, the means to achieve long-term release of the active drug, *i.e.* a 'depot effect', is very desirable. Conceptually, these demands to a photocontrolled release system have been composed in Figure 2-8.

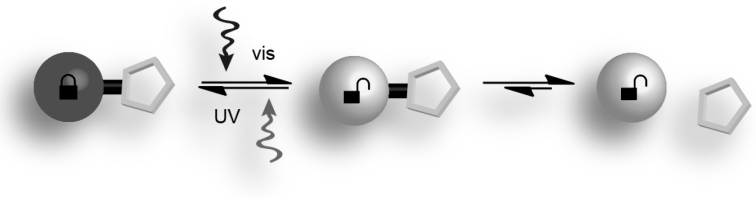

Figure 2-8: Conceptual depiction of the photoreversible activation of a release system relying on a subsequent thermal equilibrium.

The photocontrollable DA reaction highlighted in Chapter 2.1 fulfills all of the criteria defined for this task as it i) protects the maleimide derivative's reactive double bond by formation of the DA adduct thus inhibiting its biological activity,[194] ii) can lock and unlock the DA adduct photoreversibly granting external control over the release system,[95] and iii)

features a subsequent thermal equilibrium acting as a depot for long-term release of the maleimide based drug.

To the best of our knowledge, photoswitching of a DAE derivative that is soluble in physiological media has only been reported in two cases[182,183] and also literature documented examples of water-soluble DAEs are pretty rare.[243–249] As the route towards the photocontrol over the DA reaction was already covered in Chapter 2.1, the main effort for the realization of this application thus lies in the design of a photoswitchable DA system that is soluble in physiological (*i.e.* buffered aqueous) media while retaining its high photochemical efficiency therein.

2.2.2 Synthesis and Characterization of the Target Molecules

Since the methylated pyridine moiety is a reoccurring motif to solubilize DAEs in aqueous environments,[243,245] the first furyl switch that was designed to fulfill the criteria outlined in Chapter 2.2.1 was the methylpyridinium salt **14** (Scheme 2-4). Starting from the already established chloro precursor **12** the *p*-pyridyl-substituted furyl switch **13** was obtained with a yield of 76% by one-pot halogen-metal exchange and Suzuki-Miyaura type cross-coupling conditions employing the commercial hydrochloride of *p*-bromo pyridine. Subsequent methylation using methyl iodide in acetonitrile and washing with brine yielded the desired methylpyridinium chloride **14** with a good yield of 89%.

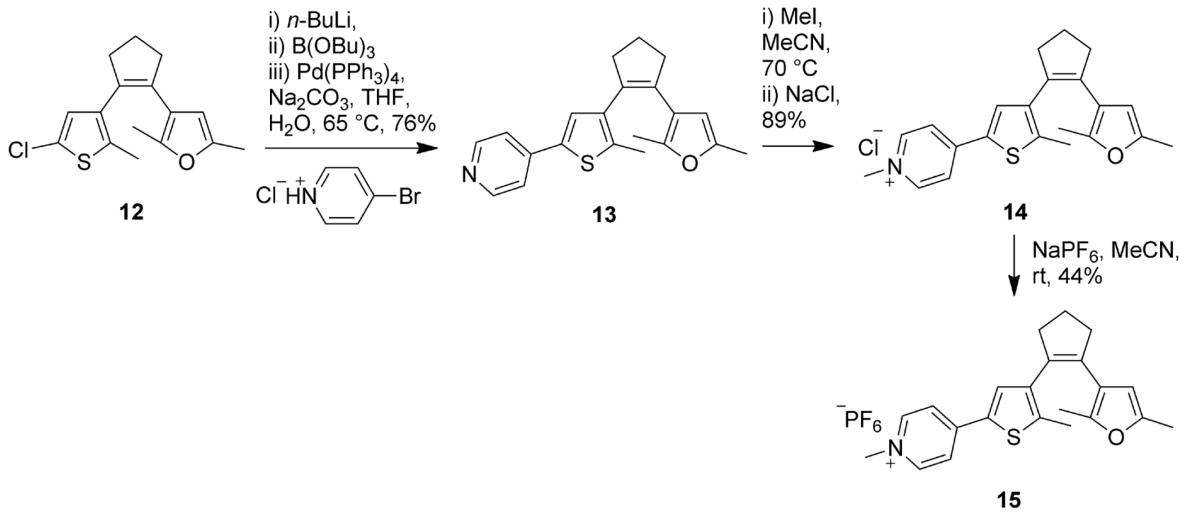

Scheme 2-4. Syntheses of water-soluble furyl-substituted DAEs **14** and **15**.

DAE **14** possesses outstanding water-solubility up to hundreds of milligrams per milliliter. Yet, no reversible photochromic behavior could be detected as upon irradiation with

UV-light only unspecific degradation could be observed. Figure 2-9a noticeably shows the development of a new absorption band around 640 nm upon irradiation of **14o** with light of the wavelength λ_{irr} = 313 nm. This absorption band, however, is depleted after a short time and a new band around 500 nm is formed. Subsequent irradiation of the resulting mixture with visible light of the wavelength λ_{irr} = 546 nm did not reproduce the ring-open form **14o** (Figure 2-9b). It was reasoned that the halogen anion could interfere with the photochemistry, *e.g.* by forming radical species, and could lead to the production of unwanted side-products during the irradiation process. Hence, the hexafluorophosphate **15** was synthesized by stirring **14** and $NaPF_6$ in acetonitrile. The repeated washing steps necessary to remove residual $NaPF_6$ are accounted for the fact that only 44% yield were received after this simple ion exchange. However, similar degradation behavior to **14o** was observed and no reversible photochromic processes could be detected while irradiating a solution of **15o** in acetonitrile with UV-light of the wavelength λ_{irr} = 313 nm. A possible reason for that irreversible photoreaction could be an initially occurring charge transfer or photoinduced electron transfer between the electron-donating furyl and the electron-withdrawing methylpyridinium moieties in the DAE's ring-open form, as indicated by the bathochromically shifted S_1-transitions of **14** and **15** (Figure 2-9).[53,250] A resulting pyridine-based radical could then engage in some irreversible subsequent reaction leading to fatigue.

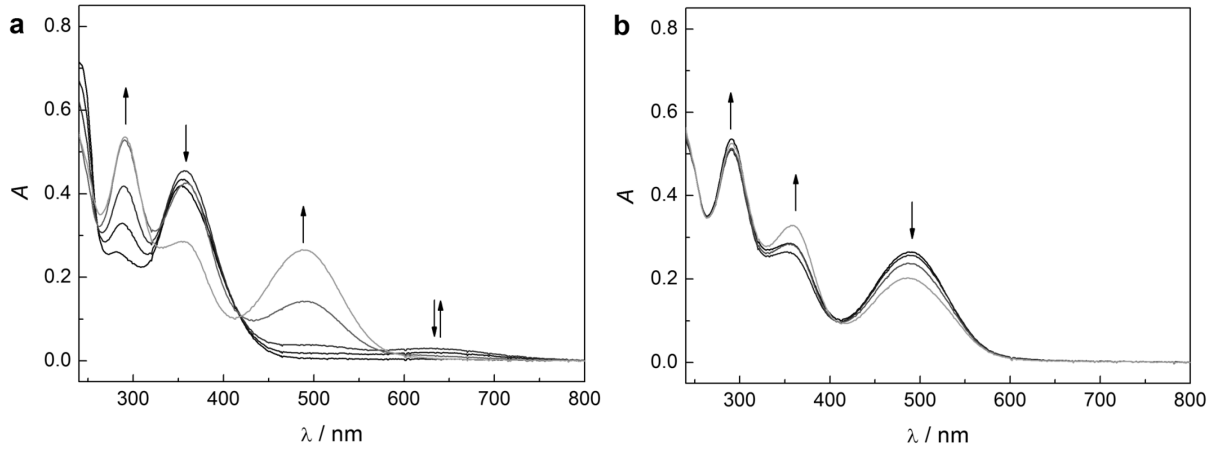

Figure 2-9: UV/vis absorption spectra during the course of a) ring-closure of DAE **14o** induced by irradiation with UV-light (λ_{irr} = 313 nm) and b) ring-opening of DAE **14c** induced by irradiation with vis-light (λ_{irr} = 546 nm) in H_2O ($c \sim 10^{-5}$ M) at 25 °C.

Consequently, the charged, electron-withdrawing species was excluded from the π-electron system that participates in the photochromic reaction leading to the design of bis(dimethylamino) ester **16** (Scheme 2-5). Starting from the chloro precursor **12**, one-pot

halogen-metal exchange, Suzuki-Miyaura type cross-coupling conditions, and subsequent precipitation with anhydrous HCl from an Et_2O solution led to bis(dimethylamino) ester hydrochloride **16** in 62% yield. Diaminoester bromide **17** employed in this reaction was synthesized in a straightforward manner by the drop-wise addition of *p*-bromobenzoyl chloride to a solution of the commercial 1,3-bis(dimethylamino)propan-2-ol in methylene chloride. Normally, this reaction should be quantitative and the comparably poor yield of 67% is caused by the contamination of the starting material with *p*-bromobenzoic acid.

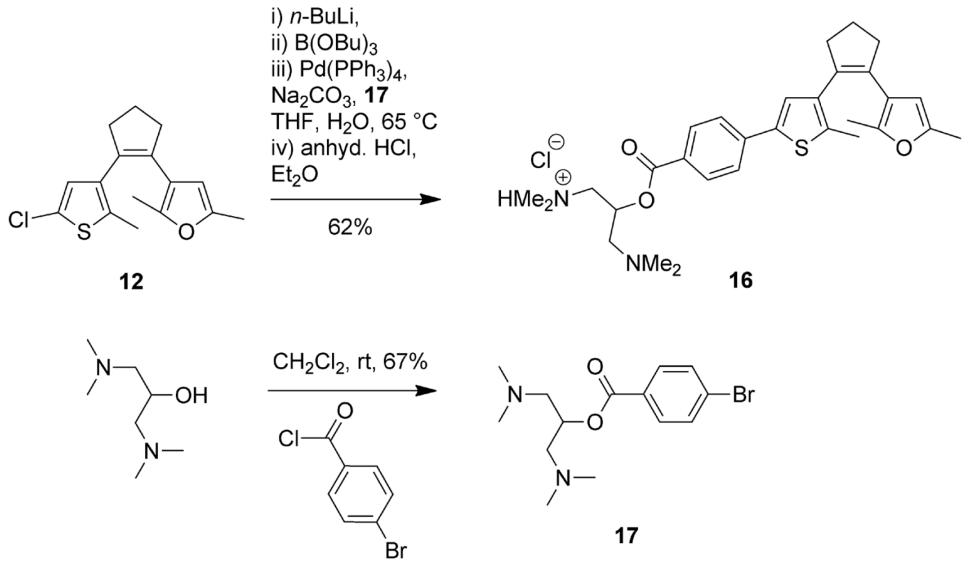

Scheme 2-5: Syntheses of water-soluble furyl-substituted ester **16** and its free base precursor building block **17**.

DAE **16o** is readily dispersed in water and exhibits reversible switching behavior, as indicated by the appearance of a band at around 540 nm upon irradiation with UV-light and its vanishing upon irradiation with vis-light (Figure 2-10a and Figure 2-10b). However, only a low fraction of ring-closed isomer **16c** could be produced at the photostationary state, strongly suggesting that effective photoisomerization is somehow hindered. Furthermore, hydrolysis of **16o** to the free acid and 1,3-bis(dimethylamino)propan-2-ol was observed over the timescale of days rendering this derivative not useful in long-term applications. The formation of aggregates becomes apparent through the increased baseline absorption attributed to unspecific scattering in solution and is most likely responsible for the unsatisfying photochromic properties as the switching process could be hampered in densely packed aggregates.

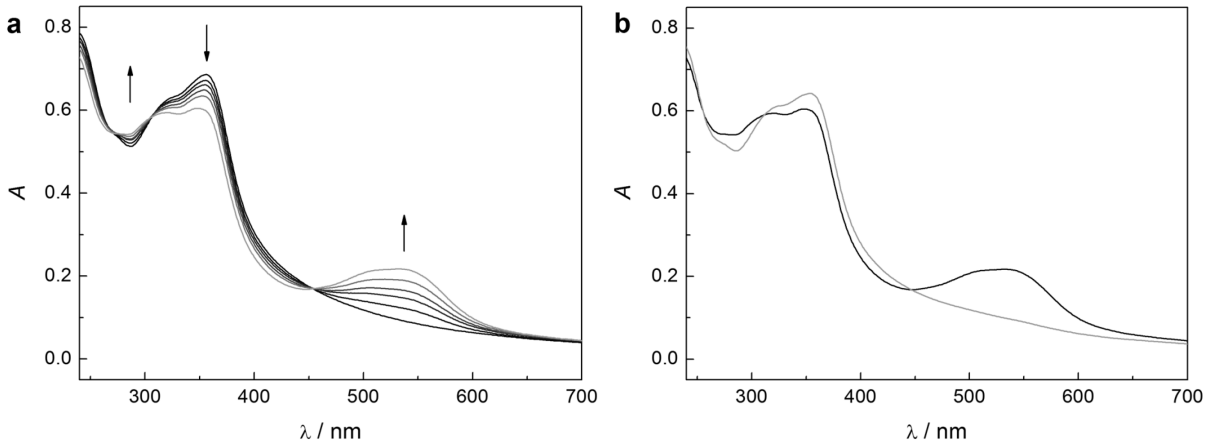

Figure 2-10: UV/vis absorption spectra during the course of a) ring-closure of DAE **16o** induced by irradiation with UV-light (λ_{irr} = 313 nm) and b) ring-opening of DAE **16c** induced by irradiation with vis-light (λ_{irr} = 546 nm) in H_2O ($c \sim 10^{-5}$ M) at 25 °C.

Subsequently, we decided to dismiss the design of DAE **16** and to synthesize the sodium salt of a carboxylic acid, as sodium carboxylates are well-known to permit solubility in aqueous media. Therefore, precursor **12** was employed in the familiar cross-coupling sequence with ethyl *p*-bromobenzoate to yield ester **18** with a yield of 67%. The latter was subsequently saponified quantitatively with NaOH in ethanol to yield desired sodium carboxylate **19** (Scheme 2-6). With a yield of 75% this otherwise quantitative reaction was again hampered by multiple washing steps. DAE **19o** exhibits excellent solubility in water and also suitable photochromic behavior, as indicated by the reversible formation of a band around 500 nm upon irradiation of **19o** to **19c** employing UV-light (Figure 2-11a). However, over time in H_2O and immediately upon dissolution in phosphate buffered saline (PBS), aggregation of **19o** was observed (compare scattering in Figure 2-11b). Efforts to elucidate this aggregation behavior will be described in Chapter 2.2.4.

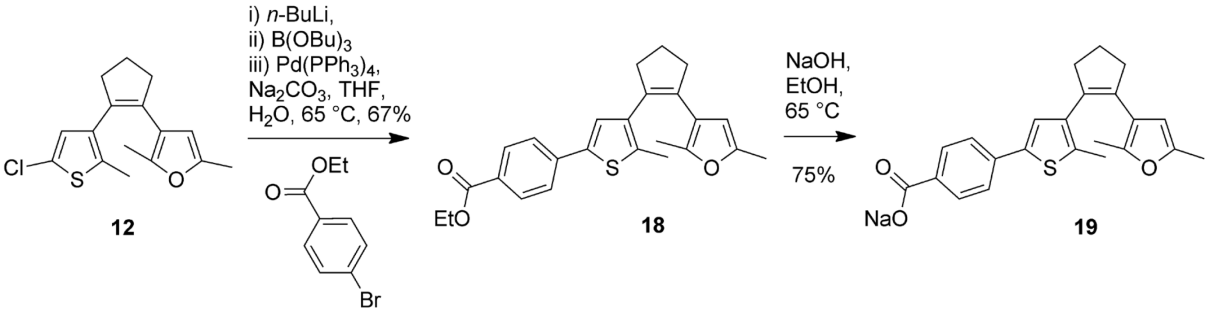

Scheme 2-6: Synthesis of water-soluble furyl-substituted sodium carboxylate **19**.

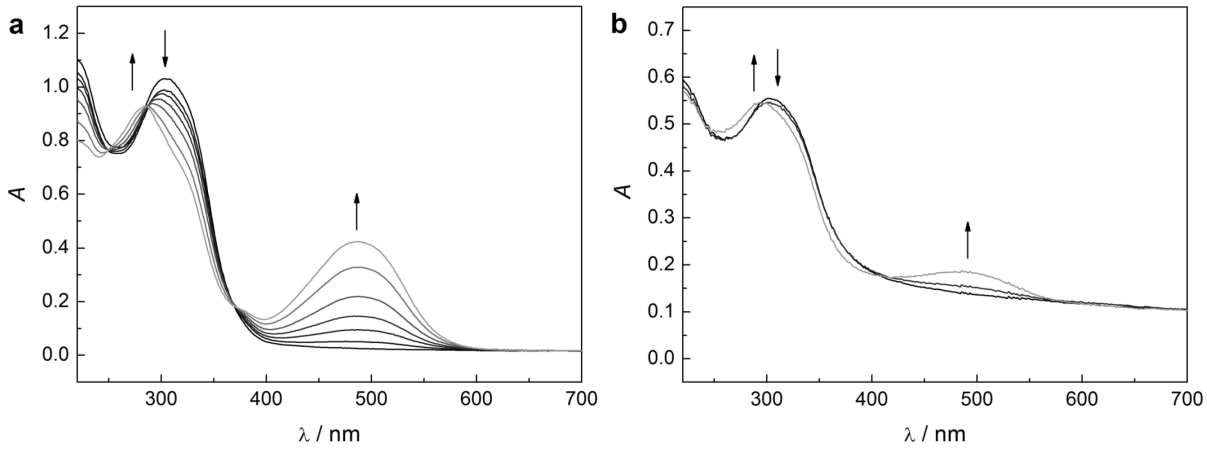

Figure 2-11: UV/vis absorption spectra during the course of ring-closure of DAE **19o** induced by irradiation to the PSS with UV-light (λ_{irr} = 313 nm, $c \sim 10^{-5}$ M) at 25 °C in a) H_2O and b) PBS.

Against our expectations, the ring-closed form **19c** was found not to be stable. As can be seen in Figure 2-12, upon stirring the mixture of **19c** and **19o** at the PSS at 25 °C, the absorption in the visible part of the spectrum fades over the period of multiple hours. This could point towards a thermal instability of the ring-closed switch, a property not usually observed in DAEs substituted with 3-thienyl or 3-furyl residues.[30,35,36] A UPLC analysis of the solution's composition after the thermal bleaching, however, reveals that the ring-open form **19o** is not regenerated (Figure 2-13). Instead, a different compound **RPo** with a molecular weight of 16 Da higher than **19o** was detected. These results, alongside with the observed sensitivity of furyl-substituted DAEs towards molecular oxygen (compare furyl DAE **1o** in Chapter 2.2.2), strongly suggest that an oxidation reaction occurs. Furthermore, the reaction product **RPo** exhibits photochromic behavior but thermally reverts to its ring-open form after a short time again. We thus reason that the chemical reaction that only takes place from the ring-closed form **19c** but not from the ring-open form **19o** leads to a novel, perhaps oxidized, ring-closed species **RPc**, which exhibits thermal reversibility and consequentially reverts back to its ring-open form **RPo**. Two major reasons for the thermal back reaction of DAEs are discussed in the literature. i) Oxidation of the closed-form leads to a DAE cation which subsequently reverts to its ring-open form[53] or ii) the aromatic stabilization energy of the aryl moieties is increased to a point where the difference in ground state energies of ring-open and ring-closed forms becomes too high and the thermal bistability is lost.[24] Up to now it is unclear which one of the suggested effects the supposed oxidation reaction is inducing. Despite its unusual photochromic and aggregation behavior, **19** will be explored as suitable molecule to form water-soluble DA adducts with maleimide derivatives, as their photochromic behavior should differ to a certain extent from **19o** due to the altered furyl moiety.

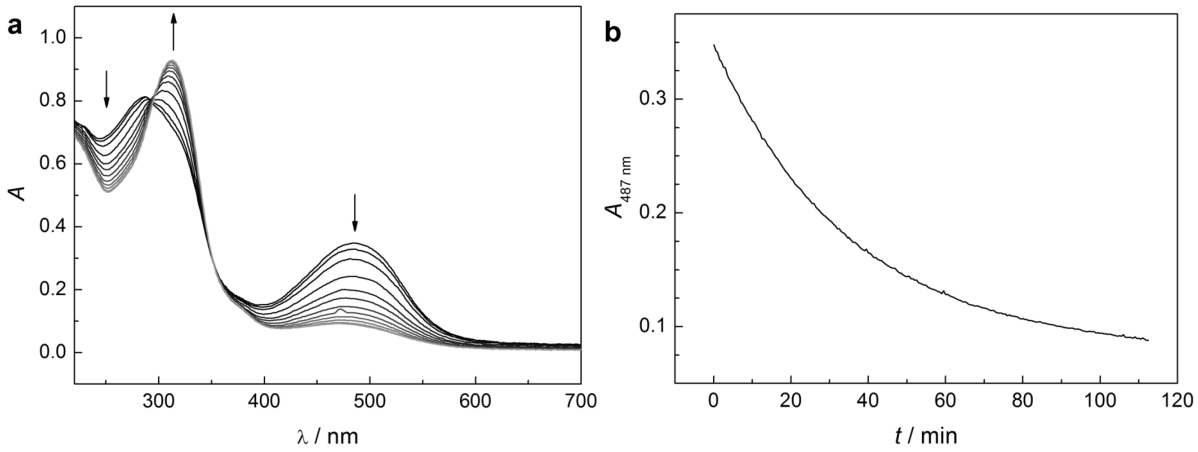

Figure 2-12: Reaction induced cycloreversion of **19c** after irradiation to the PSS with UV-light (λ_{irr} = 313 nm, $c \sim 10^{-5}$ M) at 25 °C in H_2O. a) Stacked UV/vis absorption spectra and b) exponential decay as observed at the absorption maximum of **19c** (487 nm) over time.

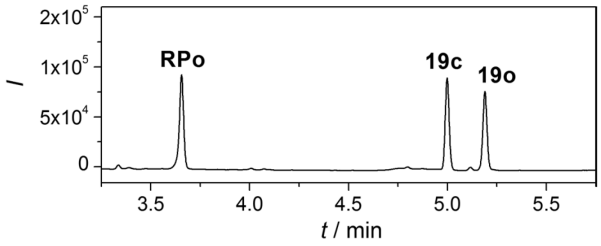

Figure 2-13: UPLC-MS DAD traces at 292 nm of DAE **19** in H_2O at the PSS after irradiation with light (λ_{irr} = 313 nm) composed of **19o**, **19c**, and reaction product **RPo**.

The DA adducts of **19** with maleimide and *N*-ethylmaleimide were considered for synthesis as both maleimide derivatives have been explored as catalytic TOP2 inhibitors as well as TOP2 poison antagonists in the literature.[193,194] Synthesis of maleimide adducts **22c** and **23c** can be carried out *via* two different routes (Scheme 2-7). The first route starts with ester **18** on which the DA reaction with the respective maleimide is subsequently performed to give adducts **20o** or **21o** in yields from 79–83% after chromatographic purification. These can then be irradiated preparatively in a photochemical chamber reactor with light of the wavelength λ_{irr} = 300 nm to yield their respective closed forms **20c** and **21c** which, in turn, can be saponificated quantitatively with NaOH to the corresponding sodium carboxylates **22c** and **23c**. While the latter step is generally quantitative, the preparative irradiation produces a decent amount of by-products that are difficult to separate by column chromatography. As additionally the intermediate ring-closed forms **20c** and **21c** are prone to oxidation, the received yields (< 38%) were rather poor. Thus, the first route was not identified as the ideal path towards the target compounds and only followed terminally in the case of adduct **22c**.

These considerations led to an alternative second route, which relies on the DA reaction of the respective maleimide derivative with the already water-soluble DAE **19** in EtOH to yield quantitative conversion to the respective DA adducts **22o** and **23o**. These are then converted to their corresponding ring-closed forms **22c** and **23c** on demand directly before the actual experiment by irradiation with light of the wavelength λ_{irr} = 313 nm generated by a 500 W medium pressure mercury lamp. This second route simplifies the handling of the compounds and also leads to target molecules of higher purity as the side-products produced during preparative irradiation in the photochemical reactor can be omitted.

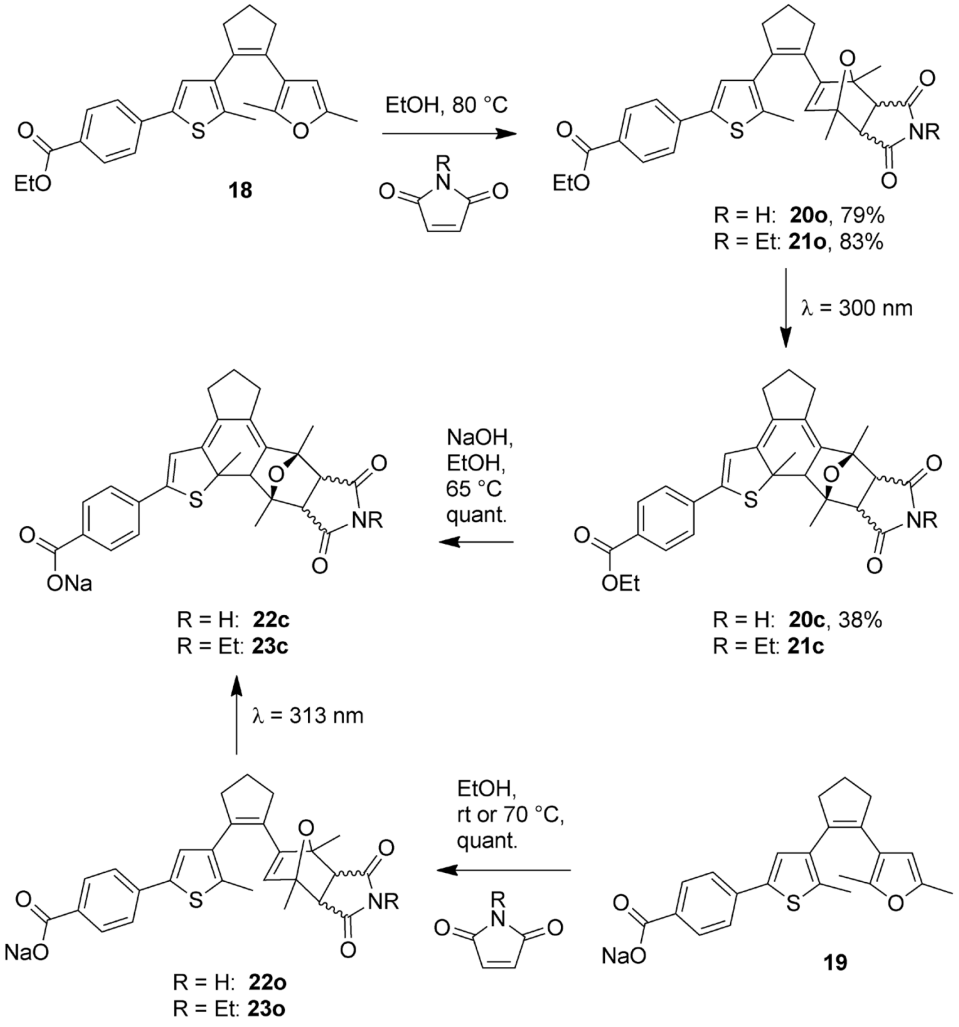

Scheme 2-7: Syntheses of water-soluble closed form maleimide and *N*-ethylmaleimide adducts **22c** and **23c**.

Expediently, the ratio of *endo* to *exo* stereoisomers produced in the DA reaction of **19** with the two different maleimides can be tuned simply by varying the reaction temperature. While furan **19** and maleimide were reacted at room temperature for 1 d to yield a mixture consisting of 40% of the *endo* and 60% of the *exo* isomer for adduct **22o**, stirring **19** and *N*-ethylmaleimide at 70 °C for 6 h led to almost exclusively (97%) the *exo* stereoisomer of **23o**.

While the *endo* to *exo* ratio can be fine-tuned regardless of the maleimide derivative employed, these two combinations were chosen to gain insight into their different release kinetics since the retro DA reaction of the *endo* stereoisomer is expected to take place at an increased rate as compared to the *exo* isomer (compare Chapter 2.2.3)

The molar absorptivities, absorption maxima, and composition at the PSS of DAEs **22** and **23** are summarized in Table 2-6. All irradiation experiments were performed in phosphate buffered saline (PBS), successfully verifying that switches **22** and **23** are applicable under *in vivo* conditions. Both derivatives almost quantitatively convert to their respective ring-closed forms **22c** and **23c** at the PSS after irradiation with UV-light. This can be observed in Figure 2-14a and Figure 2-15a and is indicated through the appearance of the characteristic bands at 412 nm. When employing light with a higher wavelength than 400 nm, the cycloreversion reaction from **22c** and **23c** to **22o** and **23o** is induced regenerating the ring-open isomers (Figure 2-14b and Figure 2-15b). Although the almost quantitative character of these ring-opening processes was confirmed by UPLC measurements, the absorption bands at 316 nm are not completely regenerated in the ring-open forms.

Table 2-6: Molar absorptivities, absorption maxima, and composition at the PSS of adducts **22** and **23** in PBS. Molar absorptivities should be regarded as preliminary as aggregation phenomena may alter them artificially.

ε / L mol^{-1}cm^{-1}				λ_{max} / nm				$PSS_{313\ nm}$ / %	
22o	**22c**	**23o**	**23c**	**22o**	**22c**	**23o**	**23c**	**22**	**23**
16700	11500	18500	12600	316	412	316	412	97	98

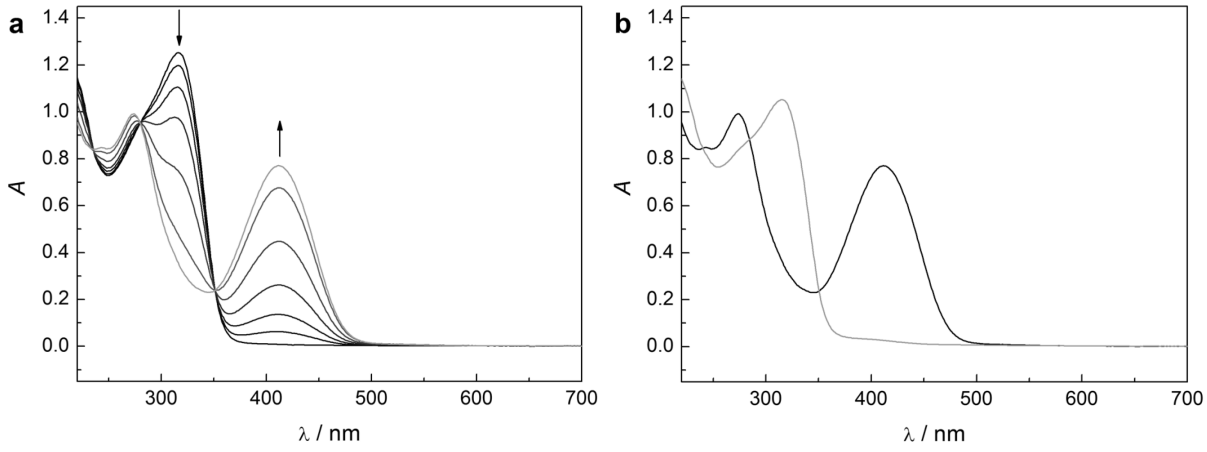

Figure 2-14: UV/vis absorption spectra during the course of a) ring-closure of DAE **22o** induced by irradiation with UV-light (λ_{irr} = 313 nm) and b) ring-opening of DAE **22c** induced by irradiation with vis-light (λ_{irr} > 400 nm) in phosphate buffered saline (PBS) (c ~ 7x10^{-5} M) at 25 °C.

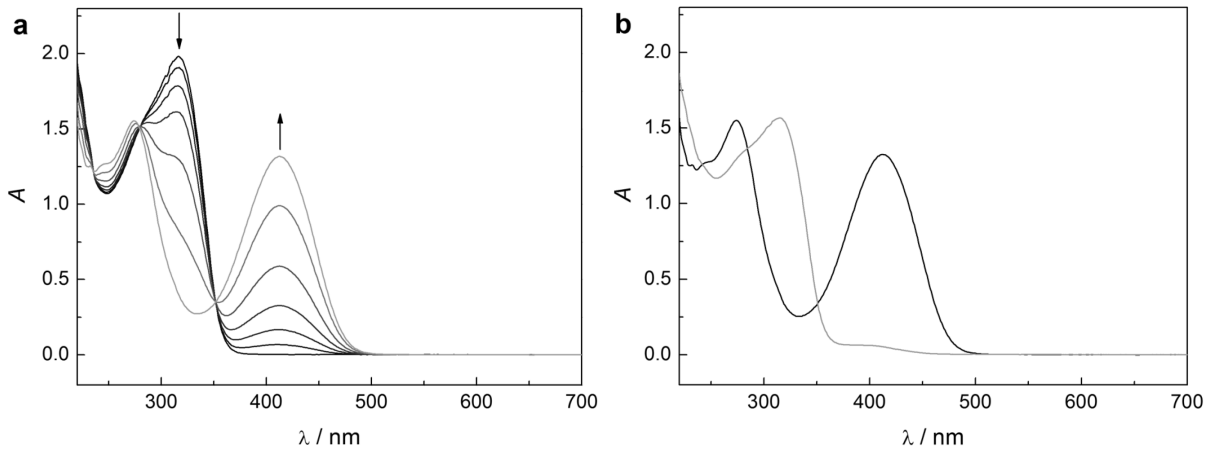

Figure 2-15: UV/vis absorption spectra during the course of a) ring-closure of DAE **23o** induced by irradiation with UV-light (λ_{irr} = 313 nm) and b) ring-opening of DAE **23c** induced by irradiation with vis-light (λ_{irr} > 400 nm) in phosphate buffered saline (PBS) ($c \sim 10^{-4}$ M) at 25 °C.

We attribute this phenomenon to the formation of aggregates in solutions of the ring-open forms that contribute to their molar absorptivities in that area and that are not homogeneously restored after the consecutive ring-opening reactions.

Importantly, a water-soluble furyl-substituted DAE **19o** has been designed that not only exhibits interesting aggregation behavior in aqueous solution but also performs a chemical reaction from its ring-closed form **19c** leading to a thermally reversible photochromic product. The usability of this system in the context of photoswitchable stoichiometric reactions still has to be explored. Moreover, two DA adducts **22** and **23** have been synthesized that are highly suitable for the release of maleimide in physiological media, as they combine all the necessary properties that are demanded: (i) they exhibit a high solubility in water as well as in PBS, (ii) their respective compositions at the PSS in physiological solution are outstanding, meaning that the ring-closed forms **22c** and **23c** can be generated basically quantitatively on demand without any further purification, and (iii) the ring-closed adducts can be transformed into their ring-open counterparts by irradiation with highly bioorthogonal visible light (λ_{irr} > 400 nm).

2.2.3 Photoinduced Release of Maleimide Derivatives

To prove the conceptual validity of triggering the release of maleimide derivatives from their respective adducts **22o** and **23o**, closed forms **22c** and **23c** have to be generated as they constitute the deactivated and presumably pharmacologically inactive form. This was realized *in situ* by irradiation of a 10^{-4} M solution of the corresponding ring-open forms **22o** and **23o**

until the photostationary state was reached (dashed lines in Figure 2-16a and Figure 2-16b). The ring-closed derivatives were then irradiated with vis-light ($\lambda_{irr} > 400$ nm) to regenerate the corresponding active ring-open forms **22o** and **23o** (grey solid lines in Figure 2-16a and Figure 2-16b) and subsequently heated at 80 °C to release maleimide or *N*-ethylmaleimide over time (black lines in Figure 2-16a and Figure 2-16b). Hence, it was demonstrated that the release of maleimide derivatives can be carried out quantitatively in PBS by applying high temperatures.

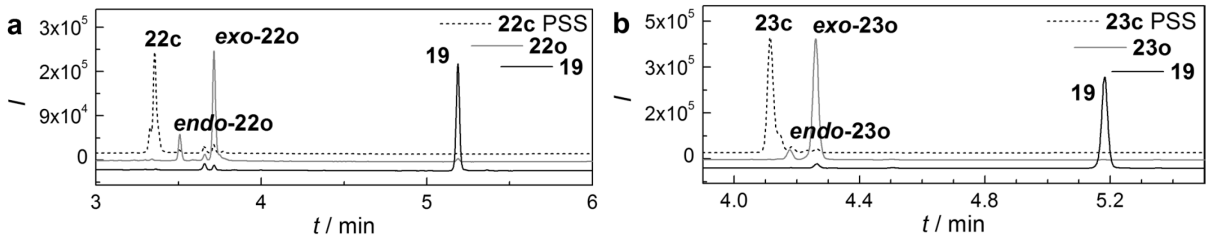

Figure 2-16: UPLC-MS DAD traces at 280 nm of the ring-closed DA adducts at the PSS, the ring-open DA adducts after irradiation with vis-light ($\lambda_{irr} > 400$ nm, 20 min) in PBS, and the successful release of a) maleimide after 3 h at 80 °C for **22c** and **22o** and b) *N*-ethylmaleimide after 5 h at 80 °C for **23c** and **23o**.

However, 80 °C are nowhere near to physiological temperatures and thus the release of maleimide from **22o** was investigated in detail at temperatures ranging from 40 °C to 80 °C (Figure 2-17). As expected, the retro DA reaction becomes increasingly slower with decreasing temperatures. Nevertheless, it can be seen that a continuous release of maleimide takes place even at 40 °C to an extent of about 50% after 92 h. However, as a mixture of the *endo* and *exo* stereoisomers of **22o** was employed for the retro DA reaction, the information content of Figure 2-17 seems rather limited and a detailed kinetic analysis of the release was carried out.

For this purpose, it is necessary to determine which reactions can actually take place in a solution of a mixture of an *endo* and *exo* DA adduct. From Scheme 2-8 it can be extracted that for the complete kinetic description of the reaction system the forward (DA) reactions from the starting materials to either *endo* or *exo* adducts, represented through their respective rate constants k^{f}_{exo} and k^{f}_{endo}, as well as the backward (retro DA) reactions, represented through their respective rate constants k^{b}_{exo} and k^{b}_{endo}, have to be taken into account. Evidently, the resulting system of rate equations cannot be solved analytically and hence some simplifications are necessary.

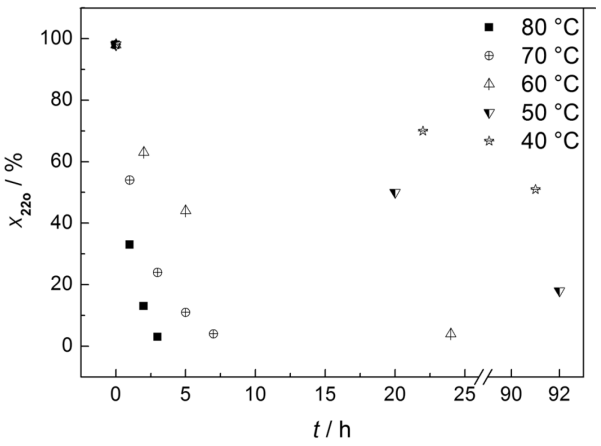

Figure 2-17: Retro DA reaction of **22o** to **19** and maleimide at different temperatures in PBS as visualized by the evolution of the adduct's molar fraction *x* over time. The compositions of the reaction mixtures were determined by integrating the peak areas of the DAD detector at 280 nm after UPLC measurements.

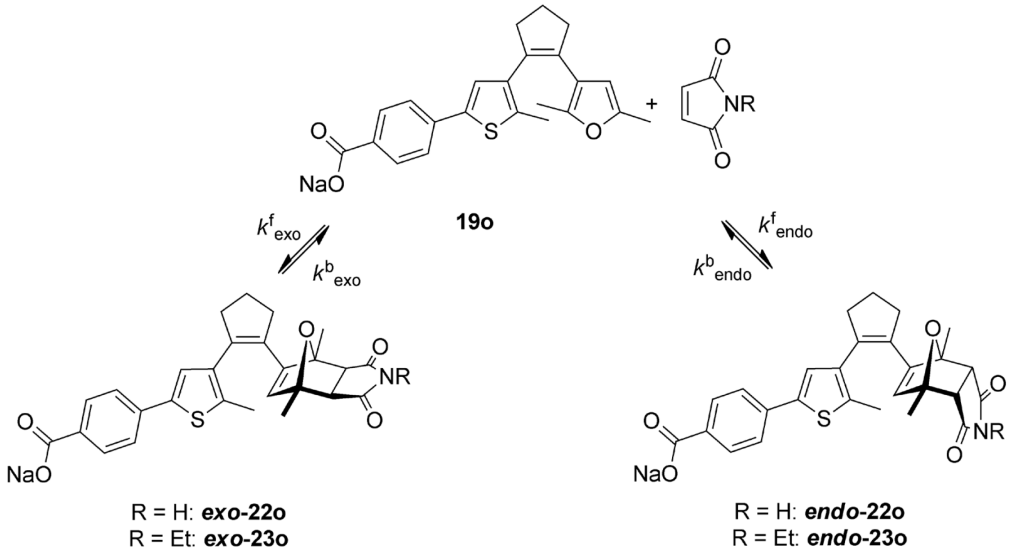

Scheme 2-8: Reversible DA reaction between DAE **19** and maleimide derivatives leading to either *endo* or *exo* stereoisomers of **22o** and **23o** respectively.

Our primary interest lies in the release of maleimide and thus in the rate constants for the retro DA reaction k^b. The retro DA reaction from adducts **22o** and **23o** to switch **19** is a unimolecular reaction and thus follows first-order kinetics (Scheme 2-8). The differential rate equation – exemplarily expressed through the concentration of the *exo* adduct – accordingly yields the expression

$$\frac{\mathrm{d}\,c_{\mathrm{exo}}}{\mathrm{d}\,t} = \dot{c}_{\mathrm{exo}} = k^{\mathrm{f}}_{\mathrm{exo}} \cdot c_{\mathbf{19}} \cdot c_{\mathrm{mal}} - k^{\mathrm{b}}_{\mathrm{exo}} \cdot c_{\mathrm{exo}} \tag{2.1}$$

where contributions of DA as well as retro DA reactions are taken into account through their respective rate constants k and concentrations of the participating species c. As at any given point of the reaction $c_{\mathbf{19}} = c_{\mathrm{mal}}$, Equation (2.1) can be simplified to

$$\dot{c}_{\mathrm{exo}} = k^{\mathrm{f}}_{\mathrm{exo}} \cdot c^2_{\mathbf{19}} - k^{\mathrm{b}}_{\mathrm{exo}} \cdot c_{\mathrm{exo}} . \tag{2.2}$$

However and as stated beforehand, no analytic solution for any of these expressions can be found. Conveniently, with decreasing adduct concentrations the bimolecular forward DA reaction becomes increasingly insignificant as the term $k^{\mathrm{f}}_{\mathrm{exo}} \cdot c^2_{\mathbf{19}}$ decreases faster than $k^{\mathrm{b}}_{\mathrm{exo}} \cdot c_{\mathrm{exo}}$. Consequently, Equation (2.2) can be approximated to

$$\dot{c}_{\mathrm{exo}} = -k^{\mathrm{b}}_{\mathrm{exo}} \cdot c_{\mathrm{exo}} \tag{2.3}$$

in diluted solutions and integrated to yield the expression

$$c_{\mathrm{exo}} = c_0 \cdot e^{-k^{\mathrm{b}}_{\mathrm{exo}} \cdot t} \tag{2.4}$$

with c_0 being the *exo* adduct's concentration at $t = 0$. Finally the rate constant can be determined by logarithmic conversion to

$$\ln\left(c_{\mathrm{exo}}\right) = -k^{\mathrm{b}}_{\mathrm{exo}} \cdot t + \ln\left(c_0\right) \tag{2.5}$$

as this expression represents a linear relationship and thus k can be extracted from the slope by simple linear regression. Certainly, equivalent expressions can be formulated for all equations with respect to the *endo* stereoisomer employing c_{endo}.

For the determination of the rate constants of the retro DA reaction the individual evolution of the *endo* and *exo* adducts of **22o** (60% *exo*, 40% *endo*) and **23o** (97% *exo*, 3% *endo*) in 10^{-4} M solutions in PBS was followed over time by integrating the DAD signal of the corresponding UPLC traces at $\lambda = 280$ nm where the DA adducts as well as **19o** exhibit approximately the same molar absorptivities (Figure 2-18). A number of expected features can be extracted from this set of figures: i) The release of maleimide is faster at 40 °C than it is at 37 °C, and ii) the release of maleimide from the *endo* stereoisomer is faster than from the corresponding *exo* stereoisomer. However, it is also easily recognized that the evolution of the individual concentrations does not follow the expected exponential decay. Instead, for the

retro DA reaction of **22o** to **19** even an intermediate increase in the amount of *exo* stereoisomer is observed completely contradicting the simplifications applied to the rate equations earlier. Thus, the forward DA reaction cannot be neglected despite supposedly being multiple orders of magnitude more slowly.

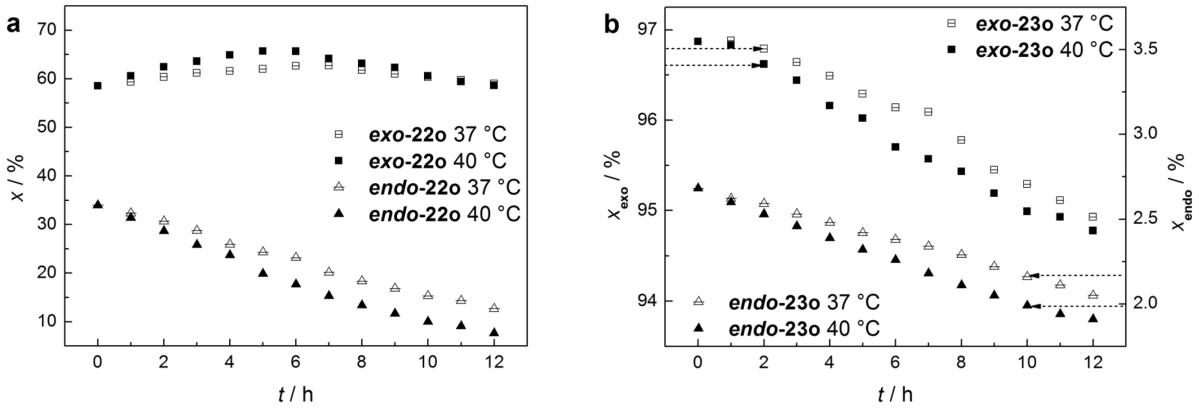

Figure 2-18: Retro DA reaction at 37 °C and 40 °C in PBS as visualized by the evolution of the *endo* and *exo* adduct's molar fraction *x* over time as determined by UPLC measurements of a) **22o** to **19** and maleimide and b) **23o** to **19** and *N*-ethylmaleimide. Ratios recorded at $t = 0$ h can slightly deviate from the ratios determined directly after synthesis as retro DA reaction did already set in.

As direct interconversion of the stereoisomers is not possible without performing the forward or backward DA reaction,[158] it is reasonable to assume that the predicted reaction pathway must be different from the pathway observed. As the forward DA reaction follows bimolecular kinetics, it is apparent that the concentrations of **19** and the respective maleimide derivative are the critical variables that have to be considered in detail. Hence, it may be possible that the effective concentration of the reactants deviates from the concentration of 10^{-4} M that would be expected in homogeneous solution. One way to rationalize the observed effects leading to the intermediate formation of ***exo*-22o** is to assume aggregation in aqueous solution causing increased local concentrations. An additional step that describes the association to (*via* k^{a}) as well as the dissociation from the aggregate (*via* k^{d}) could describe how after triggering the retro DA reaction the maleimide derivative is not covalently bound in the adduct anymore but trapped inside an aggregate increasing its effective concentration in the vicinity of unreacted **19o** (Scheme 2-9). Eventually, the forward DA reaction becomes relevant and not negligible when the dissociation from the adduct to homogeneous solution is slow enough, *i.e.* $k^{d} < k^{f}$.

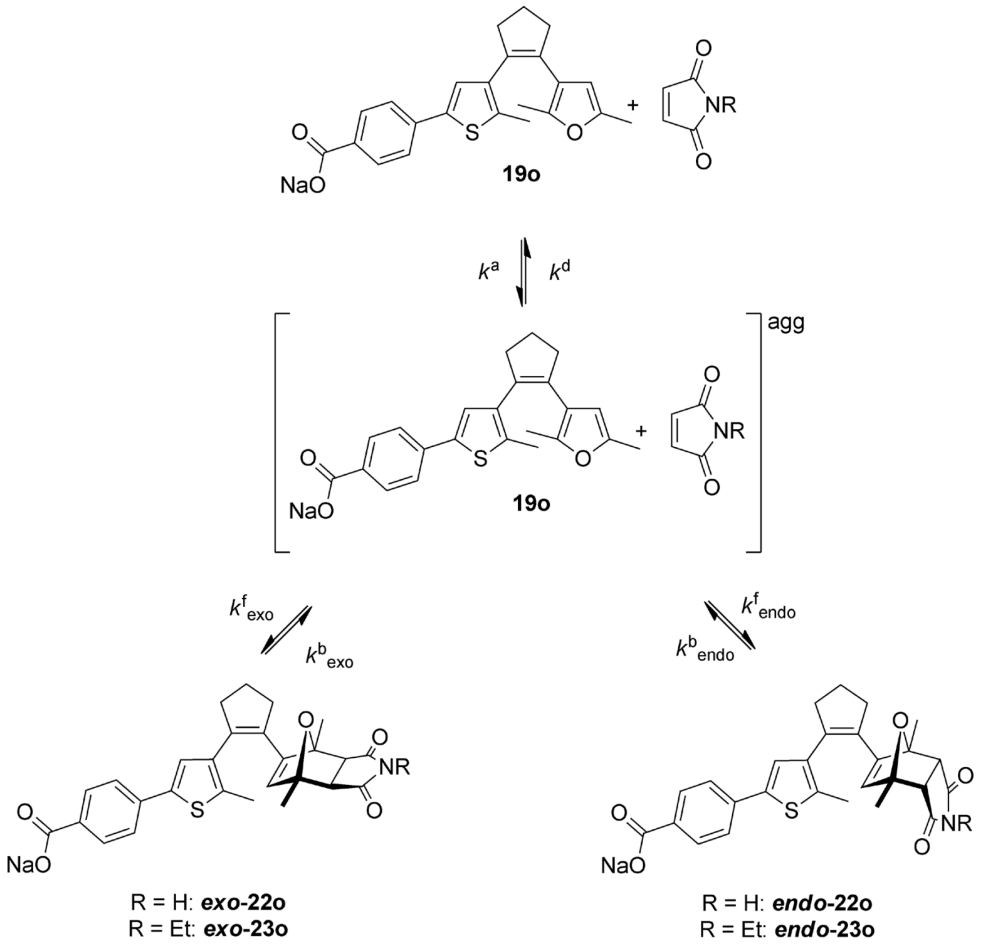

Scheme 2-9: Reversible DA reaction between DAE **19** and maleimide derivatives via association and dissociation to aggregates leading to either *endo* or *exo* stereoisomers of **22** and **23** respectively.

To gather hints whether the phenomenon is indeed related to aggregation, the release of maleimide from **22o** (60% *exo*, 40% *endo*) in a deaggregating solvent mixture (H_2O:THF:MeCN = 2:1:1) was followed at 40 °C by UPLC measurements (Figure 2-19). As can be seen in Figure 2-19a and as opposed to the measurements in PBS, the amount of ***exo*-22o** is not increasing in the deaggregating solvent mixture but conversely follows the initially expected exponential rate law. Moreover, Figure 2-19b reveals a linear relationship between the natural logarithm of the concentrations of ***exo*-22o** or ***endo*-22o** against the reaction time thus confirming the simplifications applied to yield Equation (2.5) and its pseudo first-order kinetics.

Inconveniently, this finding renders the simplifications applied to analytically solve the rate equations invalid when applied to the retro DA reaction in aggregation-inducing solvents such as PBS. Moreover, a thorough determination of the actual rate constants for the retro DA reaction in PBS would yield no noteworthy insight into the release dynamics as the back

reaction might not be the rate-determining step. Thus, it becomes necessary to compare the released amounts of the respective maleimide derivative directly.

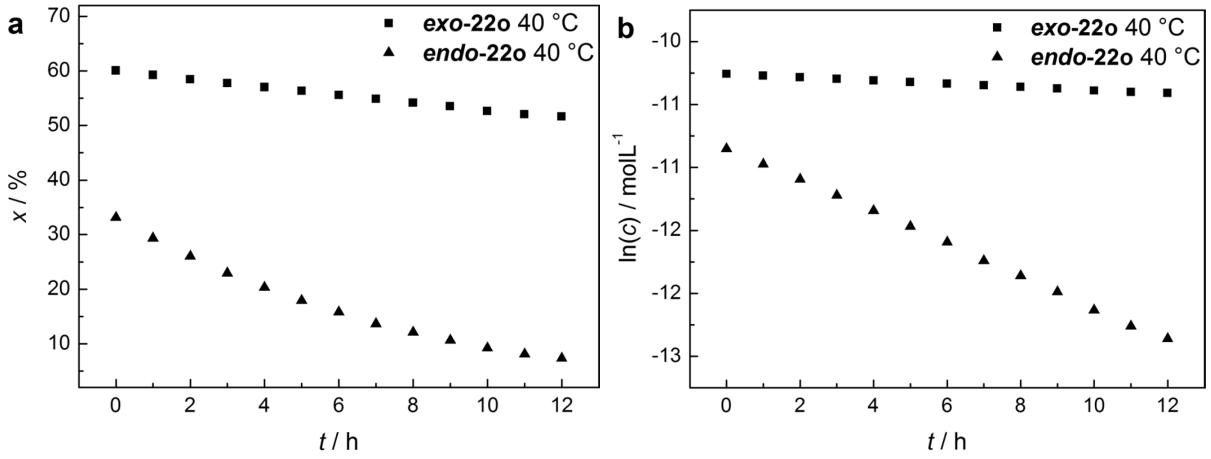

Figure 2-19: Retro DA reaction of **22o** (60% *exo*, 40% *endo*, 5×10^{-5} M) to **19** and maleimide at 40 °C in deaggregating solvent mixture (H_2O:THF:MeCN = 2:1:1) over time as visualized by the evolution of the *endo* and *exo* adduct's a) molar fraction *x* and b) natural logarithm of their concentration ln(*c*).

From the data presented in Figure 2-18, the overall concentration of released maleimide c_{MI} – or *N*-ethylmaleimide c_{NEM}, respectively – can be calculated at any point of the reaction according to

$$c = \frac{100 - x_{\mathrm{endo}} - x_{\mathrm{exo}}}{100} \cdot c_0 \tag{2.6}$$

and the graphs resulting thereof are presented in Figure 2-20. Since $k^{\mathrm{b}}_{\mathrm{endo}}$ is expected to be at least one order of magnitude higher than $k^{\mathrm{b}}_{\mathrm{exo}}$, the release of maleimide from **22o** (consisting of 40% *endo* isomer) is with 46 $\mu M d^{-1}$ at 37 °C and 59 $\mu M d^{-1}$ at 40 °C unsurprisingly much higher than the release of *N*-ethylmaleimide from **23o** (consisting of 3% *endo* isomer) with 5 $\mu M d^{-1}$ at 37 °C and 6 $\mu M d^{-1}$ at 40 °C. These daily concentrations are estimated from the release that was monitored over 12 h and most importantly lie in the range of therapeutic applicability suitable for *in vivo* applications.[194] Furthermore, these results show the possibility to conveniently fine-tune the amount of released maleimide derivative over time by synthesizing DA adducts with varying *endo* to *exo* stereoisomer compositions: While a higher *endo* fraction ensures a larger initial release of maleimide, a higher *exo* fraction leads to a slower release creating a 'depot effect'. Figure 2-20a and Figure 2-20b also show that the release from the deactivated ring-closed forms is negligible and can be disregarded. Another

feature potentially useful for *in vivo* application is the increased release rate at 40 °C as compared to 37 °C. As tumor tissue tends to exhibit higher metabolic activity than unaffected tissue, the release of maleimide derivatives can be particularly stimulated in those areas.

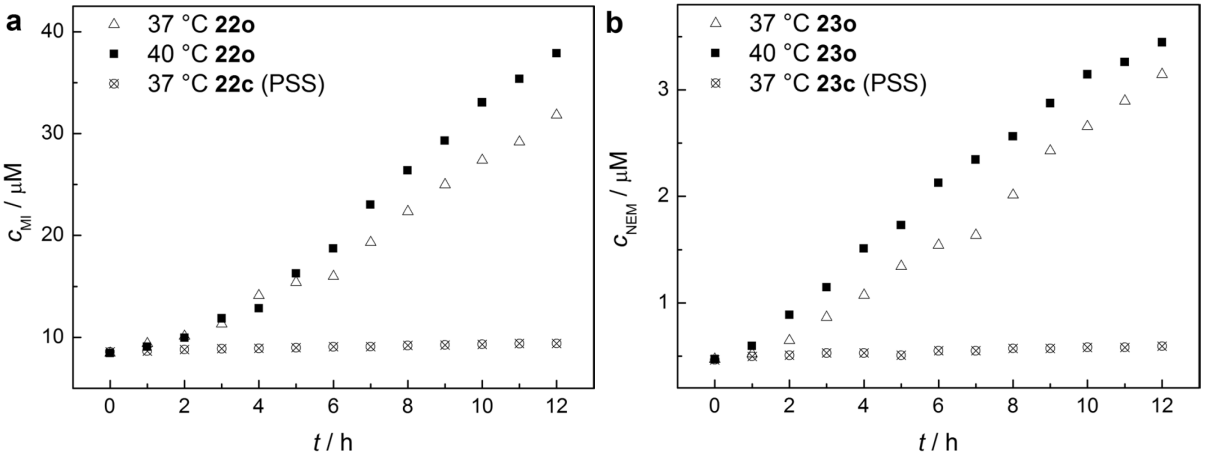

Figure 2-20: Retro DA reactions at 37 °C and 40 °C, respectively, in PBS ($c = 1\times10^{-4}$ M) as visualized by the evolution of the concentration c of a) maleimide released from **22o** and b) *N*-ethylmaleimide released from **23o** over time compared to the release from the respective closed form adducts **22c** and **23c**.

Moreover, the reversibility of the switching process in DAEs in combination with the slow thermal release allows for the 'on' and 'off' switching of the maleimide release *in situ* (Figure 2-21).

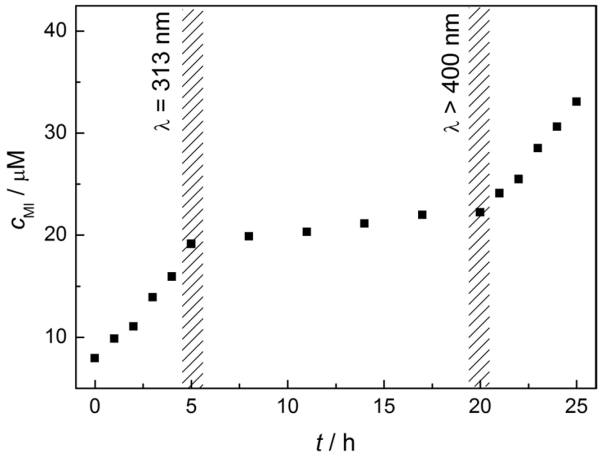

Figure 2-21: Switching the release of maleimide *in situ* 'off' from **22o** to **22c** (λ = 313 nm for 9 min) and 'on' again from **22c** to **22o** (λ > 400 nm for 20 min) at 40 °C in PBS ($c = 1\times10^{-4}$ M) as visualized by the evolution of the concentration of maleimide c_{MI} over time.

Besides the activation of the retro DA reaction by ring-opening **22c** to **22o** with vis-light, the release of maleimide could subsequently be inhibited to a wide extent by ring-closing

unreacted **22o** back to **22c** by UV-light *in situ* rendering this system potentially useful in the context of photopharmacology where the prodrug could be switched 'off' after the desired effect on the organism was observed. The system then remains inactive for the chosen time and can subsequently be reactivated on demand allowing for the release of maleimide again.

In conclusion, maleimide and *N*-ethylmaleimide could be successfully released from their corresponding DA adducts **22o** and **23o** under physiological conditions (*i.e.* at body temperature and in aqueous buffer). The active ring-open forms could be generated *in situ* by irradiation with highly bioorthogonal vis-light from their respective ring-closed forms **22c** and **23c**, the latter of which were shown not to exhibit any significant release behavior. Not only lies the amount of released maleimide derivative in the pharmacologically active μM range, it could also be stimulated conveniently by higher temperatures (as in tissue with higher metabolic activity) or the initial ratio of *endo* to *exo* stereoisomer. While a high *endo* fraction ensures immediate release, a high *exo* fraction is useful when a depot, releasing small amounts of maleimide over days, is desired. Additionally, the photoreversible character of the DAEs could be exploited to switch the adduct's release activity 'off' and 'on' again enabling *in situ* control over when the maleimide is being released.

2.2.4 Aggregation Behavior of Furyl DAE 19o

In Chapter 2.2.2, Figure 2-11 we deduced from the scattering observed when performing UV/vis spectroscopy in PBS that furyl-substituted DAE **19o** might be prone to an aggregation process dependent on the nature of the solvent employed. The formation of aggregates is highly dependent on a variety of external effects, *i.a.* concentration, *p*H, or ionic strength. Likewise, the molecular shape and relative orientation of substituents, in particular polar groups, govern the type of aggregates formed.

Though DAE **19o** exhibits no characteristically long, nonpolar chain and is thus unlikely to form typical micelles or vesicles in water, the concentration dependence of aggregation was investigated using techniques usually employed to determine critical micelle concentrations (CMCs).[251] For this purpose a 3.4×10^{-4} M solution of 1-(2-pyridylazo)-2-naphthol (PAN) in pentane was added to differently concentrated dispersions of **19o** in water. PAN as probe molecule is insoluble in aqueous solvents and indicates its inclusion into aggregates when a signal in the visible range of the spectrum can be measured. For that purpose, a UV/vis spectrum has to be recorded before and after the addition of PAN as illustrated in Figure 2-22a. The difference in absorbance ΔA at the absorption maximum

λ = 476 nm is then plotted against the concentration of the surfactant DAE **19o** (Figure 2-22b). The inclusion of PAN was first detected at a concentration of **19o** of 2×10^{-3} M, hinting towards the existence of a critical aggregation concentration (CAC) below which no aggregation takes place.

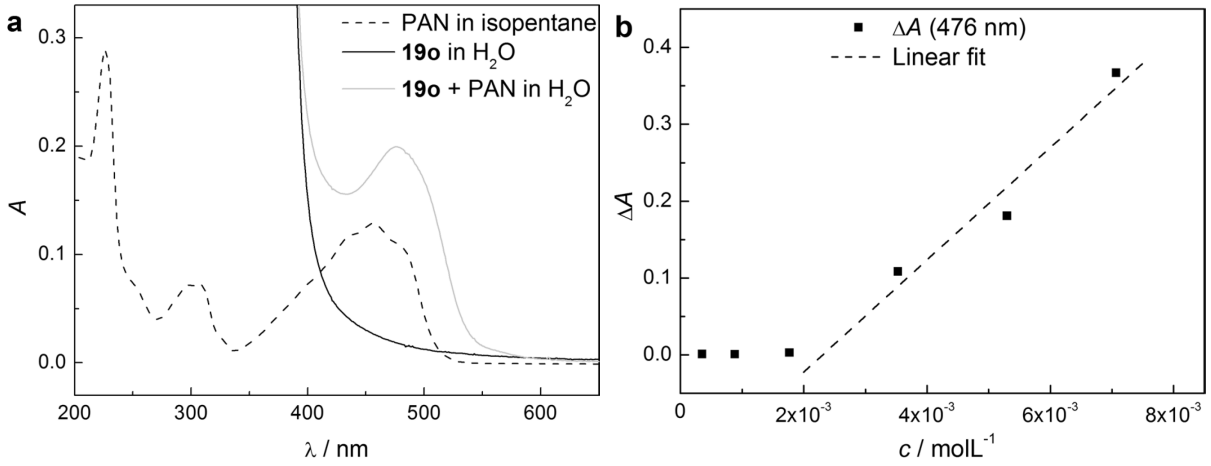

Figure 2-22: Investigation of concentration dependence of the aggregation behavior of DAE **19o** in H_2O by UV/vis spectroscopy employing PAN as probe molecule. a) Exemplary UV/vis spectra of PAN in isopentane ($c = 1\times10^{-5}$ M), **19o** in water ($c = 5.3\times10^{-3}$ M), and **19o** in water ($c = 5.3\times10^{-3}$ M) with PAN evaporated from 200 µL of a solution in isopentane ($c = 3.4\times10^{-4}$ M) for illustration. b) Difference in absorbance ΔA at λ = 476 nm plotted against the concentration of **19o**.

To verify that assumption dynamic light scattering (DLS) was performed on solutions with three different concentrations lying i) below, ii) in the range of, and iii) above the assumed CAC (Figure 2-23).

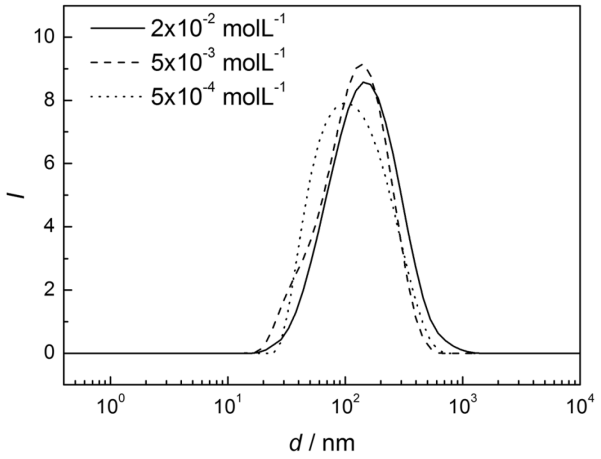

Figure 2-23: Investigation of concentration dependence of the aggregation behavior of DAE **19o** in H_2O by DLS measurements.

However, for all samples a similar signal was recorded indicating the existence of aggregates independent of concentration. An estimation of the aggregate size from these measurements appears not to be practicable as the shape of the aggregates is unknown.

Eventually, the results obtained from DLS measurements seem to contradict the finding that a CAC of 2×10^{-3} M exists. This discrepancy is most likely caused by the inapplicability of the spectro-photometric method (solvatochromism of the PAN probe) in this case. However, a definitive statement over the nature of the formed aggregates would require more elaborate techniques, such as cryo-electron microscopy, to directly observe the formed structures. In addition to the intriguing results concerning water-soluble switch **19** in the context of photoswitchable stoichiometric reactions tangentially covered in Chapter 2.2.2, the observed aggregation phenomena leave a lot of room for exploration and interpretation and could prospectively prove useful in the field of photoswitchable microenvironments and nanoreactors.

2.3 Furyl DAEs for the Reversible Covalent Functionalization of Carbon Nanotubes

2.3.1 Conceptual Outline

In Chapter 1.7 the functionalization of CNTs and furans *via* the DA reaction was introduced. A number of features were highlighted that are advantageous for this modification of sp^2-carbon allotropes, such as the non-covalent approach's reversibility and ability to regenerate an undisturbed π-lattice as well as the covalent approach's characteristically strong bonds. Employing light as a trigger to regulate this reversibility could offer a new and unprecedented level of control, especially over when and where the reversibility is switched 'on' or 'off'. Conceptually, the DA reaction of a furyl-substituted DAE with a CNT (or carbonaceous sp^2-lattice in general) is closely related to the idea of controlling covalent connection and disconnection by light that was highlighted in Chapter 2.1.[95] Scheme 2-10 summarizes the different stages that could potentially occur.

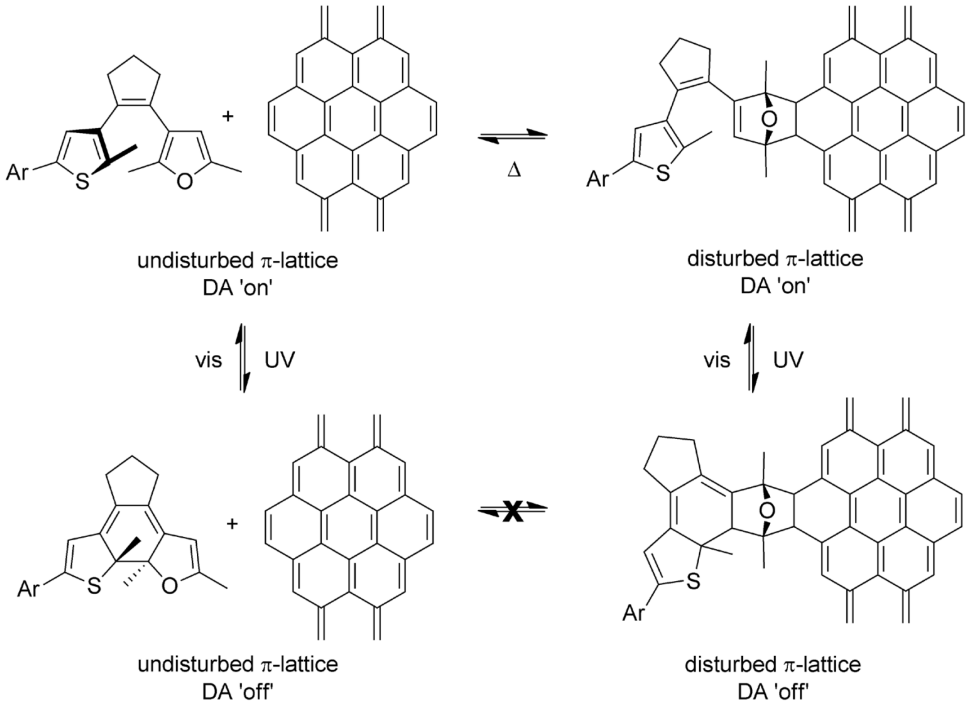

Scheme 2-10: General scheme of a DA reaction between a furyl-substituted DAE and generic, dienophilic sp^2-carbon lattice, as part of a graphene sheet.

As already established earlier, the furyl-substituted DAE could participate in a thermal DA equilibrium between its unreacted form and the adduct with the respective carbonaceous material. Both forms incorporating a DAE moiety should retain their photochromic properties

and thus be convertible reversibly to forms that switch 'off' the possibility to participate in the thermal DA equilibrium.

Besides its potential to photochemically modulate the electronic properties of the π-electron system of a CNT depending on the functionalization density, the presented system could furthermore be used to reversibly attach solubility promoting groups to the CNT. By connecting furyl DAEs bearing specifically designed solubilizing groups on their aryl moieties via the DA reaction to CNTs, a photoinduced alteration of the CNTs' solubility could be achieved. This modification would prove particularly useful in photolithography applications (Figure 2-24). A film of functionalized CNTs casted on a surface could be irradiated with UV-light through a mask to only ring-close the DAE-CNT adducts where the irradiation occurred. Afterwards, the substrate could be heated inducing the retro DA reaction only on the compartments on the surface that have not been irradiated. Subsequent washing would only remove the 'solubility-locked' CNTs leaving an inverse pattern of pristine CNTs on the substrate.

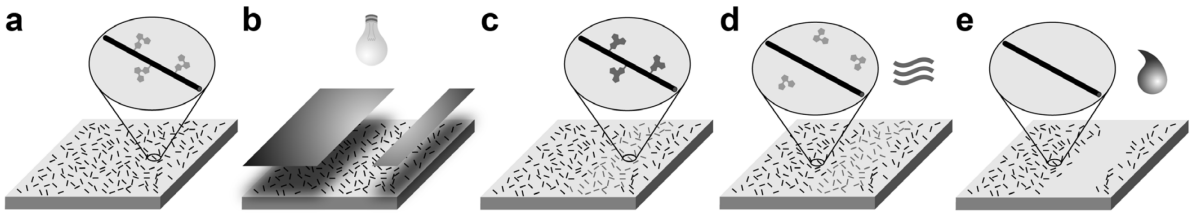

Figure 2-24: Conceptual depiction of a photolithographic process involving CNTs reversibly functionalized with furyl-substituted DAEs. a) CNTs functionalized with solubility-promoting DAEs, b) irradiation through a mask, c) selectively ring-closed and thus 'solubility-locked' fraction of the DAEs, d) heating of the substrate induces retro DA on non-irradiated fraction regenerating pristine CNTs, e) 'solubility-locked' fraction is washed away to yield negative.

Employing water-soluble furyl-substituted DAEs as solubility promoters would have the advantage to simplify analysis of the functionalized CNTs as water gives only weak reflexes in Raman spectroscopy. Hence, DAE **19o** introduced in Chapter 2.2 is envisioned as ideal candidate for this purpose. Eventually, it is important to remark that there are not many examples reported in the literature where DAEs are photoswitched in the vicinity of CNTs. Besides the covalent bridging of two tubes with different DAEs via their termini[252–255] and the blending of CNTs and DAEs in a transistor,[256] the surface or side-wall functionalization of CNTs has, to the best of our knowledge, never been carried out. Thus, it is unclear whether

the attached DAE would retain its switching performance after the functionalization event or if excitation quenching would occur.[201]

2.3.2 Functionalization and Characterization of CNTs

Before the functionalization of CNTs with target molecule **19o** can be carried out, test reactions trying to reproduce results from the literature and to optimize the reaction conditions had to be performed. As reversible covalent functionalization on CNTs is described in the literature with furfuryl alcohol (FA), it was one of the two probe molecules selected for the test reactions.[209,210] Furthermore, 3-acetyl-2,5-dimethylfuran (ADMF) was predicted to sufficiently resemble **19o** sterically as well as electronically (Scheme 2-11).

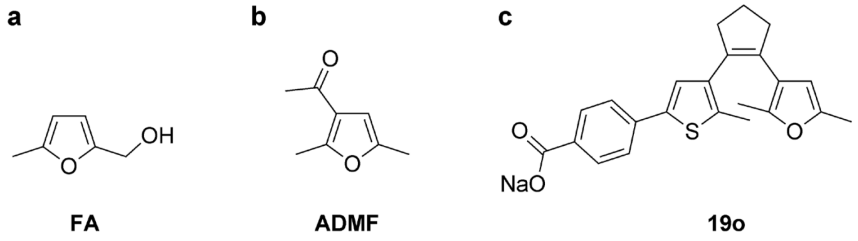

Scheme 2-11: Structural formulas of a) furfuryl alcohol, b) 3-acetyl-2,5-dimethylfuran, and c) DAE **19o**.

Various iterations of test reactions were run until proper reaction conditions were found for the DA functionalization of MWCNTs. Stirring a solution of the respective furan at 50 °C in DMSO over 3 d seemed to give most pronounced results as detected by FTIR spectroscopy and thermogravimetric analysis (TGA). Figure 2-25a shows that after the functionalization with furfuryl alcohol, an absorption band at ca. 900 cm^{-1} is visible in the IR spectrum as compared to the pristine MWCNTs and can be attributed to the C–O-stretch movement.[209] However, other expected absorption bands, such as for the C=C- or C–H-stretch movements of the resulting adduct could not be detected. TGA measurements reveal that the tubes lose approximately 2% more of their mass as compared to the pristine MWCNTs until decomposition sets in (Figure 2-25b). However, a degree of functionalization of 10% and more, such as observed by Chang and Liu in 2009, could not be reproduced.[209]

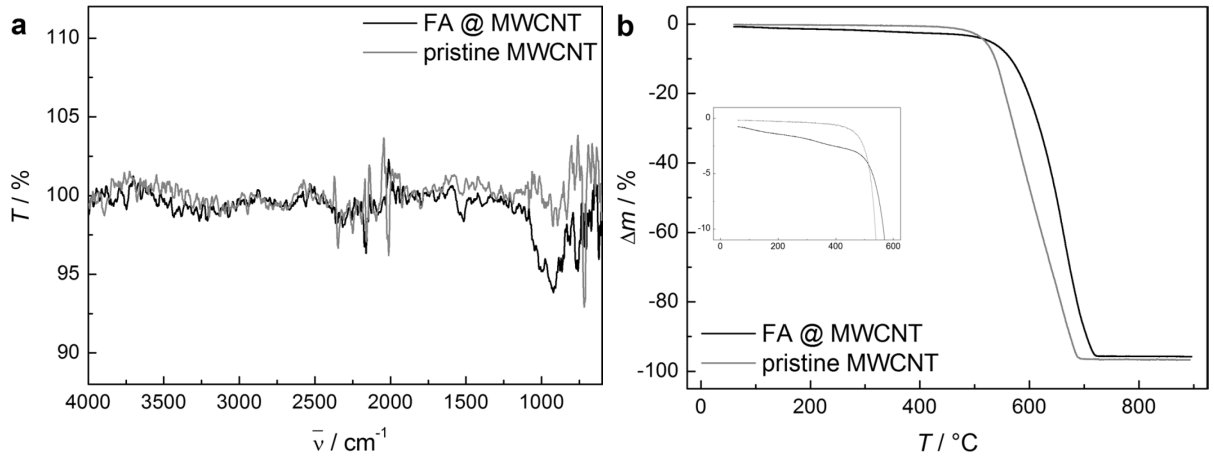

Figure 2-25: Comparison of the FTIR and TGA measurements of MWCNT before and after the reaction with FA for 3 d at 50 °C in DMSO.

Analogous results were obtained for the reaction of ADMF and MWCNTs in DMSO. Figure 2-26a expectedly misses the C–O-stretch absorption band visible in Figure 2-25a as no C–O single bond is existing in that adduct. Yet, neither the anticipated C=O-, C=C-, nor the C–H-stretch absorptions could be observed in the IR spectra after the DA reaction. The results obtained by TGA measurements for this adduct resemble the data produced from the reaction with furfuryl alcohol (Figure 2-26b). Approximately 2.5% of weight loss was found when compared to the same batch of pristine MWCNTs.

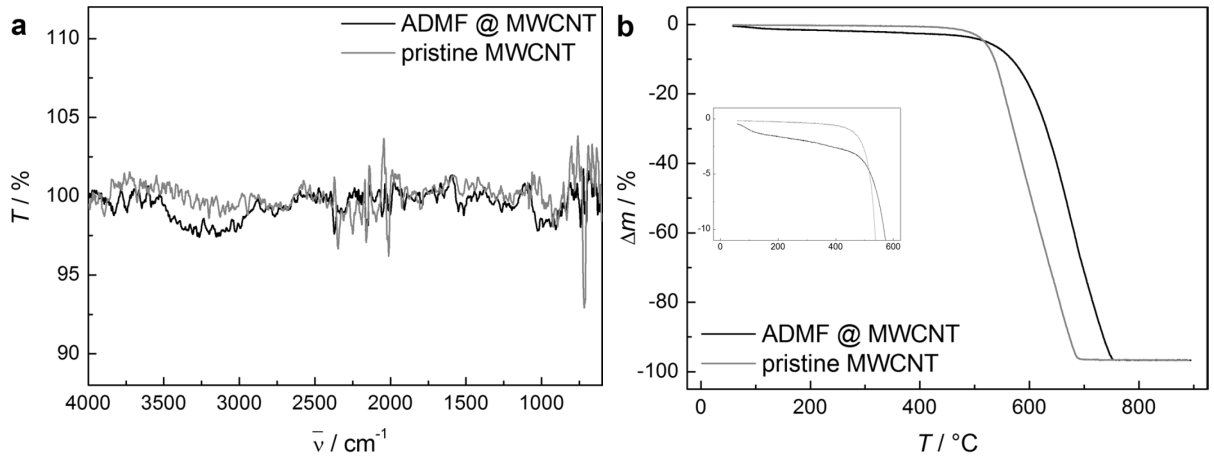

Figure 2-26: Comparison of the FTIR and TGA measurements of MWCNT before and after the reaction with ADMF for 3 d at 50 °C in DMSO.

Even though these results were not unambiguous about whether the DA functionalization had actually taken place or not, we were encouraged to submit furyl-substituted DAE **2o** to the same conditions. As can be extracted from Figure 2-27a, again none but a broad absorption band at ca. 900 cm^{-1} could be observed upon performing FTIR

spectroscopy on the processed tubes. TGA measurements also resembled the ones carried out in the test reactions beforehand with an approximate weight loss of about 2–2.5% as compared to the pristine MWCNTs (Figure 2-27b).

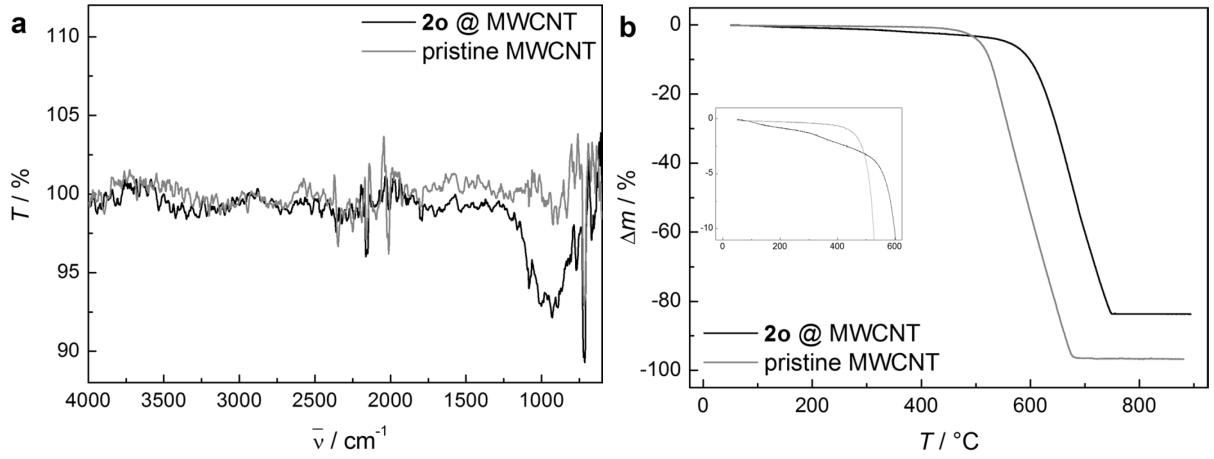

Figure 2-27: Comparison of the FTIR and TGA measurements of MWCNT before and after the reaction with **2o** for 3 d at 50 °C in DMSO.

The apparent resemblance of all the gathered data despite employing three different molecules strongly suggested that another process than the actual DA functionalization had taken place. To rule out unwanted side-reactions, the MWCNTs were heated in a blank test at 50 °C for 3 d in DMSO without any further additives and analyzed with the same methods that have been used earlier. Figure 2-28a reveals a strong similarity between the FTIR spectra of the pristine and the processed MWCNTs received from the blank test.

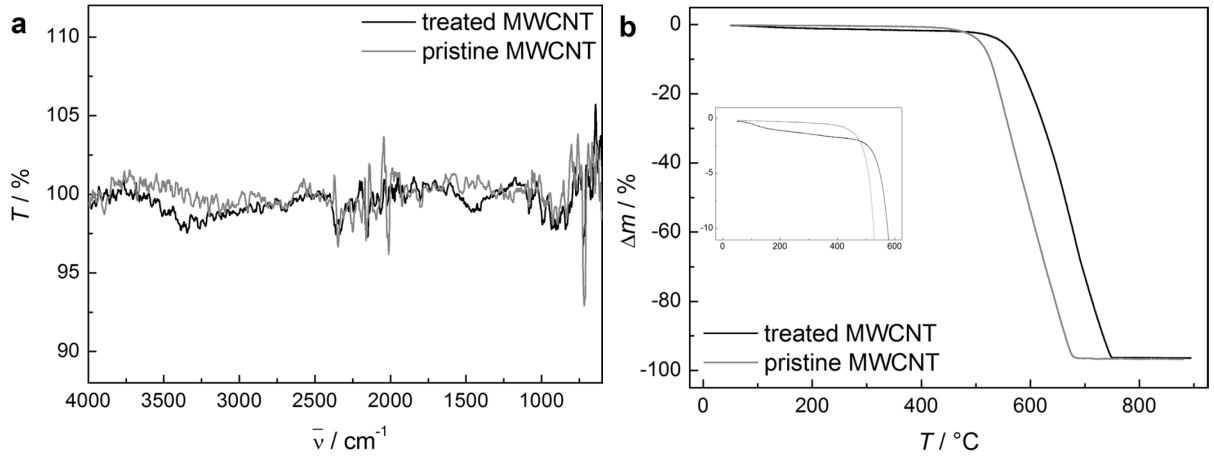

Figure 2-28: Comparison of the FTIR and TGA measurements of MWCNT before and after heating at 50 °C for 3 d in DMSO.

However, TGA analysis clearly shows that the MWCNTs are altered by stirring them in DMSO as they exhibit the same mass loss of 2–2.5% that was observed after the assumed DA functionalization. Unwanted oxidation reactions and/or the introduction of defects as well as adsorbed residual solvent could be the reason for that behavior. The latter would also explain the absorption band at 900 cm^{-1} observed in Figure 2-25a and Figure 2-27a as DMSO exhibits strong IR absorption in that region.

To exclude that the DA functionalization was actually taking place yet it could just not be detected properly, the substrate was altered to more defined SWCNTs. Importantly, SWCNTs exhibit a higher surface to overall mass ratio and thus a functionalization event should be detectable more easily. Target switch **19o** was subjected to the same reaction conditions as used earlier (50 °C, 3 d) while instead of DMSO water was employed as solvent to avoid the suspected unspecific oxidation reactions. From Figure 2-29a it can be seen that the IR spectra of the pristine SWCNTs and the supposedly DA-functionalized SWCNTs are identical as far as possible. From the TGA data, however, a significant change when compared to the pristine SWCNTs can be observed. Figure 2-29b clearly shows a mass loss of approximately 5% at a temperature around 200 °C. The delay in decomposition as compared to the pristine SWCNTs is also peculiar. However, this behavior is attributed to the removal of residual transition metal catalyst during the washing steps, as these SWCNTs have been synthesized *via* chemical vapor deposition (CVD) using CoMoCAT catalyst.

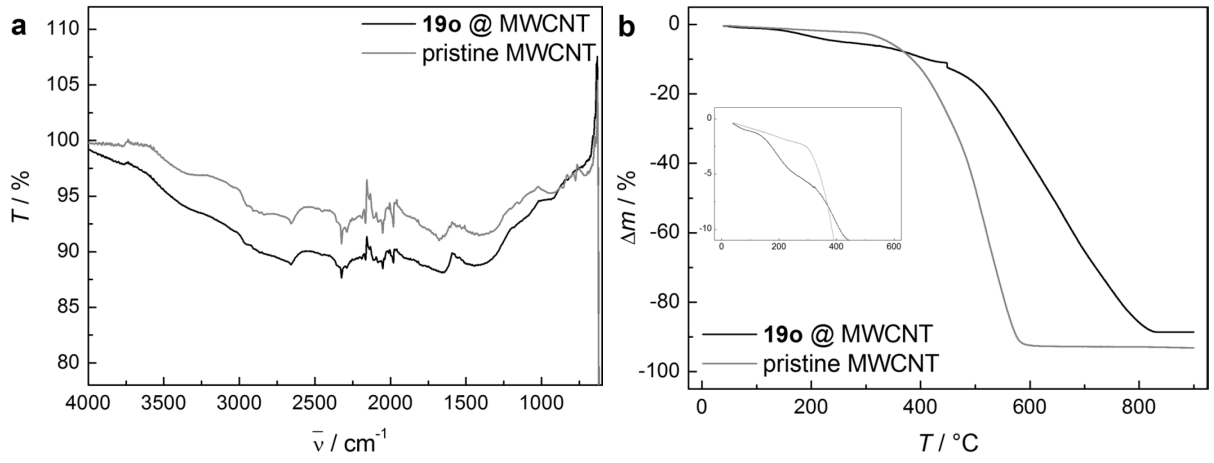

Figure 2-29: Comparison of the FTIR and TGA measurements of SWCNT before and after the reaction with **19o** for 3 d at 50 °C in water.

In order to gain further insight into whether the DA functionalization with **19o** was successful on SWCNTs, UV/vis spectroscopy measurements were carried out. For that

purpose, the supposedly functionalized SWCNTs were dispersed in DMSO, subjected to sonication, and subsequently centrifuged to yield a solution after decantation. The evolution of the UV/vis absorption spectra during the course of irradiation with light of the wavelength λ_{irr} = 313 nm is depicted in Figure 2-30a. It is clearly visible that a new band forms in the visible range of the spectrum indicating the ring-closing event of a diarylethene. However, the absorption maximum of the ring-closed form lies around 510 nm which is shifted bathochromically as compared to the DA adducts synthesized earlier (compare Chapters 2.1 and 2.2). As the DA adduct's ring-closed form typically exhibits its absorption maximum at around 400 nm, due to the lack of one double bond, it is reasonable to assume that the observed species is in fact not a DA adduct but the unreacted switch **19o**. This could either mean that a co-precipitation of SWCNTs and **19o** occurred and the latter could not be removed during the washing steps, or that **19o** adsorbed to the SWCNTs' surface. However, it can be excluded that a covalent functionalization event occurred, as a bathochromic shift of approximately 100 nm for the SWCNT-**19o** adduct as compared to the DA adducts synthesized earlier seems unlikely.

Remarkably, prolonged irradiation at 313 nm of the solution of **19o** and SWCNTs led to precipitation of the SWCNTs presumably due to bundling. To exclude that this effect is related to the presence of **19o** or **19c**, irradiation of a solution of pristine SWCNTs in DMSO was performed (Figure 2-30b). It is clearly visible that the tubes precipitate during the course of the irradiation with UV-light.

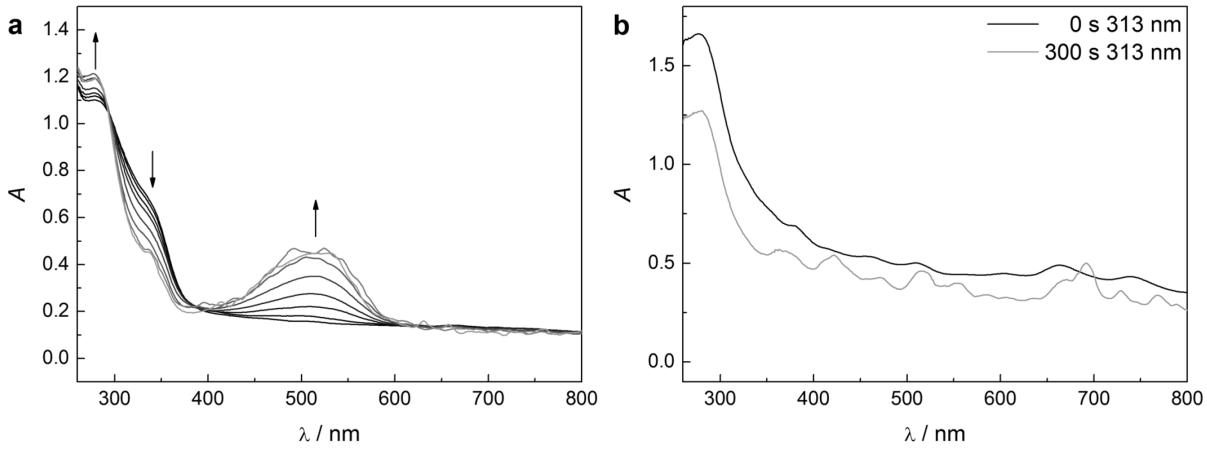

Figure 2-30: UV/vis spectra of DMSO solutions of a) the supposed adduct of **19o** and SWCNTs during the course of the irradiation with light of the wavelength λ_{irr} = 313 nm and b) pristine SWCNTs before and after irradiation with light of the wavelength λ = 313 nm.

A blind experiment in the dark without any irradiation showed that the solution of SWCNTs is stable over multiple hours excluding the thermally induced aggregation as explanation for this phenomenon. Until now, no satisfactory reasons could be found explaining this behavior of the SWCNTs in solution. However, this phenomenon appears to be an unprecedented and significant finding justifying further investigations to understand its origins and implications.

In conclusion, a covalent functionalization of CNTs could neither be achieved with the probing molecules furfuryl alcohol and 3-acetyl-2,5-dimethylfuran trying to reproduce the results reported in the literature,[209,210] nor with furyl-substituted DAEs **2o** and **19o**. The reasons for these unsuccessful attempts still remain mostly unclear. Recent calculations and findings on graphene, however, leave serious doubt over whether a DA functionalization event is actually possible on the undisturbed sp^2-lattice suggesting defective positions and vacancies in the lattice as reactive sites.[257,258] Nevertheless, the overall goal of this chapter remains highly attractive and efforts will continue to be undertaken to realize the photocontrolled reversible covalent functionalization of sp^2-carbon materials.

3. Conclusions and Outlook

3.1 Controlling Covalent Connection and Disconnection by Light

As described in Chapter 2.1, a novel set of furyl-substituted DAEs was designed and synthesized that offers an unprecedented level of control over the DA reaction. A true foundation for various purposes was laid by designing the prototypic furyl-substituted switches **1o** and **2o** that could reversibly undergo the DA reaction with maleimide to their corresponding DA adducts **3o** and **4o**. By *in situ* illumination of a reactant system consisting of **2o** and maleimide with light of different wavelengths, the outcome of the DA reaction could be biased to a considerable extent, *i.e.* the DA equilibrium could be switched between the side of the starting materials and the side of the products. This was achieved through the separate spectral addressability of the respective ring-closed derivatives **2c** and **4c** as their absorption maxima are almost fully separated in the visible part of the spectrum (compare Figure 2-5b). This manipulation of a chemical equilibrium enabled us to employ this prototypic reaction system for a variety of potential applications as it allows for the external, non-invasive, and highly orthogonal control over the formation and scission of covalent bonds only by light.

Despite the reaction system's prototypic character, there remains ample room for improvements. As visualized in Figure 2-5a, the amplification as well as the inhibition of the DA reaction is non-quantitative at any of the employed temperatures. This is an intrinsic feature of a highly reversible reaction system, as increasing the thermodynamic stability of the reaction products would render the reaction irreversible and increasing the thermodynamic stability of the starting materials would yield no conversion at all. Thus, other molecular concepts have to be identified that can overcome some of these limitations. A highly intriguing approach could, for example, exploit the photoinduced modulation of aromaticity to govern the outcome of a DA reaction. As the generation of an aromatic π-system stabilizes the DA adduct of isobenzofuran and *N*-methylmaleimide, the DA reaction becomes fast, quantitative, and only reversible at temperatures far beyond 100 °C for this particular reaction (Scheme 3-1).[159] Consequently, it would be highly fascinating to modulate the aromatic stabilization energy generated during this process to exert control over the DA equilibrium.

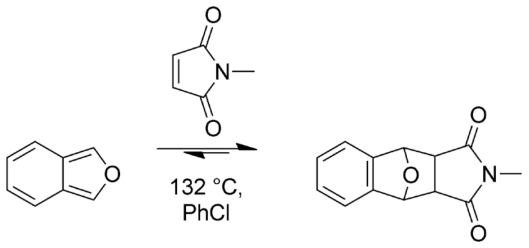

Scheme 3-1: DA reaction between isobenzofuran and *N*-methylmaleimide.

This idea could be implemented into a photoswitchable DAE in a straightforward manner (Scheme 3-2). By attaching the modified isobenzofuryl moiety in such a way, that one of the double bonds of the residual heterocycles is incorporated into the π-system of a photoswitchable DAE, the aromaticity of the DA adduct could be switched 'on' or 'off'. Through irradiation of a reaction system composed of the isobenzofuryl switch and maleimide with UV-light, the double bond granting aromatic stabilization in the adduct form could be removed enabling the retro DA reaction at far lower temperatures than in the previous state. At the same time, the thermodynamic driving force for the formation of the DA adduct from the starting materials would be withdrawn and thus the system would be switched into a state of high reversibility.

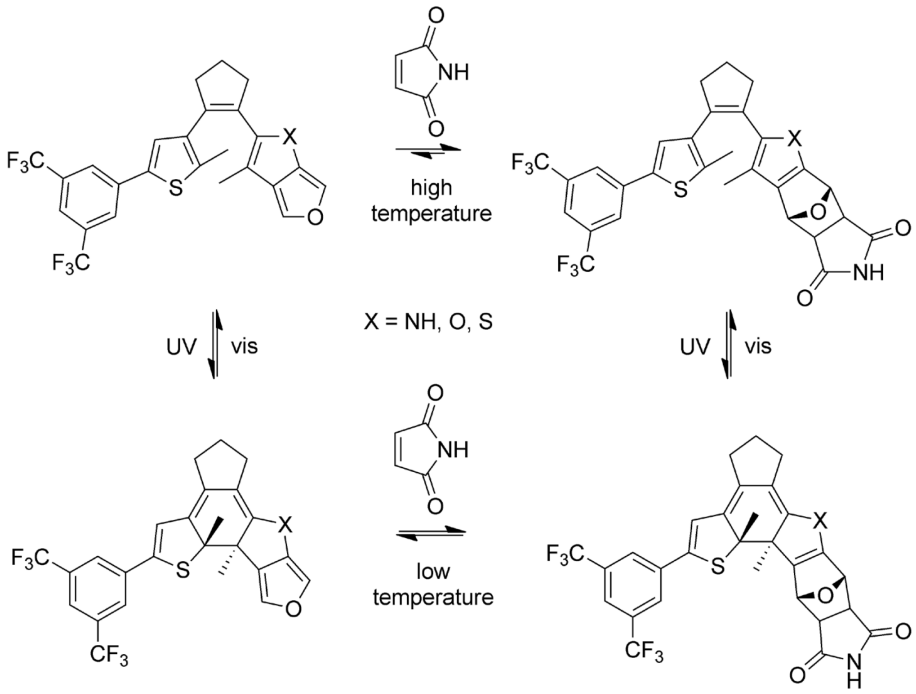

Scheme 3-2: General scheme of a DA reaction between an aromatic furyl-substituted DAE and maleimide. The reactivity towards the dienophile could be switched by changing the aromatic stabilization energy through irradiation with light.

This conceptually improved approach would solve the issue of non-quantitative turnover as observed in a reaction system constituted of **2o** and maleimide and render the isobenzofuryl-substituted switches especially useful for the release of dienophilic molecules. In a sense this system can be regarded as orthogonal to the one we reported in Chapter 2.1, since the reactants are not 'locked' but the reversibility is switched 'on' by irradiation with UV-light. Moreover, the attachment of a second heterocycle to the furan could grant facile tunability of the aromaticity achieved, as different heteroatoms introduce different amounts of aromatic stabilization energy (compare Chapter 1.5.1). The synthesis of the building blocks required for the assembly of such DAEs is also described in the literature to some extent.[259]

Another, usually omitted factor that hampers the effectiveness of the photoswitchable DA reaction is the strong concentration dependence. Naturally, a bimolecular reaction such as the DA reaction requires reactant concentrations on the molar to millimolar scale. However, the reactants' molar absorptivities in these concentration ranges would be far too high and thus for avoiding total absorption phenomena, photochemistry operates best at concentrations on the micromolar scale. One solution to overcome this limitation is to disregard the presented system's reversible character and to employ it as release device, as demonstrated in Chapter 2.2. However, focusing only on release applications would hamstring the overall potential of the reported switch **2o** and thus other solutions need to be found.

One implementation to keep the molar absorptivity low while increasing the local concentrations of the reactants would be to covalently tether the maleimide *via* its *N*-terminus to the DAE, such as proposed in Scheme 3-3. The covalent connection of the dienophile to the diene would turn the former intermolecular reaction into an intramolecular reaction accelerating the DA reaction even at low concentrations. This tethering approach, however, will only be relevant in some applications.

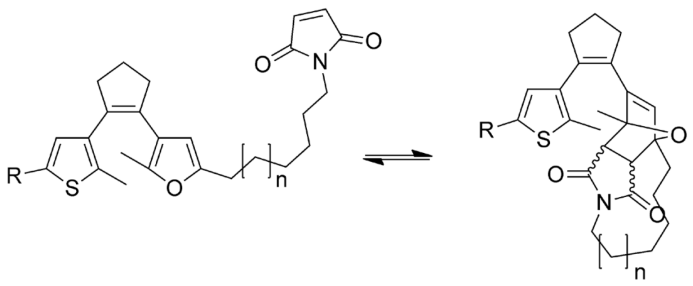

Scheme 3-3: Covalently tethering the dienophile to the diene could increase local concentrations while retaining a low molar absorptivity of the solution.

3.2 Photoinduced Release of Maleimide Derivatives in Physiological Systems

In Chapter 2.2 we reported on the successful release of a TOP2 inhibiting drug under physiological conditions employing visible light. For the first time, a water-soluble furyl-substituted DAE **19o** was synthesized that could undergo the DA reaction with maleimide or *N*-ethylmaleimide to their corresponding adducts **22o** and **23o**. These adducts were proven to exhibit outstanding switching behavior with a high composition at the PSS after irradiation with UV-light while fully retaining their solubility in physiological media. The adducts' corresponding ring-closed forms **22c** and **23c** were shown to efficiently impede the retro DA reaction back to the starting materials and readily regenerated their active, ring-open forms **22o** and **23o** upon irradiation with highly bioorthogonal vis-light. It was confirmed that **22o** and **23o** release their respective maleimide derivative under physiological temperatures over time achieving calculated daily concentrations in the micromolar range that clearly lie in the reported therapeutic window of these drugs. Not only could the extent of the 'depot effect', *i.e.* delayed release, conveniently be tuned through the adjustment of the *endo* to *exo* stereoisomer ratio in the syntheses of the DA adducts, it could also be shown that after a certain release time residual DA adduct could be reversibly deactivated by irradiation with UV-light *in situ* through ring-closing remaining **22o** or **23o**. This combination of reversibly altering a release system from its inactive to its active state whereupon the drug can be released *via* thermal equilibration is best described as 'photoswitchable prodrug'. Eventually, the presented system proved to be a potent photoswitchable prodrug for maleimide based drugs and is ready to be surveyed with various assays to prove its pharmacological effect upon TOP2 action.

Even though the presented release devices fulfill most of the criteria to be considered as successful representatives in the context of photopharmacology, there is still plenty of room for improvements. An obvious flaw is the comparably slow release of the drug that can last over days. While this feature is the prerequisite for the 'depot effect' reported earlier, the advantageous resolution in space that light can offer is lost because of the comparably faster distribution of the drug in the organism. Hence, it would be beneficial to design a device that releases the maleimide based drug on a shorter timescale. This could be performed by considering the isobenzofuryl-substituted DAEs as proposed earlier in Scheme 3-2. When substituted with solubilizing groups applicable in aqueous media, these types of switches could perform even better for the release of maleimide derivatives than **22o** or **23o**.

A further consideration can be made when recalling the content of Figure 2-19. There it was shown that aggregation phenomena possibly retain the retro DA reaction by increasing the local reactant concentrations inside of the aggregates. When releasing maleimide from **22o** in a deaggregating solvent mixture, these remarkable effects could not be observed. Hence, a molecular design preventing the aggregation of the active DA adducts would be highly desirable. As the hydrophobicity of maleimide is held responsible for the aggregation phenomena, it can be reasoned that the utilization of a more water-soluble maleimide would overcome that difficulty. For instance, polyethylene glycol chains could be attached to the maleimide's *N*-terminus.

A synthetically more challenging approach to increase the rate for the retro DA reaction would be to introduce electron-withdrawing substituents to the furyl moiety (compare Chapter 1.5.2), as exemplified in Scheme 3-4. The electron-withdrawing group would render the furyl moiety a poor diene and make the overall DA reaction endergonic.[159] Naturally, this would have consequences for the synthesis of the adducts and while maleimide is easily released from the switch, the forward DA reaction necessary to prepare the photoswitchable prodrug would be severely hampered.

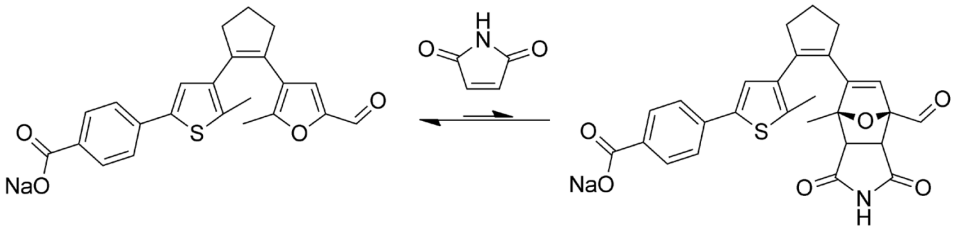

Scheme 3-4: The introduction of an electron-withdrawing formyl group would render the forward DA reaction endergonic thus facilitating the release of maleimide.

3.3 Furyl DAEs for the Reversible Covalent Functionalization of Carbon Nanotubes

It became clear in Chapter 2.3 that a covalent functionalization of CNTs could not be detected. Neither employing the probing molecules furfuryl alcohol and 3-acetyl-2,5-dimethylfuran nor with furyl-substituted DAEs **2o** and **19o** a functionalization could be observed using common analytical methods. We can only speculate over the reasons for these findings since we could not reproduce the protocols reported in the literature. As we reasoned in Chapter 2.3.2 that sp^2-carbon allotropes of lesser quality, *i.e.* such that contain a high amount of defects, could show higher reactivity towards functionalization than an undisturbed sp^2-lattice, the transition towards such low-quality CNTs could resolve the issues we encountered. Clearly, this cannot be considered as optimal solution since with increasing defect density the outstanding properties of sp^2-hybridized carbon allotropes vanish.

A further reason for the failed functionalization could be the energetic reaction profiles. Up to date, it is only scarcely investigated how exergonic DA reactions on CNTs actually are. In fact, calculations have been performed on graphene that suggest that the DA functionalization on the pristine, undisturbed sp^2-carbon lattice is in fact endergonic and thermodynamically not working at all. To empirically approach that problem, a library of furans with different substituents ranging from bulky to small and electron-donating to electron-deficient has to be employed as probes in test reactions (compare Chapter 1.5.2). The degree of functionalization, and by this the energetic profile of the DA reaction, should correlate with steric demand as well as with the electronic properties of the employed furans. Such a systematic study would allow for a conclusion whether the furan based reversible covalent functionalization on CNTs is working at all.

In addition to these suggestions, the functionalization procedures can be changed towards more elaborate methods, *e.g.* the micelle swelling technique.[260,261] In collaboration with the group of Prof. Stefanie Reich, we are currently working on the incorporation of the furyl-substituted DAEs into micelles arranged around individual SWCNTs. This method would potentially generate higher local concentrations of the furyl moieties at the SWCNT's surface, thereby facilitating the functionalization event.

Also, other sp^2-carbon structures can be considered for the functionalization, such as fullerenes.[262] In cooperation with the group of Prof. Nazario Martín, we are trying to employ fullerenes as discrete and more defined entities to investigate the principles behind the

reversible covalent functionalization employing furyl-substituted DAE **2o**. A possible eve of this is a photocontrollable modulation of the electron-accepting character of C_{60}, giving rise to a wavelength or intensity photomodulation of optoelectronic devices,[7] such as photoresponsible transistors,[263] light-emitting diodes,[264] or photovoltaic cells.[265]

4. Experimental Section

4.1 Materials and Methods

4.1.1 Analytical Instrumentation

NMR spectra were recorded on a 500 MHz (125 MHz for ^{13}C, 470 MHz for ^{19}F) Bruker AVANCE II 500 spectrometer or on a 300 MHz (75 MHz for ^{13}C) Bruker AVANCE II 300 spectrometer at 25 °C using residual protonated solvent signals[266] as internal standards (^{1}H: $\delta(CDCl_3)$ = 7.26 ppm, $\delta(C_6D_6)$ = 7.16 ppm, $\delta(CD_2Cl_2)$ = 5.32 ppm, δ(DMSO-d_6) = 2.50 ppm; ^{13}C: $\delta(CDCl_3)$ = 77.16 ppm, $\delta(C_6D_6)$ = 128.06 ppm, $\delta(CD_2Cl_2)$ = 53.84 ppm, δ(DMSO-d_6) = 39.52 ppm). Ultrahigh-performance liquid chromatography / mass spectrometry (UPLC/MS) was performed on a Waters Acquity UPLC equipped with a Waters LCT Premier XE Mass detector for high-resolution MS (HR-MS, ESI^+-ionization) and with Waters Alliance systems (consisting of a Waters Separations Module 2695, a Waters Diode Array Detector 996 and a Waters Mass Detector ZQ 2000). Dynamic light scattering (DLS) experiments were carried out on a Malvern Instruments Zetasizer Nano ZS. Thermogravimetric analysis was performed on a PerkinElmer Pyris 1 TGA equipped with a PerkinElmer Pyris 1 TGA autosampler and a PerkinElmer thermal analysis gas station. Fourier-transform infrared spectroscopy was carried out either on a Jasco FTIR-6600 or a Bruker Vertex 70v each equipped with a Specac Golden Gate single reflection diamond ATR sample holder. TLC was performed on Merck Silica Gel 60 F254 TLC plates with a fluorescent indicator employing 254 nm UV-lamp for visualization.

4.1.2 Chemicals and Solvents

Solvents and commercial starting materials were used as supplied. The solvents were dried before use, if necessary, employing an Innovative Technologies solvent purification system (multi-unit micro series). Silica gel for chromatography (0.035–0.070 mm, 60 Å) was used for column chromatography. The petroleum ether (PE) used had a boiling range of 40–60 °C. Dulbecco's phosphate buffered saline was purchased from Sigma-Aldrich and was modified, without calcium chloride and magnesium chloride, sterile-filtered, and suitable for cell culture. Multi-walled carbon nanotubes (MWCNTs) were purchased from Sigma-Aldrich, had >98% carbon basis, the specifications 6–13 nm outer diameter × 2.5–20 µm length, and were synthesized by chemical vapor deposition (CVD). Single-walled carbon nanotubes

(SWCNTs) were purchased from Sigma-Aldrich, had >90% carbon basis, a purity of >77%, the specifications 0.7–1.1 nm outer diameter × 0.3–2.3 μm length, and were synthesized by CVD on CoMoCAT.

4.2 Synthesis and Characterization data

1-(3-(2,5-Dimethylfuryl))-2-(3-(5-(*p*-tolyl))-2-methylthienyl)-cyclopentene 1o.

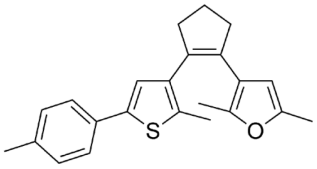

1o

1-(3-(2,5-Dimethylfuryl))-2-(3-(5-chloro-2-methylthienyl))-cyclopentene **12** (0.50 g, 1.70 mmol) was dissolved in dry THF (8 mL) under Ar. To this solution was added dropwise *n*-BuLi (0.85 mL, 1.87 mmol, 2.2 M in cyclohexane) and the resulting brownish solution was stirred at rt for 30 min. Then, $B(OEt)_3$ (0.69 mL, 2.55 mmol) was added and the mixture was stirred for 45 min at rt. Meanwhile *p*-tolyl bromide (0.44 g, 2.55 mmol) was dissolved in THF (8 mL) under Ar. To this solution was added $Pd(PPh_3)_4$ (0.20 g, 0.17 mmol) and the resulting mixture was stirred at rt for 15 min. Afterwards, aq. Na_2CO_3 solution (2 M, 15 mL) and ethylene glycol (3 drops) were added. This mixture was heated to 65 °C and then the solution containing the borate was added directly without any workup. The combined solutions were stirred at 65 °C for 1 d. Subsequently, the solution was diluted with water and extracted with EtOAc. The combined organic layers were dried over anhydr. $MgSO_4$ and the solvent was removed *in vacuo*. The resulting crude product was purified by column chromatography (silica, petroleum ether:CH_2Cl_2 = 10:1) to yield a colorless oil **1o** (61%) that was stored under Ar to prevent oxidation. **^{1}H-NMR (500 MHz, CCl_4/CD_2Cl_2):** δ(ppm) = 7.41 (s, 2H, CH_{ar}), 7.14 (s, 2H, CH_{ar}), 7.01 (s, 1H, CH_{ar}), 5.66 (s, 1H, CH_{ar}), 2.80 (m, 4H, CH_2), 2.40 (s, 3H, CH_3), 2.22 (s, 3H, CH_3), 2.13 (s, 3H, CH_3), 2.08 (m, 2H, CH_2), 2.02 (s, 3H, CH_3). **^{13}C-NMR (125 MHz, CCl_4/CD_2Cl_2):** δ(ppm) = 150.1, 147.7, 141.4, 138.4, 137.5, 134.4, 133.5, 132.9, 130.7 126.6, 124.7, 119.4, 107.9, 40.2, 39.0, 24.2, 22.6, 15.8, 14.8, 14.5. **HR-MS(ESI$^+$):** m/z = 348.1555 (calcd. 348.1548 for $C_{23}H_{24}OS^+$).

1-(3-(2,5-Dimethylfuryl))-2-(3-(5-(3,5-(bistrifluoromethyl)phenyl))-2-methylthienyl)-cyclopentene 2o

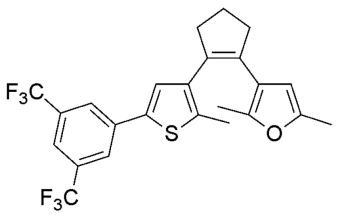

2o

1-(3-(2,5-Dimethylfuryl))-2-(3-(5-chloro-2-methylthienyl))-cyclopentene **12** (1.5 g, 5.0 mmol) was dissolved in dry THF (5 mL) under Ar. To this solution was added dropwise *n*-BuLi (2.5 mL, 5.5 mmol, 2.2 M in cyclohexane) and the resulting brownish solution was stirred at rt for 30 min. Then, $B(OBu)_3$ (2.0 mL, 7.5 mmol) was added and the mixture was stirred for 45 min at rt. Meanwhile, 3,5-bis(trifluoromethyl)bromobenzene (1.3 mL, 7.5 mmol) was dissolved in THF (5 mL) under Ar. To this solution was added $Pd(PPh_3)_4$ (0.6 g, 0.5 mmol) and the resulting mixture was stirred at rt for 15 min. Afterwards, degassed aq. Na_2CO_3 sol. (10 mL, 2 M) and ethylene glycol (3 drops) were added. This mixture was heated to 65 °C and then the solution containing the borate was added directly without any workup. The combined solutions were stirred at 65 °C for 1 d. Afterwards, the solution was diluted with water and extracted with Et_2O. The combined organic layers were dried over anhyd. $MgSO_4$ and the solvent was removed *in vacuo*. The resulting crude product was purified by column chromatography (silica, petroleum ether:CH_2Cl_2 = 10:1) to yield the target compound **2o** as a colorless solid that was recrystallized from MeOH/acetone and was stored under Ar to prevent oxidation (82%). **^{1}H-NMR (500 MHz, $CDCl_3$):** δ(ppm) = 7.90 (s, 2H, CH_{ar}), 7.70 (s, 1H, CH_{ar}), 7.19 (s, 1H, CH_{ar}), 5.64 (s, 1H, CH_{ar}), 2.76 (m, 4H, CH_2), 2.16 (s, 3H, CH_3), 2.13 (s, 3H, CH_3), 2.04 (m, 2H, CH_2), 1.98 (s, 3H, CH_3). **^{13}C-NMR (125 MHz, $CDCl_3$):** δ(ppm) = 149.5, 146.8, 138.3, 136.8, 132.9, 131.7, 126.7, 125.0, 120.2 118.1, 106.4, 38.8, 37.7, 23.0, 14.7, 13.5, 13.3. **^{19}F-NMR (470 MHz, $CDCl_3$):** δ(ppm) = -63.3. **HR-MS(ESI$^+$):** *m*/*z* = 470.1134 (calcd. 470.1139 for $C_{24}H_{20}OF_6S^+$).

1-(3-(2,5-Dimethylfuryl))-2-(3-(5-(3,5-(bistrifluoromethyl)phenyl))-2-methylthienyl)-cyclopentene 2c

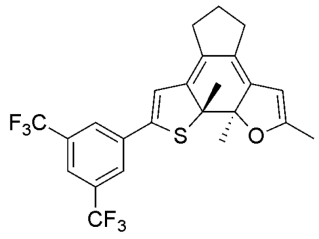

2c

1-(3-(2,5-Dimethylfuryl))-2-(3-(5-(3,5-(bistrifluoromethyl)phenyl))-2-methylthienyl)-cyclopentene **2o** was dissolved in an NMR tube in C_6D_6 and irradiated with a 313 nm UV-lamp for 5 min. **^{1}H-NMR (300 MHz, C_6D_6):** δ(ppm) = 7.80 (s, 2H, CH_{ar}), 7.58 (s, 1H, CH_{ar}), 6.19 (s, 1H, CH_{ar}), 5.08 (s, 1H, CH_{ar}), 2.71 (t, ^3J(H,H) = 7.5 Hz, 2H, CH_2), 2.61 (t, ^3J(H,H) = 7.5 Hz, 2H, CH_2), 2.18 (m, 2H, CH_2), 1.93 (s, 3H, CH_3), 1.90 (s, 3H, CH_3), 1.75 (s, 3H, CH_3).

1-(3-(2,5-Dimethylfuryl))-2-(3-(5-(*p*-tolyl))-2-methylthienyl)-cyclopentene-*N*-phenylmaleimide *exo* adduct *exo*-3o.

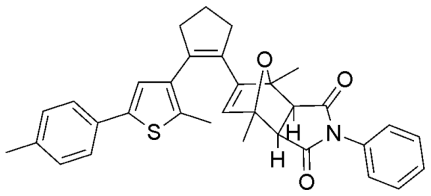

***exo*-3o**

N-phenylmaleimide (0.24 g, 0.68 mmol) and 1-(3-(2,5-dimethylfuryl))-2-(3-(5-(*p*-tolyl))-2-methylthienyl)-cyclopentene **1o** (0.12 g, 0.68 mmol) were dissolved in MeCN (5 mL) under Ar and stirred for 3 d at rt. Removal of the solvent an subsequent column chromatography (silica, petroleum ether:EtOAc = 10:6) yielded ***exo*-3o** as white foam (37%). **^{1}H-NMR (500 MHz, CCl_4/CD_2Cl_2):** δ(ppm) = 7.42 (m, 5H, CH_{ar}), 7.26 (d, ^3J(H,H) = 8.4 Hz, 2H, CH_{ar}), 7.16 (d, ^3J(H,H) = 8.4 Hz, 2H, CH_{ar}), 6.94 (s, 1H, CH_{ar}), 5.48 (s, 1H, CH_{ar}), 2.85 (m, 2H, C*H*), 2.81 (m, 2H, CH_2), 2.63 (m, 2H, CH_2), 2.39 (s, 3H, CH_3), 2.34 (s, 3H, CH_3), 2.01 (m, 2H, CH_2), 1.69 (s, 3H, CH_3), 1.63 (s, 3H, CH_3). **HR-MS(ESI$^+$):** m/z = 521.2021 (calcd. 521.2025 for $C_{33}H_{31}NO_3S^+$).

1-(3-(2,5-Dimethylfuryl))-2-(3-(5-(3,5-(bistrifluoromethyl)phenyl))-2-methylthienyl)-cyclopentene-maleimide *exo* adduct *exo*-4o

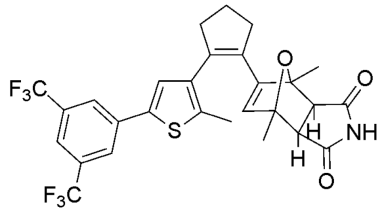

***exo*-4o**

Maleimide (1.04 g, 10.75 mmol) and 1-(3-(2,5-dimethylfuryl))-2-(3-(5-(3,5-(bistrifluoromethyl)phenyl))-2-methylthienyl)-cyclopentene **2o** (1.01 g, 2.15 mmol) were dissolved in toluene (5 mL) and stirred for 1 d at 50 °C. The solvent was removed *in vacuo* and the whole redissolved in NH_4OH (25%, 5 mL) and THF (5 ml) and stirred for 2 d at rt. After addition of aq. HCl (2 M) and extraction with Et_2O, column chromatography (silica, petroleum ether:THF = 10:2) yielded the target compound as a colorless oil. Redissolution in MeOH and precipitation with H_2O yielded ***exo*-4o** as a white powder (59%). **^{1}H-NMR (300 MHz, C_6D_6):** δ(ppm) = 8.39 (s, 1H, N*H*), 7.79 (s, 2H, CH_{ar}), 7.56 (s, 1H, CH_{ar}), 6.82 (s, 1H, CH_{ar}), 5.51 (s, 1H, CH_{ar}), 2.45 (m, 2H, CH_2), 2.41 (d, ^3J(H,H) = 6.2 Hz, 1H, C*H*), 2.31 (d, ^3J(H,H) = 6.2 Hz, 1H, C*H*), 2.16 (m, 2H, CH_2), 2.05 (s, 3H, CH_3), 1.76 (m, 2H, CH_2), 1.69 (s, 3H, CH_3), 1.56 (s, 3H, CH_3). **^{13}C-NMR (125 MHz, $CDCl_3$):** δ(ppm) = 174.4, 174.3, 151.1,

137.43, 137.41, 137.3, 137.2, 137.0, 136.8, 133.2, 133.0, 132.7, 126.9, 125.6, 89.6, 87.4, 54.8, 54.4, 39.1, 36.8, 30.6, 23.5, 16.4, 16.3, 14.9. **HR-MS(ESI$^+$):** *m*/*z* = 568.1389 (calcd. 568.1331 for $C_{28}H_{24}NO_3F_6S^+$).

1-(3-(2,5-Dimethylfuryl))-2-(3-(5-(3,5-(bistrifluoromethyl)phenyl))-2-methylthienyl)-cyclopentene-maleimide *exo* adduct *exo*-4c

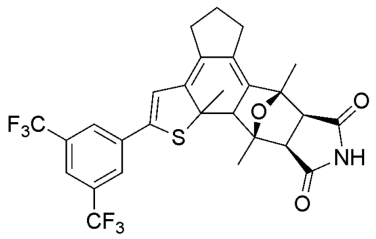

***exo*-4c**

1-(3-(2,5-Dimethylfuryl))-2-(3-(5-(3,5-(bistrifluoromethyl)phenyl))-2-methylthienyl)-cyclopentene-maleimide *exo* adduct ***exo*-4o** was dissolved in an NMR tube in C_6D_6 and irradiated with a 313 nm UV-lamp for 5 min. **^{1}H-NMR (300 MHz, C_6D_6):** δ(ppm) = 7.86 (s, 2H, CH_{ar}), 7.62 (s, 1H, CH_{ar}), 7.50 (s, 1H, N*H*), 6.28 (s, 1H, CH_{ar}), 2.82 (t, ^4J(H,H) = 2.4 Hz, 1H, C*H*), 2.43 (m, 2H, CH_2), 2.36 (d, ^3J(H,H) = 6.4 Hz, 1H, C*H*), 2.25 (d, ^3J(H,H) = 6.4 Hz, 1H, C*H*), 2.10 (m, 2H, CH_2), 1.83 (s, 3H, CH_3), 1.76 (s, 3H, CH_3), 1.75 (m, 2H, CH_2), 1.30 (s, 3H, CH_3).

2-Chloro-5-methylthiophene 5

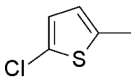

5

2-Methylthiophene (50 mL, 520 mmol) and *N*-chlorosuccinimide (76 g, 80 mmol) were dissolved in acetic acid (200 mL) and benzene (200 mL) and refluxed for 1.5 h. After cooling to rt, the solution was washed with aq. NaOH solution (3 M, 4 × 150 mL) and the solvent was removed *in vacuo*. Fractional distillation yielded a colorless liquid **5** (47%). **^{1}H-NMR (500 MHz, $CDCl_3$):** δ(ppm) = 6.60 (d, ^3J(H,H) = 3.6 Hz, 1 H, CH_{ar}), 6.43 (dq, ^3J(H,H) = 3.6 Hz, ^4J(H,H) = 1.2 Hz, 1 H, CH_{ar}), 2.32 (d, ^4J(H,H) = 1.1 Hz, 3 H, CH_3). **^{13}C-NMR (125 MHz, $CDCl_3$):** δ(ppm) = 138.5, 126.5, 125.8, 124.4, 15.5.

5-Keto-5-(3-(5-chloro-2-methylthienyl))-ethylpentanoate 6

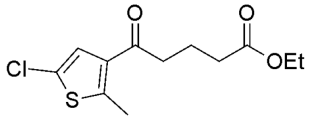

6

Glutaric acid monoethyl ester chloride (3.29 mL, 25 mmol) and 2-chloro-5-methylthiophene **5** (3.29 g, 25 mmol) were dissolved in CH_2Cl_2 (25 mL) in a Schlenk flask under Ar and cooled to 0 °C with an ice bath. To this solution was added pestled $AlCl_3$ portionwise and the whole was stirred for 1.5 h at rt. Afterwards, the mixture was poured into ice water and extracted with CH_2Cl_2. The solvent was removed *in vacuo* and purification by column chromatography (silica, PE:EtOAc = 10:1) yielded the target compound **6** as a yellow liquid (64%). **^{1}H-NMR (500 MHz, $CDCl_3$):** δ(ppm) = 7.17 (s, 1H, CH_{ar}), 4.13 (q, ^3J(H,H) = 7.2 Hz, 2H, CH_2), 2.82 (t, ^3J(H,H) = 7.2 Hz, 2H, CH_2), 2.65 (s, 3H, CH_3), 2.39 (t, ^3J(H,H) = 7.4 Hz, 2H, CH_2), 1.25 (t, ^3J(H,H) = 7.2 Hz, 3H, CH_3), 2.39 (t, ^3J(H,H) = 7.4 Hz, 2H, CH_2). **^{13}C-NMR (125 MHz, $CDCl_3$):** δ(ppm) = 194.8, 173.3, 147.9, 135.0, 126.9, 125.4, 60.5, 40.7, 33.4, 19.3, 16.2, 14.4. **HR-MS(ESI$^+$):** *m*/*z* = 275.0490 (calcd. 275.0509 for $C_{12}H_{16}O_3SCl^+$).

5-Keto-5-(3-(5-chloro-2-methylthienyl))-pentanoic acid 7

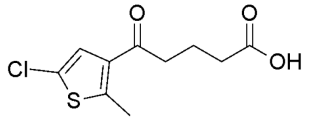

7

5-Keto-5-(3-(5-chloro-2-methylthienyl))-ethylpentanoate **6** (4.40 g, 16 mmol), EtOH (40 mL) and KOH (2.69 g, 48 mmol) were combined in a round bottom flask and the solution was refluxed for 4 h. The mixture was then diluted with water and brine and the basic aq. layer was extracted one time with Et_2O to remove unreacted ester. Afterwards the aq. layer was acidified with conc. HCl until the *p*H was acidic. The acidified aq. layer was then extracted with Et_2O, the organic layer dried over anhydrous $MgSO_4$ and the solvent removed *in vacuo* to yield the pure target compound **7** as brown oil (97%). **^{1}H-NMR (500 MHz, $CDCl_3$):** δ(ppm) = 10.65 (br, 1H, COO*H*), 7.18 (s, 1H, CH_{ar}), 2.87 (t, ^3J(H,H) = 7.1 Hz, 2H, CH_2), 2.67 (s, 3H, CH_3), 2.49 (t, ^3J(H,H) = 7.1 Hz, 2H, CH_2), 2.03 (m, 2H, CH_2). **^{13}C-NMR (125 MHz, $CDCl_3$):** δ(ppm) = 194.5, 179.4, 147.9, 134.7, 126.7, 125.4, 40.3, 43.9, 18.7, 16.0. **HR-MS(ESI$^+$):** *m*/*z* = 247.0182 (calcd. 247.0196 for $C_{10}H_{12}O_3SCl^+$).

5-Keto-5-(3-(5-chloro-2-methylthienyl))-pentanoic acid chloride 8

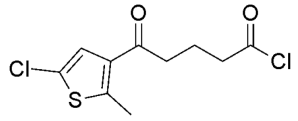

8

To a solution of 5-Keto-5-(3-(5-chloro-2-methylthienyl))-pentanoic acid **7** (3.53 g, 14.3 mmol) in CH_2Cl_2 (40 mL) in a Schlenk flask under Ar was added oxalyl chloride (3.12 mL, 35.8 mmol). The solution was stirred at rt for 3 h. The solvent and remaining reactant were removed *in vacuo* and the received crude target compound **8** was used as is.

5-Chloro-3-(3-chloropropionyl)-2-methylthiophene 9

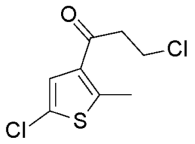

9

5-Chloro-2-methylthiophene **5** (8.3 g, 62.5 mmol) and 3-chloropropionyl chloride (6.0 mL, 62.5 mmol) were dissolved in CH_2Cl_2 (freshly distilled, 125 mL) and cooled with an ice bath. $AlCl_3$ (10.0 g, 75.0 mmol) was pestled and added carefully and portionwise. The solution was then stirred for 1.5 h at 0 °C. Afterwards, the reaction mixture was poured into ice water, acidified with HCl (2 M), extracted with CH_2Cl_2 and the combined organic layers were dried over anhydrous $MgSO_4$. The whole was filtered through a pad of silica, the solvent removed *in vacuo* and the target compound **9** received including ca. 10% regioisomer (97%) which was removed in later steps. **HR-MS (ESI$^+$)**: *m/z* = 222.9686 (calcd. 222.9715 for $C_8H_9OSCl_2^+$).

3-Acryloyl-5-chloro-2-methylthiophene 10

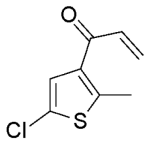

10

5-Chloro-3-(3-chloropropionyl)-2-methylthiophene **9** (13.4 g, 60.0 mmol) was dissolved in CH_2Cl_2 (125 mL) and cooled with an ice bath. To this solution was added 1,8-diazabicycloundec-7-ene, DBU, (9.0 mL, 60.0 mmol) and the whole was stirred for 1 h at rt. Afterwards, dil. aq. NH_4Cl solution was added, the reaction mixture extracted with CH_2Cl_2, the combined organic layers dried over anhydrous $MgSO_4$ and the solvent removed *in vacuo*. Column chromatography (silica, petroleum ether:EtOAc = 20:1) yielded the target

compound **10** as a colorless oil (46%) that was used immediately in the next reaction. **^{1}H-NMR (300 MHz, $CDCl_3$):** δ(ppm) = 7.12 (s, 1 H, CH_{ar}), 6.83 (d×d, ^3J(H,H) = 10.4 Hz, ^3J(H,H) = 17.1 Hz, 1 H, C*H*), 6.34 (d×d, ^3J(H,H) = 17.1 Hz, ^2J(H,H) = 1.6 Hz 1 H, CH_2), 5.83 (d×d, ^3J(H,H) = 10.4 Hz, ^2J(H,H) = 1.6 Hz 1 H, CH_2), 2.64 (s, 3 H, CH_3). **^{13}C-NMR (75 MHz, $CDCl_3$):** δ(ppm) = 185.8, 148.2, 135.3, 134.5, 129.8, 127.0, 125.6, 15.9. **HR-MS (ESI$^+$)**: *m/z* = 187.0057 (calcd. 186.9984 for $C_8H_8OSCl^+$).

1-(3-(2,5-Dimethylfuryl))-5-(3-(5-chloro-2-methylthienyl))-1,5-pentadione 11

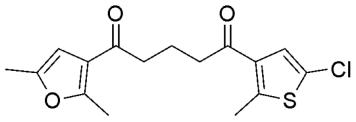

11

***Via* Michael addition:** Diisopropylamine (9.3 mL, 66.0 mmol) was dissolved in dry THF (50 mL) under Ar and cooled to -78 °C. To this solution was added *n*-BuLi (27.3 mL, 60.0 mmol, 2.2 M in cyclohexane) dropwise, the whole was allowed to warm to rt and finally stirred for further 45 min at rt. The solution was then cooled to -35 °C, 3-acetyl-1,5-dimethylfuran (6.5 mL, 60.0 mmol) was added whereupon the mixture turned yellow. The whole was then stirred for 15 min at -35 °C, subsequently allowed to warm to rt and stirred for 10 min. Afterwards, 3-acryloyl-5-chloro-2-methylthiophene **10** (11.2 g, 60 mmol) dissolved in dry THF (10 mL) was added at -30 °C, the solution stirred at that temperature for 15 min, and then allowed to warm to rt and stir for another 1 h. The mixture was then quenched with sat. aq. NH_4Cl solution and extracted with Et_2O. The combined organic layers were dried over anhydrous $MgSO_4$ and the solvent and remaining starting material removed *in vacuo* at 70 °C. Column chromatography (silica, petroleum ether:EtOAc = 10:1) yielded the target compound as a slightly yellow oil **11** that crystallized (31%). ***Via* Friedel-Crafts acylation:** 5-Keto-5-(3-(5-chloro-2-methylthienyl))-pentanoyl chloride **8** (3.79 g, 14.3 mmol) and 2,5-dimethylfuran (1.52 mL, 14.3 mmol) were dissolved in CH_2Cl_2 (25 mL) in an ice cooled Schlenk flask under Ar. To this solution was added $SnCl_4$ (2.0 mL, 17.2 mmol) and the whole was stirred for 2 h at 0 °C. Afterwards, the mixture was poured onto ice water and extracted with CH_2Cl_2. The combined organic layers were dried over anhydrous $MgSO_4$, the solvent was removed *in vacuo* and the obtained crude product was purified by column chromatography (silica, PE:EtOAc = 10:1) to yield a yellowish solid **11** (20%). **^{1}H-NMR (500 MHz, $CDCl_3$):** δ(ppm) = 7.18 (s, 1H, CH_{ar}), 6.20 (s, 1H, CH_{ar}), 2.84 (t, ^3J(H,H) = 7.0 Hz, 2H, CH_2), 2.76 (t, ^3J(H,H) = 7.0 Hz, 2H, CH_2), 2.65 (s, 3H, CH_3), 2.53 (s, 3H, CH_3),

2.24 (s, 3H, CH_3), 2.04 (quin, ^3J(H,H) = 7.0 Hz, 2H, CH_2). **HR-MS(ESI$^+$):** *m*/*z* = 325.0648 (calcd. 325.0665 for $C_{16}H_{18}O_3SCl^+$).

1-(3-(2,5-Dimethylfuryl))-2-(3-(5-chloro-2-methylthienyl))-cyclopentene 12

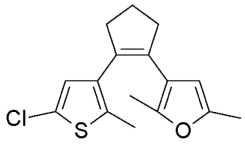

12

$TiCl_4$ (5.3 mL, 48.0 mmol) was added very cautiously dropwise to ice cooled dry THF (150 mL) under Ar whereupon the solution turned yellow. To this mixture was added Zn dust (6.3 g, 96 mmol) and the slurry was then stirred for 45 min at 65 °C. Afterwards, the solution was cooled with an ice bath, pyridine (1.9 mL, 24.0 mmol) was added, the solution was stirred for 10 min at 0 °C and subsequently 1-(3-(2,5-dimethylfuryl))-5-(3-(5-chloro-2-methylthienyl))-1,5-pentadione **11** (5.2 g, 16 mmol) was added. The mixture was then reheated to 65 °C for 2 h, successively cooled to rt, and quenched with sat. aq. K_2CO_3 solution. The mixture was then acidified with aq. HCl (2 M), extracted with Et_2O, the combined organic layers washed with brine, dried over anhydrous $MgSO_4$, and the solvent was removed *in vacuo*. The resulting crude product was purified by column chromatography (silica, petroleum ether:CH_2Cl_2 = 20:1) to yield a colorless oil **12** (59%) that crystallized and was stored under Ar to prevent oxidation. **^{1}H-NMR (500 MHz, $CDCl_3$):** δ(ppm) = 6.59 (s, 1H, CH_{ar}), 5.56 (s, 1H, CH_{ar}), 2.72 (t, ^3J(H,H) = 7 Hz, 2H, CH_2), 2.66 (t, ^3J(H,H) = 7.0 Hz, 2H, CH_2), 2.18 (s, 3H, CH_3), 2.00 (m, 2H, CH_2), 1.98 (s, 3H, CH_3), 1.94 (s, 3H, CH_3). **^{13}C-NMR (125 MHz, $CDCl_3$):** δ(ppm) = 148.9, 146.4, 135.5, 132.4, 131.1, 126.8, 125.3, 117.7, 106.4, 38.5, 37.6, 22.7, 14.3, 13.4, 13.1. **HR-MS(ESI$^+$):** m/z = 293.0772 (calcd. 293.0767 for $C_{16}H_{18}OSCl^+$).

1-(3-(2,5-Dimethylfuryl))-2-(3-(5-*p*-pyridyl)-2-methylthienyl)-cyclopentene 13

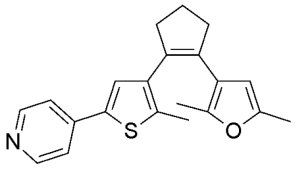

13

1-(3-(2,5-Dimethylfuryl))-2-(3-(5-chloro-2-methylthienyl))-cyclopentene **12** (2.84 g, 9.7 mmol) was dissolved in dry THF (10 mL) in a Schlenk tube under Ar. To this solution was added dropwise *n*-BuLi (4.9 mL, 2.2 M) and the resulting brownish solution was stirred at rt

for 30 min. Then, $B(OBu)_3$ (3.93 mL, 14.6 mmol) was added and the mixture was stirred for 45 min at rt Meanwhile, 4-bromopyridine hydrochloride (2.83 g, 14.6 mmol) was dissolved in THF (15 mL) in a Schlenk flask under Ar. To this solution was added $Pd(PPh_3)_4$ (1.12 g, 1.0 mmol) and the resulting mixture was stirred at rt for 15 min. Afterwards, degassed aq. Na_2CO_3 solution and ethylene glycol (3 drops) were added. This mixture was heated to 65 °C and then the solution containing the borate was added directly without any workup. The combined solutions were stirred at 65 °C for 1 d. Afterwards, the solution was diluted with water and extracted with Et_2O. The combined organic layers were dried over anhyd. $MgSO_4$ and the solvent was removed *in vacuo*. The resulting crude product was purified by column chromatography (silica, petroleum ether:EtOAc = 2:1) to yield the target compound **13** as a colorless oil that was recrystallized from MeOH/water (76%). **^{1}H-NMR (500 MHz, C_6D_6):** δ(ppm) = 8.48 (d, ^3J(H,H) = 5.9 Hz 2H, CH_{ar}), 7.17 (s, 1H, CH_{ar}), 7.05 (d, ^3J(H,H) = 5.9 Hz 2H, CH_{ar}), 5.76 (s, 1H, C*H*), 2.68 (m, 4H, CH_2), 2.03 (s, 3H, CH_3), 1.97 (s, 3H, CH_3), 1.95 (s, 3H, CH_3), 1.91 (m, 2H, CH_2). **^{13}C-NMR (125 MHz, CD_3CN):** δ(ppm) = 151.2, 150.1, 147.4, 141.5, 138.7, 137.9, 137.1, 133.2, 132.3, 127.3, 127.1, 119.7, 107.2, 39.3, 38.3, 23.5, 14.9, 13.64, 13.61. **HR-MS(ESI$^+$):** m/z = 336.1356 (calcd. 336.1422 for $C_{21}H_{22}NOS^+$).

1-(3-(2,5-Dimethylfuryl))-2-(3-(5-*p*-methylpyridinium)-2-methylthienyl)-cyclopentene chloride 14

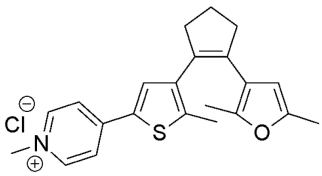

14

1-(3-(2,5-Dimethylfuryl))-2-(3-(5-*p*-pyridyl)-2-methylthienyl)-cyclopentene **13** (0.80 g, 2.40 mmol) was dissolved in MeCN (50 mL) under Ar and MeI (0.38 mL, 6.0 mmol) was added. The solution was stirred at 70 °C for 4 h. Then, the solvent was evaporated *in vacuo* and CH_2Cl_2 was added. Subsequently, the solution was washed with brine, dried over anhyd. $MgSO_4$, and the solvent removed *in vacuo* to yield **14** as orange solid (89%). **^{1}H-NMR (500 MHz, CD_3CN):** δ(ppm) = 8.48 (d, ^3J(H,H) = 6.8 Hz 2H, CH_{ar}), 7.98 (d, ^3J(H,H) = 6.8 Hz 2H, CH_{ar}), 7.81 (s, 1H, CH_{ar}), 5.68 (s, 1H, CH_{ar}), 4.18 (s, 3H, CH_3), 2.76 (m, 4H, CH_2), 2.16 (s, 3H, CH_3), 2.11 (s, 3H, CH_3), 2.04 (m, 2H, CH_2), 1.91 (s, 3H, CH_3). **^{13}C-NMR (125 MHz, CD_3CN):** δ(ppm) = 162.0, 151.0, 150.1, 147.9, 146.3, 141.5, 135.2, 134.7, 134.1, 132.2, 122.9, 119.2, 107.7, 48.4, 39.5, 38.7, 23.9, 15.6, 13.7, 13.6. **HR-MS(ESI$^+$):** m/z = 350.0214 (calcd. 350.1579 for $C_{22}H_{24}NOS^+$).

1-(3-(2,5-Dimethylfuryl))-2-(3-(5-*p*-methylpyridinium)-2-methylthienyl)-cyclopentene hexafluorophosphate 15

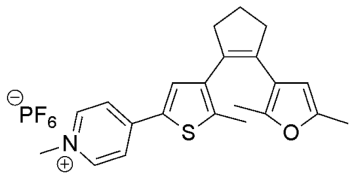

15

1-(3-(2,5-Dimethylfuryl))-2-(3-(5-*p*-methylpyridinium)-2-methylthienyl)-cyclopentene chloride **14** (0.71 g, 1.85 mmol) was dissolved in MeCN (50 mL) whereupon $NaPF_6$ (2.52 g, 15 mmol) and H_2O (1 mL) were added. The solution was stirred at rt for 1 h and subsequently the solvent was evaporated *in vacuo*. The precipitate was washed extensively with H_2O and dried *in vacuo* to yield the target compound **15** as red solid (44%). **^{1}H-NMR (500 MHz, C_6D_6):** δ(ppm) = 7.88 (d, ^3J(H,H) = 6.8 Hz 2H, CH_{ar}), 7.37 (s, 1H, CH_{ar}), 7.14 (d, ^3J(H,H) = 6.8 Hz 2H, CH_{ar}), 5.66 (s, 1H, CH_{ar}), 3.95 (s, 3H, CH_3), 2.69 (m, 4H, CH_2), 1.99 (s, 3H, CH_3), 1.95 (m, 2H, CH_2), 1.94 (s, 3H, CH_3), 1.91 (s, 3H, CH_3). **^{13}C-NMR (125 MHz, C_6D_6):** δ(ppm) = 150.3, 148.4, 147.4, 144.8, 144.4, 140.6, 134.4, 133.6, 133.1, 131.5, 121.8, 118.7, 107.1, 47.5, 39.2, 38.4, 23.5, 15.2, 13.63, 13.56. **^{19}F-NMR (470 MHz, C_6D_6):** δ(ppm) = -70.2, -71.7. **HR-MS(ESI$^+$):** m/z = 350.1513 (calcd. 350.1579 for $C_{22}H_{24}NOS^+$).

1-(3-(2,5-Dimethylfuryl))-2-(3-(5-(*p*-benzoic acid 1,3-bis(dimethylamino))-2-propanoate)-2-methylthienyl)-cyclopentene hydrochloride 16

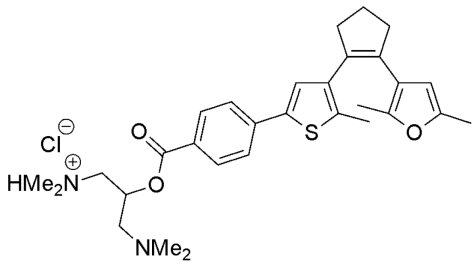

16

1-(3-(2,5-Dimethylfuryl))-2-(3-(5-chloro-2-methylthienyl))-cyclopentene **12** (0.69 g, 2.35 mmol) was dissolved in dry THF (5 mL) in a Schlenk tube under Ar. To this solution was added dropwise *n*-BuLi (1.2 mL, 2.2 M) and the resulting brownish solution was stirred at rt for 30 min. Then, $B(OBu)_3$ (0.95 mL, 3.5 mmol) was added and the mixture was stirred for 45 min at rt. Meanwhile, **17** (1.16 g, 3.5 mmol) was dissolved in THF (5 mL) in a Schlenk flask under Ar. To this solution was added $Pd(PPh_3)_4$ (0.14 g, 0.1 mmol) and the resulting mixture was stirred at rt for 15 min. Afterwards, degassed aq. Na_2CO_3 solution (10 mL, 2 M) and ethylene glycol (3 drops) were added. This mixture was heated to 65 °C and then the

solution containing the borate was added directly without any workup. The combined solutions were stirred at 65 °C for 1 d. Afterwards, the solution was diluted with water and extracted with Et_2O. The combined organic layers were washed with brine, dried over anhyd. $MgSO_4$, and the solvent was removed *in vacuo*. The resulting crude product was purified by column chromatography (silica, acetone with 1% Et_3N) to yield the free base (93%) which was converted to the hydrochloride by passing anhyd. HCl (generated from dripping muriatic acid into conc. H_2SO_4) through a solution of the free base in anhyd. Et_2O. The received compound was recrystallized from MeCN/Et_2O to yield the target hydrochloride as off-white solid **16** (62%). **^{1}H-NMR (500 MHz, CD_3CN):** δ(ppm) = 8.06 (d, ^3J(H,H) = 8.7 Hz 2H, CH_{ar}), 7.64 (d, ^3J(H,H) = 8.7 Hz 2H, CH_{ar}), 7.30 (s, 1H, CH_{ar}), 5.95 (m, 1H, C*H*), 5.67 (s, 1H, CH_{ar}), 3.90 (m, 2H, CH_2), 3.52 (m, 2H, CH_2), 2.82 (s, 12H, CH_3), 2.72 (m, 4H, CH_2), 2.08 (s, 3H, CH_3), 2.05 (s, 3H, CH_3), 1.98 (m, 2H, CH_2), 1.89 (s, 3H, CH_3). **^{13}C-NMR (125 MHz, CD_3CN):** δ(ppm) = 165.8, 150.3, 147.3, 140.2, 139.0, 138.8, 137.2, 133.3, 132.9, 132.7, 131.7, 128.0, 127.6, 125.6, 119.0, 107.3, 66.0, 58.5, 44.3, 39.1, 38.1, 23.4, 14.5, 13.3, 13.1. **HR-MS(ESI$^+$):** m/z = 507.2584 (calcd. 507.2681 for $C_{30}H_{39}N_2O_3S^+$).

***p*-Bromobenzoic acid 1,3-bis(dimethylamino)-2-propanoate 17**

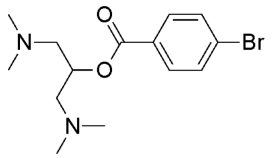

17

To an ice-cooled solution of 1,3-bis(dimethylamino)-2-propanol (3.26 mL, 20 mmol) in CH_2Cl_2 (20 mL) was added 4-bromobenzoyl chloride (5.27 g, 24 mmol) in CH_2Cl_2 (20 mL) dropwise via addition funnel. The resulting mixture was stirred at rt overnight whereupon precipitate was formed. Subsequently, the formed hydrochloride was dissolved with sat. aq. Na_2CO_3 sol., the organic layer was washed with brine, and the solvent was removed *in vacuo*. The crude mixture was dissolved in petroleum ether and precipitate was filtered off. The filtrate was concentrated in vacuo to yield the target compound as **17** a yellow oil (67%). **^{1}H-NMR (300 MHz, C_6D_6):** δ(ppm) = 7.84 (m, 1H, CH_{ar}), 7.82 (m, 1H, CH_{ar}), 7.15 (m, 1H, CH_{ar}), 7.12 (m, 1H, CH_{ar}), 5.58 (m, 1H, C*H*), 2.47 (m, 4H, CH_2), 2.14 (s, 12H, CH_3). **^{13}C-NMR (75 MHz, C_6D_6):** δ(ppm) = 165.6, 154.1, 132.2, 131.8, 130.6, 71.5, 61.9, 46.5. **HR-MS(ESI$^+$):** m/z = 329.0737 (calcd. 329.0865 for $C_{14}H_{22}N_2O_2Br^+$).

1-(3-(2,5-Dimethylfuryl))-2-(3-(5-*p*-ethylbenzoyl)-2-methylthienyl)-cyclopentene 18

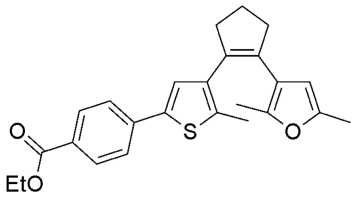

18

To a solution of 1-(3-(2,5-dimethylfuryl))-2-(3-(5-chloro-2-methylthienyl))-cyclopentene **12** (1.00 g, 3.4 mmol) in dry THF (6 mL) under Ar was added *n*-BuLi (1.7 mL, 2.2 M). The reaction mixture turned dark and was stirred at rt for 30 min. Afterwards, $B(OiPr)_3$ (0.96 g, 5.1 mmol) was added and the mixture was stirred at rt for 1 h. Meanwhile, *p*-bromo ethylbenzoate (1.17 g, 5.1 mmol) was dissolved in THF (3 mL) and to this solution $Pd(PPh_3)_4$ (0.39 g, 0.34 mmol) was added. The resulting mixture was stirred at rt for 45 min. Then, degassed aq. Na_2CO_3 sol. (6 mL, 2 M) and ethylene glycol (4 drops) were added. The resulting solution was heated to 65 °C and the borate was added to this solution via a syringe without any workup. The combined solutions were stirred at 65 °C for 1 d. Afterwards, the solution was diluted with water and extracted with Et_2O. The combined organic layers were washed with brine, dried over anhyd. $MgSO_4$, and the solvent was removed in vacuo. The resulting crude product was purified by column chromatography (silica, PE:CH_2Cl_2 = 2:1) to yield the target compound **18** as a yellowish oil (67%). **^{1}H-NMR (500 MHz, C_6D_6):** δ(ppm) = 8.13 (d, ^3J(H,H) = 8.5 Hz, 2H, CH_{ar}), 7.48 (d, ^3J(H,H) = 8.5 Hz, 2H, CH_{ar}), 7.17 (s, 1H, CH_{ar}), 5.76 (s, 1H, CH_{ar}), 4.15 (q, ^3J(H,H) = 7.1 Hz, 2H, CH_2), 2.70 (m, 4H, CH_2), 2.06 (s, 3H, CH_3), 2.00 (s, 3H, CH_3), 1.96 (s, 3H, CH_3), 1.91 (m, 2H, CH_2), 1.05 (t, ^3J(H,H) = 7.1 Hz, 3H, CH_3). **^{13}C-NMR (125 MHz, C_6D_6):** δ(ppm) = 166.0, 149.6, 147.1, 139.3, 139.0, 138.3, 136.0, 132.6, 132.2, 131.9, 131.4, 130.7, 129.4, 126.1, 125.2, 118.6, 107.0, 60.8, 39.1, 38.0, 23.2, 14.6, 14.3, 13.4, 13.3. **HR-MS(ESI$^+$):** m/z = 407.1458 (calcd. 407.1681 for $C_{25}H_{27}O_3S^+$).

1-(3-(2,5-Dimethylfuryl))-2-(3-(5-*p*-sodiumbenzoyl)-2-methylthienyl)-cyclopentene 19

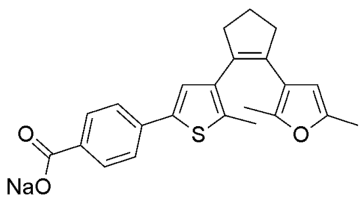

19

To ester **19** (0.077 g, 0.19 mmol) was added NaOH sol. in EtOH (1.9 mL, 0.1 M). The whole was stirred at 65 °C for 3 h and subsequently the solvent was removed *in vacuo*. The residue was suspended in MeCN, filtered off by vacuum filtration, and washed repeatedly with MeCN

to yield the target compound **19** as a white solid (75%). **^{1}H-NMR (500 MHz, DMSO-d$_6$):** δ(ppm) = 7.92 (d, ^3J(H,H) = 8.1 Hz, 2H, CH_{ar}), 7.47 (d, ^3J(H,H) = 8.1 Hz, 2H, CH_{ar}), 7.27 (s, 1H, CH_{ar}), 5.73 (s, 1H, CH_{ar}), 2.72 (mb, 4H, CH_2), 2.10 (s, 3H, CH_3), 2.00 (s, 3H, CH_3), 1.96 (m, 2H, CH_2), 1.90 (s, 3H, CH_3). **^{13}C-NMR (125 MHz, DMSO-d$_6$):** δ(ppm) = 169.8, 148.6, 145.7, 139.0, 138.6, 137.0, 133.9, 133.0, 131.7, 131.0, 129.7, 124.2, 123.5, 117.6, 106.2, 38.1, 37.0, 21.9, 13.9, 12.9. 12.6. **HR-MS(ESI$^+$):** m/z = 379.1354 (calcd. 379.1368 for $C_{23}H_{23}O_3S^+$).

1-(3-(2,5-Dimethylfuryl))-2-(3-(5-*p*-ethylbenzoyl)-2-methylthienyl)-cyclopentene-maleimide adduct 20o

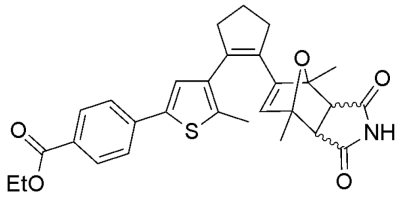

20o

Maleimide (0.24 g, 2.50 mmol) and 1-(3-(2,5-dimethylfuryl))-2-(3-(5-*p*-ethylbenzoyl)-2-methylthienyl))-cyclopentene **18** (0.20 g, 0.50 mmol) were dissolved in EtOH (2 mL) under Ar and stirred for 3 h at 80 °C. Removal of the solvent an subsequent column chromatography (silica, petroleum ether:EtOAc = 2:1) yielded **20o** as white foam as a mixture of 90% of the *exo* isomer and 10% of the *endo* isomer (79% overall yield). **^{1}H-NMR (500 MHz, C$_6$D$_6$):** δ(ppm) = 8.14 (d, ^3J(H,H) = 8.7 Hz, 2H, CH_{ar}), 7.49 (d, ^3J(H,H) = 8.7 Hz, 2H, CH_{ar}), 7.48 (sb, 1H, N*H*), 7.00 (s, 1H, CH_{ar}), 5.85 (s, 1H, *endo*-C*H*), 5.51 (s, 1H, *exo*-C*H*), 4.41 (q, ^3J(H,H) = 6.9 Hz, 2H, CH_2), 2.64 (d, ^3J(H,H) = 2.5 Hz, 1H, *endo*-C*H*), 2.52 (m, 2H, CH_2, *endo*-C*H*), 2.42 (m, 2H, CH_2), 2.40 (d, ^3J(H,H) = 6.5 Hz, 1H, *exo*-C*H*), 2.25 (d, ^3J(H,H) = 6.5 Hz, 1H, *exo*-C*H*), 2.16 (m, 1H, CH_2), 2.14 (s, 3H, *endo*-CH_3), 2.09 (s, 3H, *exo*-CH_3), 1.76 (m, 2H, CH_2), 1.72 (s, 3H, *exo*-CH_3), 1.58 (s, 3H, *endo*-CH_3), 1.52 (s, 3H, *exo*-CH_3), 1.43 (s, 3H, e*ndo*-CH_3), 1.03 (t, ^3J(H,H) = 7.1 Hz, 3H, CH_3). **^{13}C-NMR (125 MHz, C$_6$D$_6$):** δ(ppm) = *exo*: 174.7, 170.4, 166.3, 151.0, 140.0, 139.0, 137.4, 137.1, 136.0, 134.4, 132.8, 131.1, 130.0, 126.2, 125.6, 89.7, 87.4, 61.2, 54.8, 54.4, 39.1, 36.7, 23.6, 16.41, 16.39, 15.1, 14.4. **HR-MS(ESI$^+$):** m/z = 504.1792 (calcd. 504.1845 for $C_{29}H_{30}NO_5S^+$).

1-(3-(2,5-Dimethylfuryl))-2-(3-(5-*p*-ethylbenzoyl)-2-methylthienyl)-cyclopentene-maleimide adduct 20c

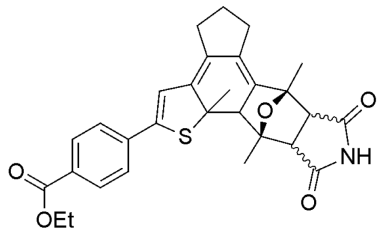

20c

1-(3-(2,5-Dimethylfuryl))-2-(3-(5-*p*-ethylbenzoyl)-2-methylthienyl)-cyclopentene-maleimide adduct **20o** (0.05 g, 0.10 mmol) was dissolved in degassed MeCN (150 mL) and irradiated in a Rayonet RPR 100 reactor equipped with 300 nm lamps for 5 min while agitated every 1 min. Column chromatography (silica, PE:EtOAc = 2:1) yielded the ring-closed form **20c** as a mixture of the *endo* and *exo* adduct (38%). **^{1}H-NMR (500 MHz, C_6D_6):** δ(ppm) = 8.17 (d, ^3J(H,H) = 8.4 Hz 2H, CH_{ar}), 7.68 (s, 1H, N*H*), 7.49 (d, ^3J(H,H) = 8.4 Hz 2H, CH_{ar}), 6.44 (s, 1H, CH_{ar}), 4.14 (q, ^3J(H,H) = 7.1 Hz, 2H, CH_2), 2.87 (s, 1H, *exo*-C*H*), 2.72 (s, 1H, *endo*-C*H*), 2.44 (d, ^3J(H,H) = 5.3 Hz, 2H, *exo*-C*H*), 2.43 (m, 2H, CH_2, *endo*-C*H*), 2.21 (d, ^3J(H,H) = 5.3 Hz, 2H, *exo*-C*H*), 2.23 (m, 1H, CH_2), 2.11 (m, 3H, CH_2, *endo*-C*H*), 2.00 (s, 3H, *endo*-CH_3), 1.92 (s, 3H, *exo*-CH_3), 1.83 (s, 3H, *endo*-CH_3), 1.77 (s, 3H, *exo*-CH_3), 1.59 (m, 2H, CH_2), 1.40 (s, 3H, e*ndo*-CH_3), 1.34 (s, 3H, *exo*-CH_3), 1.03 (t, ^3J(H,H) = 7.1 Hz, 3H, CH_3). **HR-MS(ESI$^+$):** m/z = 503.1548 (calcd. 503.1766 for $C_{29}H_{29}NO_5S^+$).

1-(3-(2,5-Dimethylfuryl))-2-(3-(5-*p*-ethylbenzoyl)-2-methylthienyl)-cyclopentene-*N*-ethylmaleimide adduct 21o

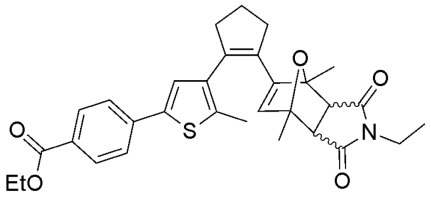

21o

N-ethylmaleimide (0.31 g, 2.50 mmol) and 1-(3-(2,5-dimethylfuryl))-2-(3-(5-*p*-ethylbenzoyl)-2-methylthienyl))-cyclopentene **18** (0.20 g, 0.50 mmol) were dissolved in EtOH (2 mL) under Ar and stirred for 3 h at 80 °C. Removal of the solvent an subsequent column chromatography (silica, PE:THF = 5:1) yielded **21o** as yellowish oil as a mixture of 90% of the *exo* isomer and 10% of the *endo* isomer (83% overall yield). **^{1}H-NMR (500 MHz, C_6D_6):** δ(ppm) = 8.14 (d, ^3J(H,H) = 8.7 Hz, 2H, CH_{ar}), 7.49 (d, ^3J(H,H) = 8.7 Hz, 2H, *exo*-CH_{ar}), 7.44 (d, ^3J(H,H) = 8.7 Hz, 2H, *endo*-CH_{ar}), 7.03 (s, 1H, *exo*-CH_{ar}), 6.99 (s, 1H, *endo*-CH_{ar}), 5.56 (s, 1H, *exo*-C*H*),

5.46 (m, 1H, *endo*-C*H*), 4.14 (q, ^3J(H,H) = 7.1 Hz, 2H, CH_2), 3.35 (q, ^3J(H,H) = 7.1 Hz, 2H, *exo*-CH_2), 3.24 (m, 2H, *endo*-CH_2), 2.71 (d, ^3J(H,H) = 7.8 Hz, 1H, *endo*-C*H*), 2.66 (d, ^3J(H,H) = 7.8 Hz, 1H, *endo*-C*H*), 2.56 (m, 1H, CH_2), 2.45 (m, 2H, CH_2), 2.44 (d, ^3J(H,H) = 6.5 Hz, 1H, *exo*-C*H*), 2.30 (d, ^3J(H,H) = 6.5 Hz, 1H, *exo*-C*H*), 2.20 (m, 1H, CH_2), 2.11 (s, 3H, CH_3), 1.76 (m, 2H, CH_2), 1.75 (s, 3H, *exo*-CH_3), 1.66 (s, 3H, *endo*-CH_3), 1.55 (s, 3H, *exo*-CH_3), 1.46 (s, 3H, *endo*-CH_3), 1.43 (s, 3H, e*ndo*-CH_3), 1.03 (t, ^3J(H,H) = 7.1 Hz, 3H, CH_3), 0.96 (t, ^3J(H,H) = 7.1 Hz, 3H, CH_3). **^{13}C-NMR (125 MHz, C_6D_6):** δ(ppm) = *exo*: 174.6, 174.4, 166.2, 151.1, 140.0, 139.0, 137.5, 137.3, 136.0, 132.9, 130.0, 131.1, 126.2, 125.6, 108.4, 89.7, 87.4, 67.6, 53.6, 53.2, 39.1, 36.8, 34.0, 29.5, 16.54, 16.50, 15.1, 14.6, 13.4. **HR-MS(ESI$^+$):** m/z = 531.2094 (calcd. 531.2097 for $C_{31}H_{33}NO_5S^+$).

1-(3-(2,5-Dimethylfuryl))-2-(3-(5-*p*-sodiumbenzoyl)-2-methylthienyl)-cyclopentene-maleimide adduct 22o

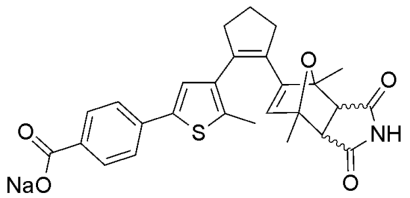

22o

1-(3-(2,5-Dimethylfuryl))-2-(3-(5-*p*-sodiumbenzoyl)-2-methylthienyl)-cyclopentene **19** (0.100 g, 0.25 mmol) and maleimide (0.121 g, 1.25 mmol) were dissolved in EtOH (2.0 mL) and stirred at rt for 1 d. Subsequently, the solvent was removed *in vacuo*, the crude compound dispersed in acetone, filtered off and washed with acetone repeatedly to remove residual maleimide yielding **22o** as a mixture of the *endo* (40%) and *exo* adduct (60%) (quant.). **^{1}H-NMR (500 MHz, D_2O):** δ(ppm) = 7.80 (m, 2H, CH_{ar}), 7.40 (m, 2H, CH_{ar}), 6.93 (m, 1H, CH_{ar}), 5.63 (s, 1H, *endo*-CH_{ar}), 5.55 (s, 1H, *exo*-CH_{ar}) 3.32 (d, ^3J(H,H) = 7.1 Hz, 1H, *endo*-C*H*), 3.27 (d, ^3J(H,H) = 7.1 Hz, 1H, *endo*-C*H*), 2.65 (d, ^3J(H,H) = 6.2 Hz, 1H, *exo*-C*H*), 2.59 (d, ^3J(H,H) = 6.2 Hz, 1H, *exo*-C*H*), 2.35 (m, 4H, CH_2), 2.02 (s, 3H, CH_3), 1.69 (m, 2H, CH_2), 1.42 (s, 3H, *endo*-CH_3), 1.38 (s, 3H, *endo*-CH_3), 1.33 (s, 3H, *exo*-CH_3), 1.32 (s, 3H, *exo*-CH_3). **HR-MS(ESI$^+$):** m/z = 476.1455 (calcd. 476.1532 for $C_{27}H_{26}NO_5S^+$).

1-(3-(2,5-Dimethylfuryl))-2-(3-(5-*p*-sodiumbenzoyl)-2-methylthienyl)-cyclopentene-maleimide adduct 22c

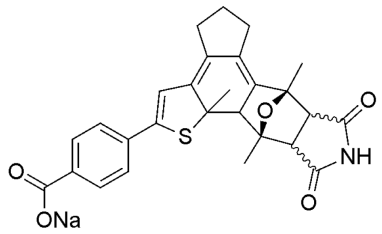

22c

1-(3-(2,5-Dimethylfuryl))-2-(3-(5-*p*-ethylbenzoyl)-2-methylthienyl)-cyclopentene-maleimide adduct **20c** (0.019 g, 0.038 mmol) was dissolved in NaOH in EtOH (0.38 mL, 0.1 M) and stirred at 70 °C for 3 h. Evaporation of the solvent yielded the ring-closed form **22c** as a mixture of the *endo* and *exo* adduct (quant.). **^{1}H-NMR (500 MHz, D_2O):** δ(ppm) = 7.72 (s, 1H, N*H*), 7.71 (d, ^3J(H,H) = 8.1 Hz, 2H, CH_{ar}), 7.60 (d, ^3J(H,H) = 8.1 Hz, 2H, CH_{ar}), 6.72 (s, 1H, CH_{ar}), 2.82 (s, 1H, C*H*), 2.76 (m, 1H, C*H*), 2.71 (m, 1H, C*H*), 2.38 (m, 2H, CH_2), 2.26 (m, 2H, CH_2), 1.67 (m, 2H, CH_2), 1.51 (s, 3H, CH_3), 1.47 (s, 3H, CH_3), 1.00 (s, 3H, CH_3). **HR-MS(ESI$^+$):** m/z = 476.1394 (calcd. 476.1532 for $C_{27}H_{26}NO_5S^+$).

1-(3-(2,5-Dimethylfuryl))-2-(3-(5-*p*-sodiumbenzoyl)-2-methylthienyl)-cyclopentene-*N*-ethylmaleimide adduct 23o

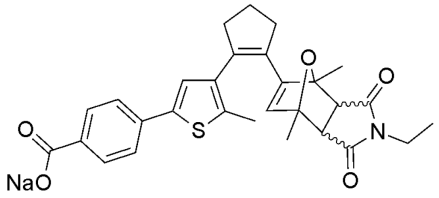

23o

1-(3-(2,5-Dimethylfuryl))-2-(3-(5-*p*-sodiumbenzoyl)-2-methylthienyl)-cyclopentene **19** (0.100 g, 0.25 mmol) and *N*-ethylmaleimide (0.156 g, 1.25 mmol) were dissolved in EtOH (2.0 mL) and stirred at 70 °C for 6 h. Subsequently, the solvent was removed *in vacuo*, the crude compound dispersed in acetone, filtered off and washed with acetone repeatedly to remove residual *N*-ethylmaleimide yielding **23o** as mixture of the *endo* (3%) and the *exo* adduct (97%) (quant.). **^{1}H-NMR (500 MHz, DMSO, D_2O):** *exo* adduct**:** δ(ppm) = 7.76 (d, ^3J(H,H) = 7.5 Hz, 2H, CH_{ar}), 7.49 (d, ^3J(H,H) = 7.5 Hz, 2H, CH_{ar}), 7.17 (s, 1H, CH_{ar}), 5.89 (s, 1H, CH_{ar}), 3.27 (q, ^3J(H,H) = 6.5 Hz, 2H, CH_2), 2.84 (d, ^3J(H,H) = 5.6 Hz, 1H, C*H*), 2.78 (d, ^3J(H,H) = 5.6 Hz, 1H, C*H*), 2.65 (m, 2H, CH_2), 2.43 (m, 2H, CH_2), 2.17 (s, 3H, CH_3), 1.90 (m, 2H, CH_2), 1.36 (s, 6H, CH_3), 0.90 (t, ^3J(H,H) = 6.5 Hz, 3H, CH_3). **HR-MS(ESI$^+$):** m/z = 526.1635 (calcd. 526.1664 for $C_{29}H_{29}NO_5NaS^+$).

Functionalization Attempts on MWCNTs

Method A. The functionalization attempts on MWCNTs were carried out in Schlenk tubes under Ar according to procedures in the literature.[210] Neat furfuryl alcohol or 3-acetyl-2,5-dimethylfuran (3 mL) were degassed by repeated sonication and pump cycles whereupon MWCNTs (50 mg) were added to the reactant. The dispersions were stirred for 1 d at either 75 °C or 150 °C. Subsequently the mixtures were cooled to r.t., the tubes collected by vacuum filtration, and washed extensively with THF. When TGA and FTIR analysis did not prove any visible functionalization the protocol was altered adding a 1 h sonication step before the heating.

Method B. As Method A did not produce any visible functionalization, the protocol was changed to the one published by Chang and Liu.[209] Furfuryl alcohol or 3-acetyl-2,5-dimethylfuran (3 mL) were dissolved in DMSO (15 mL) and degassed by repeated sonication and pump cycles. Afterwards, MWCNTs (50 mg) were added to the solution and stirred at 50 °C or 75 °C for 3 d. Subsequently the mixtures were cooled to r.t., the tubes collected by vacuum filtration, and washed extensively with THF. TGA and FTIR analysis showed ambiguous results for the runs at 50 °C so Method B was used with switch **2o** in a 0.2 M solution in DMSO.

Functionalization attempts on SWCNTs

Method B optimized earlier with MWCNTs was used for the functionalization of SWCNTs using water instead of DMSO and switch **19o** (0.1 M).

4.3 Procedures and Photochemistry

4.3.1 General Remarks

All procedures linked to photochemistry were performed using spectrophotometric grade solvents. UV/vis absorption spectroscopy was performed on a Varian Cary 60 UV/vis spectrophotometer equipped with a Peltier thermostated cell holder at 25 ± 0.05 °C if not indicated otherwise. Analytical irradiation was performed employing an Oriel 500 W mercury arc lamp model 68810 in an Oriel universal arc lamp housing model 66055 equipped with an Oriel ¼ m grating monochromator model 77200, an Oriel timed shutter and water filter either at 313 nm or 334 nm for ring-closure or at 436 nm or 546 nm for ring-opening reactions or on an Oriel 1000 W xenon arc lamp model 66924 using an Oriel timed shutter, water filter, and various cut-off filters. The lamp output beam was wired into the spectrophotometer orthogonal to the beamline of the respective spectrophotometer employing fiber-optics to enable simultaneous irradiation and probing.

Quantum yields were determined using the initial slope method according to Equation (1.9) presented in Chapter 1.3.3. Due to the intrinsic error in the mathematical approximation (linear fitting of the initial slope) employed and the varying time intervals for cyclization and cycloreversion reactions (longer in the case of cycloreversion), the quantum yields obtained by this method exhibit an estimated relative uncertainty in measurement of 10% of the obtained value for photocyclization and for cycloreversion reactions. Quantum yields were determined by comparing the initial reaction yields for the cyclization and the cycloreversion of the diarylethenes with the isomerization of commercial azobenzene in methanol[106] and commercial furyl fulgide Aberchrome 670 in toluene,[267] respectively.

4.3.2 *In situ* Diels-Alder Studies

In situ Diels-Alder studies were carried out in a quartz cuvette employing DAE **2o** (10^{-5} M) and maleimide (10^{-2} M) in spectroscopy grade toluene. The solutions were kept at temperatures from 25 °C to 60 °C employing a Varian Cary 60 UV/vis spectrophotometer equipped with a Peltier thermostated cell holder for a given time. Simultaneous irradiation was performed by employing Roithner LEDs (UVTOP335-BL-TO18, LED375-06, LED395-02V, LED405-06V, and LED535-01) driven by a GW Instek GPD-3303S linear DC power supply. After the given time, the composition of the solutions was analyzed by UPLC/MS. The retention times of the involved species were determined independently. The diode array

detector signal at 270 nm was chosen for relative integration of the signals as the molar absorptivities of the relevant species **2o**, **2c**, **4o**, and **4c** are almost similar at this wavelength (compare Figure 2-5a).

Thermal reaction of **2o** and maleimide without irradiation was carried out for 1 d. Amplification of the Diels-Alder reaction was performed by thermal reaction for 6 h while irradiating with 335 nm and 535 nm light. UVTOP335-BL-TO18 at 1 mA and 6.2 V and LED535-01 at 20 mA and 4.0 V were employed. Inhibition of the Diels-Alder reaction was performed by thermal reaction for 1 d while irradiating with 375 nm light. An LED375-06 at 20 mA and 4.3 V during the first hour and 1 mA and 4.3 V for the remaining 23 h was employed.

4.3.3 Photoinduced Release of Maleimide Derivatives

The photoinduced releases of maleimide from **22c** and the release of *N*-ethylmaleimide from **23c** were carried out *in situ* in a quartz cuvette using phosphate buffered saline as solvent. 10^{-4} M solutions were employed and tempered using a Varian Cary 60 or Cary 50 UV/vis spectrophotometer equipped with a Peltier thermostated cell holder for a given time. Generation of the ring-closed isomers was carried out *in situ* by irradiation of the respective DAEs **22o** or **23o** employing the Oriel 500 W mercury arc lamp until the quasi quantitative PSS was reached. The compositions of the solutions at a certain time were determined by UPLC/MS measurements through integration of the DAD signals at 280 nm where the molar absorptivity of all participating species was approximately identical. For preparation of the UPLC samples, an aliquot of 100 µL was pipetted out of the cuvette and diluted with 50 µL MeCN and 50 µL THF to avoid the formation of aggregates that could stick on the column. The retention times of the involved species were determined independently on the isolated compounds.

The *in situ* step experiment for the release of maleimide from **22c** was carried out by initial irradiation of **22o** to the PSS consisting almost exclusively of **22c** employing the Oriel 500 W mercury arc lamp and the grating monochromator. Ring-opening to **22o** was then performed on the Oriel 1000 W xenon arc lamp using cut-off filters with transmission only at wavelengths greater than 400 nm. The following release process was observed by UPLC/MS measurements as specified earlier. After 5 h, ring-closing for deactivation was then initiated by irradiation of the mixture until **22** reached its PSS employing the Oriel 500 W mercury arc lamp and the grating monochromator. Tempering for 15 h was then again observed by

UPLC/MS until the **22c** was activated, *i.e.* ring-opened to **22o** again by employing the Oriel 1000 W xenon arc lamp using cut-off filters and followed by subsequent tempering.

References

[1] R. Exelby, R. Grinter, *Chem. Rev.* **1965**, *65*, 247–260.

[2] H. Bouas-Laurent, H. Dürr, *Pure Appl. Chem.* **2001**, *73*, 639–665.

[3] R. Göstl, A. Senf, S. Hecht, *Chem. Soc. Rev.* **2014**, *43*, 1982–1996.

[4] M.-M. Russew, S. Hecht, *Adv. Mater.* **2010**, *22*, 3348–3360.

[5] B. M. Neilson, C. W. Bielawski, *ACS Catal.* **2013**, 1874–1885.

[6] J. Zhang, Q. Zou, H. Tian, *Adv. Mater.* **2013**, *25*, 378–399.

[7] E. Orgiu, P. Samorì, *Adv. Mater.* **2014**, *26*, 1827–1845.

[8] H. Dürr, H. Bouas-Laurent, *Photochromism: Molecules and Systems*, Elsevier Ltd, Oxford, **2003**.

[9] B. L. Feringa, W. R. Browne, *Molecular Switches*, John Wiley & Sons, **2011**.

[10] M. Irie, T. Seki, Y. Yokoyama, *New Frontiers in Photochromism*, Springer, Tokyo; London, **2013**.

[11] C. Dugave, L. Demange, *Chem. Rev.* **2003**, *103*, 2475–2532.

[12] R. Klajn, *Pure Appl. Chem.* **2010**, *82*, 2247–2279.

[13] R. Klajn, J. F. Stoddart, B. A. Grzybowski, *Chem. Soc. Rev.* **2010**, *39*, 2203–2237.

[14] A. Goulet-Hanssens, C. J. Barrett, *J. Polym. Sci. Part Polym. Chem.* **2013**, *51*, 3058–3070.

[15] G. Berkovic, V. Krongauz, V. Weiss, *Chem. Rev.* **2000**, *100*, 1741–1754.

[16] R. Klajn, *Chem. Soc. Rev.* **2013**, *43*, 148–184.

[17] B. V. Gemert, *Mol. Cryst. Liq. Cryst. Sci. Technol. Sect. Mol. Cryst. Liq. Cryst.* **2000**, *344*, 57–62.

[18] M. Kawano, T. Sano, J. Abe, Y. Ohashi, *J. Am. Chem. Soc.* **1999**, *121*, 8106–8107.

[19] A. Kikuchi, F. Iwahori, J. Abe, *J. Am. Chem. Soc.* **2004**, *126*, 6526–6527.

[20] Y. Kishimoto, J. Abe, *J. Am. Chem. Soc.* **2009**, *131*, 4227–4229.

[21] R. H. Mitchell, *Eur. J. Org. Chem.* **1999**, *1999*, 2695–2703.

[22] K. Ayub, R. Li, C. Bohne, R. V. Williams, R. H. Mitchell, *J. Am. Chem. Soc.* **2011**, *133*, 4040–4045.

[23] W. A. Velema, W. Szymanski, B. L. Feringa, *J. Am. Chem. Soc.* **2014**, *136*, 2178–2191.

[24] M. Irie, *Chem. Rev.* **2000**, *100*, 1683–1684.

[25] H. Tian, S. Yang, *Chem. Soc. Rev.* **2004**, *33*, 85.

[26] M. Irie, *Photochem. Photobiol. Sci.* **2010**, *9*, 1535–1542.

[27] H. D. Samachetty, N. R. Branda, *Chem. Commun.* **2005**, 2840–2842.

[28] H. D. Samachetty, N. R. Branda, *Pure Appl. Chem.* **2006**, *78*, 2351–2359.

[29] H. D. Samachetty, V. Lemieux, N. R. Branda, *Tetrahedron* **2008**, *64*, 8292–8300.

[30] R. M. Kellogg, M. B. Groen, H. Wynberg, *J. Org. Chem.* **1967**, *32*, 3093–3100.

[31] M. Irie, O. Miyatake, K. Uchida, T. Eriguchi, *J. Am. Chem. Soc.* **1994**, *116*, 9894–9900.

[32] Y. Yokoyama, H. Shiraishi, Y. Tani, Y. Yokoyama, Y. Yamaguchi, *J. Am. Chem. Soc.* **2003**, *125*, 7194–7195.

[33] H. Nakagawa, S. Kawai, T. Nakashima, T. Kawai, *Org. Lett.* **2009**, *11*, 1475–1478.

[34] T. Nakashima, Y. Kajiki, S. Fukumoto, M. Taguchi, S. Nagao, S. Hirota, T. Kawai, *J. Am. Chem. Soc.* **2012**, *134*, 19877–19883.

[35] M. Irie, K. Uchida, *Bull. Chem. Soc. Jpn.* **1998**, *71*, 985–996.

[36] T. Yamaguchi, M. Irie, *J. Mater. Chem.* **2006**, *16*, 4690.

[37] D. Sysoiev, A. Fedoseev, Y. Kim, T. E. Exner, J. Boneberg, T. Huhn, P. Leiderer, E. Scheer, U. Groth, U. E. Steiner, *Chem. – Eur. J.* **2011**, *17*, 6663–6672.

[38] D. Sysoiev, T. Yushchenko, E. Scheer, U. Groth, U. E. Steiner, T. E. Exner, T. Huhn, *Chem. Commun.* **2012**, *48*, 11355–11357.

[39] J. Wolf, I. Eberspächer, U. Groth, T. Huhn, *J. Org. Chem.* **2013**, *78*, 8366–8375.

[40] P. Ren, R. Wang, S. Pu, G. Liu, C. Fan, *J. Phys. Org. Chem.* **2014**, *27*, 183–190.

[41] X. Li, S. Pu, H. Li, G. Liu, *Dyes Pigments* **2014**, *105*, 47–56.

[42] H. Li, S. Pu, G. Liu, B. Chen, *Dyes Pigments* **2014**, *101*, 15–24.

[43] H. Li, G. Liu, S. Pu, B. Chen, *Dyes Pigments* **2013**, *99*, 812–821.

[44] S. Pu, R. Wang, G. Liu, W. Liu, S. Cui, P. Yan, *Dyes Pigments* **2012**, *94*, 195–206.

[45] T. Yoshida, K. Arishima, F. Ebisawa, M. Hoshino, K. Sukegawa, A. Ishikawa, T. Kobayashi, M. Hanazawa, Y. Horikawa, *J. Photochem. Photobiol. Chem.* **1996**, *95*, 265–270.

[46] Z. Sun, H. Li, G. Liu, C. Fan, S. Pu, *Dyes Pigments* **2014**, *106*, 94–104.

[47] S. Pu, H. Li, G. Liu, W. Liu, S. Cui, C. Fan, *Tetrahedron* **2011**, *67*, 1438–1447.

[48] K. Uchida, T. Ishikawa, M. Takeshita, M. Irie, *Tetrahedron* **1998**, *54*, 6627–6638.

[49] T. Nakashima, M. Goto, S. Kawai, T. Kawai, *J. Am. Chem. Soc.* **2008**, *130*, 14570–14575.

[50] J. Piard, R. Métivier, M. Giraud, A. Léaustic, P. Yu, K. Nakatani, *New J. Chem.* **2009**, *33*, 1420–1426.

[51] M. Herder, M. Pätzel, L. Grubert, S. Hecht, *Chem. Commun.* **2010**, *47*, 460–462.

[52] H. Li, S. Pu, G. Liu, W. Liu, *J. Phys. Conf. Ser.* **2011**, *276*, 012132.

[53] M. Herder, M. Utecht, N. Manicke, L. Grubert, M. Pätzel, P. Saalfrank, S. Hecht, *Chem. Sci.* **2013**, *4*, 1028–1040.

[54] K. Yuan, J. Boixel, H. L. Bozec, A. Boucekkine, H. Doucet, V. Guerchais, D. Jacquemin, *Chem. Commun.* **2013**, *49*, 7896–7898.

[55] G. Liu, S. Pu, R. Wang, *Org. Lett.* **2013**, *15*, 980–983.

[56] H. Liu, S. Pu, G. Liu, B. Chen, *Dyes Pigments* **2014**, *102*, 159–168.

[57] S. Pu, P. Yan, G. Liu, W. Miao, W. Liu, *Tetrahedron Lett.* **2011**, *52*, 143–147.

[58] R. Wang, S. Pu, G. Liu, S. Cui, W. Liu, *Tetrahedron Lett.* **2012**, *53*, 320–324.

[59] S. Pu, C. Zheng, Q. Sun, G. Liu, C. Fan, *Chem. Commun.* **2013**, *49*, 8036–8038.

[60] C. Zheng, S. Pu, G. Liu, B. Chen, *Tetrahedron Lett.* **2013**, *54*, 7024–7028.

[61] S. Castellanos, L. Grubert, R. Stößer, S. Hecht, *J. Phys. Chem. C* **2013**, *117*, 23529–23538.

[62] S. Pu, C. Fan, W. Miao, G. Liu, *Tetrahedron* **2008**, *64*, 9464–9470.

[63] T. Wang, S. Pu, S. Cui, G. Liu, *J. Phys. Conf. Ser.* **2011**, *276*, 012192.

[64] R. Wang, S. Pu, G. Liu, S. Cui, H. Li, *Tetrahedron Lett.* **2013**, *54*, 5307–5310.

[65] M. Irie, *Chem. Rev.* **2000**, *100*, 1685–1716.

[66] L. N. Lucas, J. J. D. de Jong, J. H. van Esch, R. M. Kellogg, B. L. Feringa, *Eur. J. Org. Chem.* **2003**, *2003*, 155–166.

[67] G. Hohlneicher, M. Mueller, M. Demmer, J. Lex, J. H. Penn, L. X. Gan, P. D. Loesel, *J. Am. Chem. Soc.* **1988**, *110*, 4483–4494.

[68] M. Hanazawa, R. Sumiya, Y. Horikawa, M. Irie, *J. Chem. Soc. Chem. Commun.* **1992**, 206.

[69] M. M. Krayushkin, S. N. Ivanov, A. Y. Martynkin, B. V. Lichitsky, A. A. Dudinov, B. M. Uzhinov, *Russ. Chem. Bull.* **2001**, *50*, 2424–2427.

[70] M. M. Krayushkin, D. V. Pashchenko, B. V. Lichitskii, T. M. Valova, Y. P. Strokach, V. A. Barachevskii, *Russ. J. Org. Chem.* **2006**, *42*, 1816–1821.

[71] Z. Erno, A. M. Asadirad, V. Lemieux, N. R. Branda, *Org. Biomol. Chem.* **2012**, *10*, 2787–2792.

[72] H. Liu, Y. Chen, *J. Phys. Chem. A* **2009**, *113*, 5550–5553.

[73] L. Bougdid, A. Samat, C. Moustrou, *New J. Chem.* **2009**, *33*, 1357–1361.

[74] T. Nakashima, K. Atsumi, S. Kawai, T. Nakagawa, Y. Hasegawa, T. Kawai, *Eur. J. Org. Chem.* **2007**, *2007*, 3212–3218.

[75] S. Kawai, T. Nakashima, Y. Kutsunugi, H. Nakagawa, H. Nakano, T. Kawai, *J. Mater. Chem.* **2009**, *19*, 3606.

[76] H. Nakagawa, T. Nakashima, T. Kawai, *Eur. J. Org. Chem.* **2012**, *2012*, 4493–4500.

[77] X. Li, H. Tian, *Tetrahedron Lett.* **2005**, *46*, 5409–5412.

[78] C.-T. Poon, W. H. Lam, H.-L. Wong, V. W.-W. Yam, *J. Am. Chem. Soc.* **2010**, *132*, 13992–13993.

[79] H. Liu, Y. Chen, *J. Mater. Chem.* **2011**, *21*, 1246–1249.

[80] X. Deng, L. S. Liebeskind, *J. Am. Chem. Soc.* **2001**, *123*, 7703–7704.

[81] K. Morinaka, T. Ubukata, Y. Yokoyama, *Org. Lett.* **2009**, *11*, 3890–3893.

[82] S. Fukumoto, T. Nakagawa, S. Kawai, T. Nakashima, T. Kawai, *Dyes Pigments* **2011**, *89*, 297–304.

[83] S. Fukumoto, T. Nakashima, T. Kawai, *Eur. J. Org. Chem.* **2011**, *2011*, 5047–5053.

[84] S. Fukumoto, T. Nakashima, T. Kawai, *Angew. Chem. Int. Ed.* **2011**, *50*, 1565–1568.

[85] M. Kose, Ç. Yi. Sekerci, K. Suzuki, Y. Yokoyama, *J. Photochem. Photobiol. Chem.* **2011**, *219*, 58–61.

[86] J. He, T. Wang, S. Chen, R. Zheng, H. Chen, J. Li, H. Zeng, *J. Photochem. Photobiol. Chem.* **2014**, *277*, 45–52.

[87] M. M. Krayushkin, D. V. Pashchenko, B. V. Lichitsky, M. Irie, L. G. Vorontsova, Z. A. Starikova, *Mendeleev Commun.* **2007**, *17*, 301–302.

[88] R. Göstl, B. Kobin, L. Grubert, M. Pätzel, S. Hecht, *Chem. – Eur. J.* **2012**, *18*, 14282–14285.

[89] V. Z. Shirinian, A. A. Shimkin, D. V. Lonshakov, A. G. Lvov, M. M. Krayushkin, *J. Photochem. Photobiol. Chem.* **2012**, *233*, 1–14.

[90] V. Z. Shirinian, D. V. Lonshakov, A. G. Lvov, A. A. Shimkin, M. M. Krayushkin, *Photochem. Photobiol. Sci.* **2013**, *12*, 1717–1725.

[91] V. Z. Shirinian, A. G. Lvov, M. M. Krayushkin, E. D. Lubuzh, B. V. Nabatov, *J. Org. Chem.* **2014**, *79*, 3440–3451.

[92] G. Szalóki, J.-L. Pozzo, *Chem. – Eur. J.* **2013**, *19*, 11124–11132.

[93] S. Hiroto, K. Suzuki, H. Kamiya, H. Shinokubo, *Chem. Commun.* **2011**, *47*, 7149.

[94] V. A. Migulin, M. M. Krayushkin, V. A. Barachevsky, O. I. Kobeleva, T. M. Valova, K. A. Lyssenko, *J. Org. Chem.* **2011**, *77*, 332–340.

[95] R. Göstl, S. Hecht, *Angew. Chem. Int. Ed.* **2014**, *53*, 8784–8787.

[96] K. Yuan, J. Boixel, A. Chantzis, D. Jacquemin, V. Guerchais, H. Doucet, *Chem. – Eur. J.* **2014**, *20*, 10073–10083.

[97] Q. Zheng, M. F. Juette, S. Jockusch, M. R. Wasserman, Z. Zhou, R. B. Altman, S. C. Blanchard, *Chem. Soc. Rev.* **2014**, *43*, 1044–1056.

[98] Q. Zheng, S. Jockusch, Z. Zhou, S. C. Blanchard, *Photochem. Photobiol.* **2014**, *90*, 448–454.

[99] M. Irie, T. Lifka, K. Uchida, S. Kobatake, Y. Shindo, *Chem. Commun.* **1999**, 747–750.

[100] P. D. Patel, I. A. Mikhailov, K. D. Belfield, A. E. Masunov, *Int. J. Quantum Chem.* **2009**, *109*, 3711–3722.

[101] K. Higashiguchi, K. Matsuda, T. Yamada, T. Kawai, M. Irie, *Chem. Lett.* **2000**, *29*, 1358–1359.

[102] M. Montalti, A. Credi, L. Prodi, M. T. Gandolfi, *Handbook of Photochemistry*, CRC Press, **2006**.

[103] H. J. Kuhn, S. E. Braslavsky, R. Schmidt, *Pure Appl. Chem.* **2004**, *76*, 2105–2146.

[104] G. Gauglitz, *J. Photochem.* **1976**, *5*, 41–47.

[105] G. Gauglitz, S. Hubig, *J. Photochem.* **1981**, *15*, 255–257.

[106] G. Gauglitz, S. Hubig, *J. Photochem.* **1985**, *30*, 121–125.

[107] T. Kudernac, T. Kobayashi, A. Uyama, K. Uchida, S. Nakamura, B. L. Feringa, *J. Phys. Chem. A* **2013**, *117*, 8222–8229.

[108] S. Nakamura, K. Uchida, M. Hatakeyama, *Molecules* **2013**, *18*, 5091–5103.

[109] M. Takeshita, T. Kodama, Y. Wada, N. Hatcho, *Chem. Lett.* **2013**, *42*, 1358–1359.

[110] A. Perrier, S. Aloise, M. Olivucci, D. Jacquemin, *J. Phys. Chem. Lett.* **2013**, *4*, 2190–2196.

[111] H. Shoji, D. Kitagawa, S. Kobatake, *New J. Chem.* **2014**, *38*, 933–941.

[112] S. Lee, Y. You, K. Ohkubo, S. Fukuzumi, W. Nam, *Chem. Sci.* **2014**, *5*, 1463–1474.

[113] R. Hoffmann, R. B. Woodward, *Acc. Chem. Res.* **1968**, *1*, 17–22.

[114] F. Stellacci, C. Bertarelli, F. Toscano, M. C. Gallazzi, G. Zotti, G. Zerbi, *Adv. Mater.* **1999**, *11*, 292–295.

[115] K. Uchida, E. Tsuchida, Y. Aoi, S. Nakamura, M. Irie, *Chem. Lett.* **1999**, *28*, 63–64.

[116] S. Kobatake, K. Uchida, E. Tsuchida, M. Irie, *Chem. Lett.* **2000**, *29*, 1340–1341.

[117] K. Uchida, D. Guillaumont, E. Tsuchida, G. Mochizuki, M. Irie, A. Murakami, S. Nakamura, *J. Mol. Struct. THEOCHEM* **2002**, *579*, 115–120.

[118] S. Kobatake, M. Irie, *Chem. Lett.* **2003**, *32*, 1078–1079.

[119] T. Yamaguchi, M. Hosaka, K. Shinohara, T. Ozeki, M. Fukuda, S. Takami, Y. Ishibashi, T. Asahi, M. Morimoto, *J. Photochem. Photobiol. Chem.* **2014**, *285*, 44–51.

[120] M. Takeshita, M. Nagai, T. Yamato, *Chem. Commun.* **2003**, 1496–1497.

[121] M. Kamrul Hossain, M. Takeshita, T. Yamato, *Eur. J. Org. Chem.* **2005**, *2005*, 2771–2776.

[122] S. Aloïse, M. Sliwa, Z. Pawlowska, J. Réhault, J. Dubois, O. Poizat, G. Buntinx, A. Perrier, F. Maurel, S. Yamaguchi, et al., *J. Am. Chem. Soc.* **2010**, *132*, 7379–7390.

[123] W. Li, C. Jiao, X. Li, Y. Xie, K. Nakatani, H. Tian, W. Zhu, *Angew. Chem. Int. Ed.* **2014**, *53*, 4603–4607.

[124] S.-Z. Pu, F.-S. Zhang, F. Sun, R.-J. Wang, X.-H. Zhou, S.-K. Chan, *Tetrahedron Lett.* **2003**, *44*, 1011–1014.

[125] G. Pariani, A. Bianco, R. Castagna, C. Bertarelli, *J. Phys. Chem. A* **2011**, *115*, 12184–12193.

[126] V. Lemieux, N. R. Branda, *Org. Lett.* **2005**, *7*, 2969–2972.

[127] V. Lemieux, S. Gauthier, N. R. Branda, *Angew. Chem. Int. Ed.* **2006**, *45*, 6820–6824.

[128] T. Wu, H. Tang, C. Bohne, N. R. Branda, *Angew. Chem. Int. Ed.* **2012**, *51*, 2741–2744.

[129] A. M. Asadirad, S. Boutault, Z. Erno, N. R. Branda, *J. Am. Chem. Soc.* **2014**, *136*, 3024–3027.

[130] R. S. Stoll, S. Hecht, *Angew. Chem. Int. Ed.* **2010**, *49*, 5054–5075.

[131] N. Kano, F. Komatsu, T. Kawashima, *J. Am. Chem. Soc.* **2001**, *123*, 10778–10779.

[132] N. Kano, M. Yamamura, T. Kawashima, *J. Am. Chem. Soc.* **2004**, *126*, 6250–6251.

[133] M. Yamamura, N. Kano, T. Kawashima, *J. Organomet. Chem.* **2007**, *692*, 313–325.

[134] M. Yamamura, N. Kano, T. Kawashima, *Tetrahedron Lett.* **2007**, *48*, 4033–4036.

[135] M. Morimoto, K. Murata, T. Michinobu, *Chem. Commun.* **2011**, *47*, 9819–9821.

[136] F. Würthner, J. Rebek, *Angew. Chem. Int. Ed.* **1995**, *34*, 446–448.

[137] F. Würthner, J. Rebek, *J. Chem. Soc. Perkin Trans. 2* **1995**, 1727–1734.

[138] M. J. Barrell, A. G. Campaña, M. von Delius, E. M. Geertsema, D. A. Leigh, *Angew. Chem. Int. Ed.* **2011**, *50*, 285–290.

[139] L. A. Ingerman, M. L. Waters, *J. Org. Chem.* **2009**, *74*, 111–117.

[140] A. Coskun, M. Banaszak, R. D. Astumian, J. F. Stoddart, B. A. Grzybowski, *Chem. Soc. Rev.* **2011**, *41*, 19–30.

[141] O. Diels, K. Alder, *Berichte Dtsch. Chem. Ges. B Ser.* **1929**, *62*, 2081–2087.

[142] J. Sauer, *Angew. Chem. Int. Ed.* **1966**, *5*, 211–230.

[143] F. Fringuelli, A. Taticchi, *The Diels-Alder Reaction: Selected Practical Methods*, John Wiley And Sons, **2002**.

[144] Y. G. Shtyrlin, D. G. Murzin, N. A. Luzanova, G. G. Iskhakova, V. D. Kiselev, A. I. Konovalov, *Tetrahedron* **1998**, *54*, 2631–2646.

[145] A. Kumar, *Chem. Rev.* **2001**, *101*, 1–20.

[146] C. Oliver Kappe, S. Shaun Murphree, A. Padwa, *Tetrahedron* **1997**, *53*, 14179–14233.

[147] A. Gandini, M. N. Belgacem, *Prog. Polym. Sci.* **1997**, *22*, 1203–1379.

[148] X. Chen, M. A. Dam, K. Ono, A. Mal, H. Shen, S. R. Nutt, K. Sheran, F. Wudl, *Science* **2002**, *295*, 1698–1702.

[149] J. A. Syrett, C. R. Becer, D. M. Haddleton, *Polym. Chem.* **2010**, *1*, 978–987.

[150] A. Gandini, *Prog. Polym. Sci.* **2013**, *38*, 1–29.

[151] N. Zydziak, B. Yameen, C. Barner-Kowollik, *Polym. Chem.* **2013**, *4*, 4072–4086.

[152] H. Kwart, I. Burchuk, *J. Am. Chem. Soc.* **1952**, *74*, 3094–3097.

[153] Y. Imai, H. Itoh, K. Naka, Y. Chujo, *Macromolecules* **2000**, *33*, 4343–4346.

[154] J. R. McElhanon, D. R. Wheeler, *Org. Lett.* **2001**, *3*, 2681–2683.

[155] M. L. Szalai, D. V. McGrath, D. R. Wheeler, T. Zifer, J. R. McElhanon, *Macromolecules* **2007**, *40*, 818–823.

[156] B. Gotsmann, U. Duerig, J. Frommer, C. J. Hawker, *Adv. Funct. Mater.* **2006**, *16*, 1499–1505.

[157] B. J. Adzima, C. J. Kloxin, C. A. DeForest, K. S. Anseth, C. N. Bowman, *Macromol. Rapid Commun.* **2012**, *33*, 2092–2096.

[158] L. Rulíšek, P. Šebek, Z. Havlas, R. Hrabal, P. Čapek, A. Svatoš, *J. Org. Chem.* **2005**, *70*, 6295–6302.

[159] R. C. Boutelle, B. H. Northrop, *J. Org. Chem.* **2011**, *76*, 7994–8002.

[160] J. Sauer, *Angew. Chem. Int. Ed.* **1967**, *6*, 16–33.

[161] K. N. Houk, L. J. Luskus, *J. Am. Chem. Soc.* **1971**, *93*, 4606–4607.

[162] Y. Kobuke, T. Sugimoto, J. Furukawa, T. Fueno, *J. Am. Chem. Soc.* **1972**, *94*, 3633–3635.

[163] I. Willner, S. Rubin, *Angew. Chem. Int. Ed. Engl.* **1996**, *35*, 367–385.

[164] W. Szymański, J. M. Beierle, H. A. V. Kistemaker, W. A. Velema, B. L. Feringa, *Chem. Rev.* **2013**, *113*, 6114–6178.

[165] B. W. Henderson, T. J. Dougherty, *Photochem. Photobiol.* **1992**, *55*, 145–157.

[166] R. Bonnett, *Chem. Soc. Rev.* **1995**, *24*, 19–33.

[167] T. J. Dougherty, C. J. Gomer, B. W. Henderson, G. Jori, D. Kessel, M. Korbelik, J. Moan, Q. Peng, *J. Natl. Cancer Inst.* **1998**, *90*, 889–905.

[168] R. Bonnett, G. Martínez, *Tetrahedron* **2001**, *57*, 9513–9547.

[169] D. K. Chatterjee, Z. Yong, *Nanomed.* **2008**, *3*, 73–82.

[170] P. Agostinis, K. Berg, K. A. Cengel, T. H. Foster, A. W. Girotti, S. O. Gollnick, S. M. Hahn, M. R. Hamblin, A. Juzeniene, D. Kessel, et al., *CA. Cancer J. Clin.* **2011**, *61*, 250–281.

[171] W. J. Deal, B. F. Erlanger, D. Nachmansohn, *Proc. Natl. Acad. Sci. U. S. A.* **1969**, *64*, 1230–1234.

[172] J. Bieth, N. Wassermann, S. M. Vratsanos, B. F. Erlanger, *Proc. Natl. Acad. Sci. U. S. A.* **1970**, *66*, 850–854.

[173] E. Bartels, N. H. Wassermann, B. F. Erlanger, *Proc. Natl. Acad. Sci. U. S. A.* **1971**, *68*, 1820–1823.

[174] M. R. Banghart, A. Mourot, D. L. Fortin, J. Z. Yao, R. H. Kramer, D. Trauner, *Angew. Chem. Int. Ed.* **2009**, *48*, 9097–9101.

[175] A. Mourot, M. A. Kienzler, M. R. Banghart, T. Fehrentz, F. M. E. Huber, M. Stein, R. H. Kramer, D. Trauner, *ACS Chem. Neurosci.* **2011**, *2*, 536–543.

[176] P. Stawski, M. Sumser, D. Trauner, *Angew. Chem. Int. Ed.* **2012**, *51*, 5748–5751.

[177] A. Mourot, T. Fehrentz, Y. Le Feuvre, C. M. Smith, C. Herold, D. Dalkara, F. Nagy, D. Trauner, R. H. Kramer, *Nat. Methods* **2012**, *9*, 396–402.

[178] M. Stein, A. Breit, T. Fehrentz, T. Gudermann, D. Trauner, *Angew. Chem. Int. Ed.* **2013**, *52*, 9845–9848.

[179] M. Stein, S. J. Middendorp, V. Carta, E. Pejo, D. E. Raines, S. A. Forman, E. Sigel, D. Trauner, *Angew. Chem. Int. Ed.* **2012**, *51*, 10500–10504.

[180] W. A. Velema, J. P. van der Berg, M. J. Hansen, W. Szymanski, A. J. M. Driessen, B. L. Feringa, *Nat. Chem.* **2013**, *5*, 924–928.

[181] A. D. Abell, M. A. Jones, A. T. Neffe, S. G. Aitken, T. P. Cain, R. J. Payne, S. B. McNabb, J. M. Coxon, B. G. Stuart, D. Pearson, et al., *J. Med. Chem.* **2007**, *50*, 2916–2920.

[182] D. Vomasta, C. Högner, N. R. Branda, B. König, *Angew. Chem. Int. Ed.* **2008**, *47*, 7644–7647.

[183] O. Babii, S. Afonin, M. Berditsch, S. Reiβer, P. K. Mykhailiuk, V. S. Kubyshkin, T. Steinbrecher, A. S. Ulrich, I. V. Komarov, *Angew. Chem. Int. Ed.* **2014**, *53*, 3392–3395.

[184] J. L. Nitiss, *Nat. Rev. Cancer* **2009**, *9*, 327–337.

[185] N. Osheroff, E. L. Zechiedrich, K. C. Gale, *BioEssays* **1991**, *13*, 269–275.

[186] D. A. Burden, N. Osheroff, *Biochim. Biophys. Acta BBA - Gene Struct. Expr.* **1998**, *1400*, 139–154.

[187] J. V. Walker, J. L. Nitiss, *Cancer Invest.* **2002**, *20*, 570–589.

[188] J. L. Nitiss, *Nat. Rev. Cancer* **2009**, *9*, 338–350.

[189] A. K. McClendon, N. Osheroff, *Mutat. Res. Mol. Mech. Mutagen.* **2007**, *623*, 83–97.

[190] P. B. Jenen, M. Sehested, *Biochem. Pharmacol.* **1997**, *54*, 755–759.

[191] T. Andoh, R. Ishida, *Biochim. Biophys. Acta BBA - Gene Struct. Expr.* **1998**, *1400*, 155–171.

[192] A. K. Larsen, A. E. Escargueil, A. Skladanowski, *Pharmacol. Ther.* **2003**, *99*, 167–181.

[193] H. Wang, Y. Mao, A. Y. Chen, N. Zhou, E. J. LaVoie, L. F. Liu, *Biochemistry (Mosc.)* **2001**, *40*, 3316–3323.

[194] L. H. Jensen, A. Renodon-Corniere, I. Wessel, S. W. Langer, B. Søkilde, E. V. Carstensen, M. Sehested, P. B. Jensen, *Mol. Pharmacol.* **2002**, *61*, 1235–1243.

[195] L. P. Swift, S. M. Cutts, A. Nudelman, I. Levovich, A. Rephaeli, D. R. Phillips, *Cancer Chemother. Pharmacol.* **2008**, *61*, 739–749.

[196] M. Gersch, J. Kreuzer, S. A. Sieber, *Nat. Prod. Rep.* **2012**, *29*, 659–682.

[197] T. Braun, A. P. Schubert, R. N. Kostoff, *Chem. Rev.* **2000**, *100*, 23–38.

[198] M. J. Allen, V. C. Tung, R. B. Kaner, *Chem. Rev.* **2010**, *110*, 132–145.

[199] J. K. Wassei, R. B. Kaner, *Acc. Chem. Res.* **2013**, *46*, 2244–2253.

[200] P. M. Ajayan, *Chem. Rev.* **1999**, *99*, 1787–1800.

[201] K. Dirian, M. Á. Herranz, G. Katsukis, J. Malig, L. Rodríguez-Pérez, C. Romero-Nieto, V. Strauss, N. Martín, D. M. Guldi, *Chem. Sci.* **2013**, *4*, 4335–4353.

[202] C. A. Dyke, J. M. Tour, *J. Phys. Chem. A* **2004**, *108*, 11151–11159.

[203] A. Hirsch, O. Vostrowsky, in *Funct. Mol. Nanostructures* (Ed.: A.D. Schlüter), Springer Berlin Heidelberg, **2005**, pp. 193–237.

[204] N. Karousis, N. Tagmatarchis, D. Tasis, *Chem. Rev.* **2010**, *110*, 5366–5397.

[205] A. de Juan, Y. Pouillon, L. Ruiz-González, A. Torres-Pardo, S. Casado, N. Martín, Á. Rubio, E. M. Pérez, *Angew. Chem. Int. Ed.* **2014**, *53*, 5394–5400.

[206] S. Sarkar, E. Bekyarova, S. Niyogi, R. C. Haddon, *J. Am. Chem. Soc.* **2011**, *133*, 3324–3327.

[207] S. Sarkar, E. Bekyarova, R. C. Haddon, *Acc Chem Res* **2012**, *45*, 673–682.

[208] A. Gergely, J. Telegdi, E. Mészáros, Z. Pászti, G. Tárkányi, F. H. Kármán, E. Kálmán, *J. Nanosci. Nanotechnol.* **2007**, *7*, 2795–2807.

[209] C.-M. Chang, Y.-L. Liu, *Carbon* **2009**, *47*, 3041–3049.

[210] S. Munirasu, J. Albuerne, A. Boschetti-de-Fierro, V. Abetz, *Macromol. Rapid Commun.* **2010**, *31*, 574–579.

[211] L. Zhang, J. Yang, C. L. Edwards, L. B. Alemany, V. N. Khabashesku, A. R. Barron, *Chem. Commun.* **2005**, 3265–3267.

[212] J.-T. Sun, L.-Y. Zhao, C.-Y. Hong, C.-Y. Pan, *Chem. Commun.* **2011**, *47*, 10704.

[213] C. Ménard-Moyon, F. Dumas, E. Doris, C. Mioskowski, *J. Am. Chem. Soc.* **2006**, *128*, 14764–14765.

[214] T. Yang, X. Zhao, S. Nagase, *Org. Lett.* **2013**, *15*, 5960–5963.

[215] X. Lu, F. Tian, N. Wang, Q. Zhang, *Org. Lett.* **2002**, *4*, 4313–4315.

[216] J. L. Delgado, P. de la Cruz, F. Langa, A. Urbina, J. Casado, J. T. L. Navarrete, *Chem. Commun.* **2004**, 1734–1735.

[217] G. Sakellariou, H. Ji, J. W. Mays, D. Baskaran, *Chem. Mater.* **2008**, *20*, 6217–6230.

[218] F. Mercuri, A. Sgamellotti, *Phys. Chem. Chem. Phys.* **2009**, *11*, 563–567.

[219] N. Zydziak, C. Hübner, M. Bruns, C. Barner-Kowollik, *Macromolecules* **2011**, *44*, 3374–3380.

[220] B. Yameen, N. Zydziak, S. M. Weidner, M. Bruns, C. Barner-Kowollik, *Macromolecules* **2013**, *46*, 2606–2615.

[221] N. Zydziak, C. Hübner, M. Bruns, A. P. Vogt, C. Barner-Kowollik, *Polym. Chem.* **2013**, *4*, 1525–1537.

[222] N. Zydziak, C. M. Preuss, V. Winkler, M. Bruns, C. Hübner, C. Barner-Kowollik, *Macromol. Rapid Commun.* **2013**, *34*, 672–680.

[223] M. M. Bernal, M. Liras, R. Verdejo, M. A. López-Manchado, I. Quijada-Garrido, R. París, *Polymer* **2011**, *52*, 5739–5745.

[224] C.-M. Chang, Y.-L. Liu, *ACS Appl. Mater. Interfaces* **2011**, *3*, 2204–2208.

[225] J. M. García-García, M. M. Bernal, R. Verdejo, M. A. López-Manchado, E. Doncel-Pérez, L. Garrido, I. Quijada-Garrido, *J. Polym. Sci. Part B Polym. Phys.* **2014**, *52*, 349–360.

[226] J. Li, G. Jia, Y. Zhang, *Chem. – Eur. J.* **2007**, *13*, 6430–6436.

[227] Z. Chen, S. Nagase, A. Hirsch, R. C. Haddon, W. Thiel, P. von R. Schleyer, *Angew. Chem. Int. Ed.* **2004**, *43*, 1552–1554.

[228] S. Osuna, K. N. Houk, *Chem. – Eur. J.* **2009**, *15*, 13219–13231.

[229] T. Ito, S. Okazaki, *Nature* **2000**, *406*, 1027–1031.

[230] F. M. Raymo, *Adv. Mater.* **2002**, *14*, 401–414.

[231] G. Gasparini, M. Dal Molin, A. Lovato, L. J. Prins, in *Supramol. Chem.*, John Wiley & Sons, Ltd, **2012**.

[232] B. L. Miller, *Dynamic Combinatorial Chemistry in Drug Discovery, Bioorganic Chemistry, and Materials Science*, Wiley, Hoboken, NJ, **2010**.

[233] M. Barboiu, *Constitutional Dynamic Chemistry*, Springer, **2012**.

[234] J. M. A. Carnall, C. A. Waudby, A. M. Belenguer, M. C. A. Stuart, J. J.-P. Peyralans, S. Otto, *Science* **2010**, *327*, 1502–1506.

[235] S. J. Rowan, S. J. Cantrill, G. R. L. Cousins, J. K. M. Sanders, J. F. Stoddart, *Angew. Chem. Int. Ed.* **2002**, *41*, 898–952.

[236] M. E. Belowich, J. F. Stoddart, *Chem. Soc. Rev.* **2012**, *41*, 2003–2024.

[237] S. Otto, *Acc. Chem. Res.* **2012**, *45*, 2200–2210.

[238] D. Roy, J. N. Cambre, B. S. Sumerlin, *Prog. Polym. Sci.* **2010**, *35*, 278–301.

[239] A. Dirksen, S. Dirksen, T. M. Hackeng, P. E. Dawson, *J. Am. Chem. Soc.* **2006**, *128*, 15602–15603.

[240] J. A. Joule, K. Mills, *Heterocyclic Chemistry*, John Wiley & Sons, **2010**.

[241] Y. Ishibashi, T. Umesato, S. Kobatake, M. Irie, H. Miyasaka, *J Phys Chem C* **2012**, *116*, 4862–4869.

[242] D. Dulić, T. Kudernac, A. Pužys, B. L. Feringa, B. J. van Wees, *Adv. Mater.* **2007**, *19*, 2898–2902.

[243] K. Matsuda, Y. Shinkai, T. Yamaguchi, K. Nomiyama, M. Isayama, M. Irie, *Chem. Lett.* **2003**, *32*, 1178–1179.

[244] T. Hirose, M. Irie, K. Matsuda, *Adv. Mater.* **2008**, *20*, 2137–2141.

[245] Y. Zou, T. Yi, S. Xiao, F. Li, C. Li, X. Gao, J. Wu, M. Yu, C. Huang, *J. Am. Chem. Soc.* **2008**, *130*, 15750–15751.

[246] Y. Shoji, A. Yagi, M. Horiuchi, M. Morimoto, M. Irie, *Isr. J. Chem.* **2013**, *53*, 303–311.

[247] Z. Tong, S. Pu, Q. Xiao, G. Liu, S. Cui, *Tetrahedron Lett.* **2013**, *54*, 474–477.

[248] S. Pu, H. Liu, G. Liu, B. Chen, Z. Tong, *Tetrahedron* **2014**, *70*, 852–858.

[249] X. Yao, T. Li, S. Wang, X. Ma, H. Tian, *Chem. Commun.* **2014**, *50*, 7166–7168.

[250] M. Irie, K. Sayo, *J. Phys. Chem.* **1992**, *96*, 7671–7674.

[251] T. Nasiru, L. Avila, M. Levine, *J. High Sch. Res.* **2011**, *2*, 1–5.

[252] A. C. Whalley, M. L. Steigerwald, X. Guo, C. Nuckolls, *J. Am. Chem. Soc.* **2007**, *129*, 12590–12591.

[253] J. Huang, Q. Li, H. Su, J. Yang, *Chem. Phys. Lett.* **2009**, *479*, 120–124.

[254] P. Zhao, P. Wang, Z. Zhang, C. Fang, Y. Wang, Y. Zhai, D. Liu, *Solid State Commun.* **2009**, *149*, 928–931.

[255] M. K. Ashraf, N. A. Bruque, J. L. Tan, G. J. O. Beran, R. K. Lake, *J. Chem. Phys.* **2011**, *134*, 024524–024524–9.

[256] C. Sciascia, R. Castagna, M. Dekermenjian, R. Martel, A. R. Srimath Kandada, F. Di Fonzo, A. Bianco, C. Bertarelli, M. Meneghetti, G. Lanzani, *J. Phys. Chem. C* **2012**, *116*, 19483–19489.

[257] P. A. Denis, *Chem. – Eur. J.* **2013**, *19*, 15719–15725.

[258] Y. Cao, S. Osuna, Y. Liang, R. C. Haddon, K. N. Houk, *J. Am. Chem. Soc.* **2013**, *135*, 17643–17649.

[259] W. M. Abdou, A. A. Kamel, *Tetrahedron* **2000**, *56*, 7573–7580.

[260] F. Ernst, S. Heeg, T. Heek, A. Setaro, R. Haag, S. Reich, *Phys. Status Solidi RRL – Rapid Res. Lett.* **2013**, *7*, 546–549.

[261] F. Ernst, T. Heek, A. Setaro, R. Haag, S. Reich, *Adv. Funct. Mater.* **2012**, *22*, 3921–3926.

[262] B. González, A. Herrera, B. Illescas, N. Martín, R. Martínez, F. Moreno, L. Sánchez, A. Sánchez, *J. Org. Chem.* **1998**, *63*, 6807–6813.

[263] E. Orgiu, N. Crivillers, M. Herder, L. Grubert, M. Pätzel, J. Frisch, E. Pavlica, D. T. Duong, G. Bratina, A. Salleo, et al., *Nat. Chem.* **2012**, *4*, 675–679.

[264] P. Zacharias, M. C. Gather, A. Köhnen, N. Rehmann, K. Meerholz, *Angew. Chem. Int. Ed.* **2009**, *48*, 4038–4041.

[265] S. Castellanos, A. A. Vieira, B. M. Illescas, V. Sacchetti, C. Schubert, J. Moreno, D. M. Guldi, S. Hecht, N. Martín, *Angew. Chem. Int. Ed.* **2013**, *52*, 13985–13990.

[266] H. E. Gottlieb, V. Kotlyar, A. Nudelman, *J. Org. Chem.* **1997**, *62*, 7512–7515.

[267] A. P. Glaze, H. G. Heller, J. Whittall, *J. Chem. Soc. Perkin Trans. 2* **1992**, 591–594.

List of Abbreviations

ADMF	—	3-acetyl-2,5-dimethylfuran
ATR	—	attenuated total reflection
BODIPY	—	boron-dipyrromethene
CAC	—	critical aggregate concentration
CMC	—	critical micelle concentration
CNT	—	carbon nanotube
CVD	—	chemical vapor deposition
DA	—	Diels-Alder
DAD	—	diode array detector
DAE	—	diarylethene
DBU	—	1,8-diazabicycloundec-7-ene
DCC	—	dynamic covalent chemistry
DLS	—	dynamic light scattering
DMSO	—	dimethyl sulfoxide
DNA	—	deoxyribonucleic acid
ESI	—	electrospray ionization
FA	—	furfuryl alcohol
FTIR	—	Fourier transform infrared

GABA	—	γ-aminobutyric acid
hCAI	—	human carbonic anhydrase 1
HOMO	—	highest occupied molecular orbital
LED	—	light emitting diode
LUMO	—	lowest unoccupied molecular orbital
MeCN	—	acetonitrile
MI	—	maleimide
MINT	—	mechanically interlocked nanotubes
MS	—	mass spectrometry
MWCNT	—	multi-walled carbon nanotube
NEM	—	*N*-ethylmaleimide
NMR	—	nuclear magnetic resonance
PAN	—	1-(2-pyridylazo)-2-naphthol
PBS	—	phosphate buffered saline
PDT	—	photodynamic therapy
PE	—	petroleum ether
PSS	—	photostationary state
rt	—	room temperature
SWCNT	—	single-walled carbon nanotube
TGA	—	thermogravimetric analysis
THF	—	tetrahydrofuran

TLC	—	thin layer chromatography
TOP2	—	DNA topoisomerase II
TRPV1	—	transient receptor potential cation channel subfamily V member 1
UPLC	—	ultra-high performance liquid chromatography
UV	—	ultraviolet
vis	—	visible
XPhos	—	2-dicyclohexylphosphino-2‘,4‘,6‘-triisopropylbiphenyl